Interplay Between Viral and Cellular Factors Determines the Fate of Herpes Simplex Virus type I Infection

By

Heba Hamdy Mabrouk Mostafa

Submitted to the graduate degree program in Molecular Biosciences and the Graduate Faculty of the University of Kansas in partial fulfillment of the requirements for the degree of Doctor of Philosophy.

_____

Chairperson David Davido

_____

Kristi Neufeld

_____

Steven Benedict

_____

Scott Hefty

_____

Susan Egan

_____

Thomas Yankee

Date Defended: 25 March 2014

The Dissertation Committee for Heba Hamdy Mabrouk Mostafa

certifies that this is the approved version of the following dissertation:

Interplay Between Viral and Cellular Factors Determines the Fate of Herpes Simplex Virus type I Infection

_____

Chairperson David Davido

Date approved: 8 April 2014

To my beloved husband

Maged Zeineldin

To my dear parents

Hamdy Mabrouk and Hafsa Zaitoun

To my precious sons

Adam and Zane

إلى زوجى الحبيب

ماجد

إلي أبي وأمى الحبيبين

حمدى مبروك وحفصة زيتون

إلى أولادى

آدم وزين

Abstract

The herpes simplex virus type I (HSV-1) is a major human pathogen that infects the majority of the world's population. The life cycle of HSV-1 is controlled by interactions with its hosts. Understanding virus-host interactions will be necessary for developing new therapeutic and preventive strategies against HSV-1, especially in immuno-compromised patients and neonates. An interesting aspect of HSV-1 is how it switches from a productive (lytic) replication cycle to a lifelong latent infection in the sensory neurons; the molecular events involved in this switch are not clearly understood. Consequently, the major goal of this thesis is to examine the role and interactions of viral and cellular proteins in determining the outcome of viral infection. In this thesis, I studied two viral regulatory immediate early proteins (IE), namely infected cell protein 0 (ICP0) and infected cell protein 22 (ICP22). Both proteins are required for efficient viral replication *in vivo*. Specifically, I characterized in cell culture and in mice how ICP0's functions are regulated via phosphorylation, and I distinguished the functions between ICP22 versus its N-terminally truncated form, $U_S1.5$. In the latter experiments, we also identified a novel role for ICP22 in counteracting the type I interferon (IFN) response. Furthermore, I characterized the viral mutant, KOS-NA that contains novel mutation/s within the UL39 gene, which encodes for the large subunit of ribonucleotide reducatese enzyme (ICP6). These mutations in KOS-NA resulted in ICP6 amino acid substitutions that reduced its protein levels, and attenuated viral pathogenesis *in vivo,* making KOS-NA a potential therapeutic vector in treating HSV-1 diseases. Lastly, I discovered a new relation between the cellular kinase CDK-5, its activating partner p35, and HSV-1 acute infection of neurons. Overall, the data presented in this thesis indicates that multiple

viral encoded factors, phosphorylation, cellular factors, and their interactions with one another affect the HSV-1 life cycle.

Acknowledgments

I would like to thank my wonderful Ph.D. mentor, Dr. David Davido, as I was fortunate to join his lab, for all his help and support with this dissertation. Dr. Davido offered me his extensive knowledge of HSV-1 and supported me in learning various techniques, formulating and addressing hypotheses, and helped with trouble shooting when I encountered technical problems. He was always available and willing to help. Furthermore, Dr. Davido taught me about writing grants and reviewing manuscripts, which gave me a great opportunity to critically evaluate science, develop new hypotheses, and propose new approaches and techniques. He provided me with a very friendly, family oriented, no-stress work environment, allowing me to be very productive. I would like to thank all current and former members of Davido lab for assistance; this especially includes Miles Smith and Mirna Perusina Lanfranca. Also, I would like to thank Dr. Kristi Neufeld, Dr. Yoshi Azuma, Dr. Stephen Rice, Dr. Steven Benedict, and Dr. Priscilla Schaffer and members of their labs for providing reagents and equipment.

I would like to thank my graduate advisory committee members; Dr Kristi Neufeld, Dr Stephen Benedict, Dr Scott Hefty, Dr Susan Egan, and Dr Thomas Yankee for the guidance and encouragement they provided me over the years.

All my sincerest thanks and appreciation to my dear husband, Maged Zeineldin, dear parents, Hamdy Mabrouk and Hafsa Zaitoun, my dear sister Hend, my dear brother Mohammed, and my family and friends in Egypt and in Lawrence, Kansas.

I would like to thank the different sources of funding including the NIH, KU, and Hirata fellowship for making this work possible.

Table of contents

List of Figures

Chapter 1

Introduction

1.1 Significance of the research

HSV-1 is a major ubiquitous human pathogen that infects ~80% of the human population. Typical HSV-1 infections result in vesicular eruptions around the mouth, which are also known as cold sores. In addition, HSV-1 infects the cornea of the eyes resulting in keratitis, which in its recurrent form can lead to corneal opacification and blindness (1). The life threatening forms of HSV-1 infection are apparent in neonates (2) and immunocompromised individuals (3) and can be manifested as encephalitis and pneumonia. Although lethal HSV-1 infections are rare, the prevalence of HSV-1 disease causes a significant burden on human health. It is notable that even common forms of infections are painful and recurrent. With the advent of acyclovir (4), it has been feasible to treat HSV-1 infections, although recent data indicates that resistance to acyclovir is growing (5). Furthermore, the lack of effective vaccines to prevent or therapeutically treat recurrent HSV-1 infections emphasizes a critical need to understand HSV-1 replication and pathogenesis.

1.2. HSV-1

The herpes simplex virus 1 (HSV-1) is an alphaherpesvirus of the *herpesviridae* family. The virus has a large double-stranded DNA genome, which contains ~80 open reading frames (ORFs). The DNA core is surrounded by an icosahedral capsid. The nucleocapsid is embedded in an amorphous proteinaceous layer known as the

tegument, which is surrounded by a lipid bilayer envelope. The envelope carries viral glycoproteins that are required for viral attachment and penetration in the host cell (1). Like other herpesviruses, a hallmark of HSV-1 infection is its ability to switch between lytic and latent replication cycles. Lytic replication occurs in the epithelial cells and fibroblasts at the primary site of infection and sensory neurons. The latent form of infection occurs in the sensory neurons that innervate at the primary site of infection, leading to a lifelong infection. During latent infection, no infectious virus is produced. Sites of HSV-1 latency include the trigeminal ganglia (TG), superior cervical ganglion, and ciliary ganglion among others (6). Latent infections can occasionally be reactivated under stress stimuli.

1.3. HSV-1 lytic infection

Infection is initiated by fusion of the viral envelope with the cellular plasma membrane, a process which is facilitated by viral glycoproteins and a subset of cellular receptors. The nucleocapsid is transported to the nuclear pore, and the viral DNA is then released into the nucleus where transcription is initiated by the host cell RNA polymerase II. Viral gene transcription is expressed in a temporal cascade that follows the pattern of immediate-early (IE), followed by early (E), and then late (L) genes. Generally, the IE proteins have regulatory and immune evasion functions and help transactivate the E and L genes. The expression of IE proteins requires the activity of the tegument protein, VP16, which recruits the cellular transcription factors Oct-1 and HCF to form a complex on IE promoters to activate their transcription (7, 8). The IE proteins include: ICP4, an essential transcription factor to stimulate the expression of E

and L genes (9-11); ICP27, an essential viral protein that facilitates transport of viral messenger RNAs (12); and ICP47, which facilitates evasion of the immune system through down-regulation of MHC class I (13). The remaining two IE proteins, ICP0 and ICP22, play important roles in HSV replication, and their functions will be discussed in more detail later in this chapter. Following IE gene expression, the E proteins are synthesized and play direct or indirect roles in viral DNA replication. Lastly, the L proteins are assembly factors, structural components of infectious virions, or facilitate viral egress.

1.4. Latent infection and reactivation from latency

Once the virus reaches the sensory nerve endings innervating the primary site of infection, the virion envelope is lost, and the viral nucleocapsid surrounded by the tegument spreads retrograde to the neuronal cell bodies (14). Once the nucleocapsid reaches the neuronal nucleus, the viral DNA is released into the nucleus, and a productive replication cycle can occur following the same steps as in infected epithelial cell. As a productive replication cycle is lethal to neurons, it has been hypothesized that neuronal and viral factors suppress viral replication, leading to a dormant or latent infection. One recent report suggests that some neuronal subtypes might support productive infection while others might favor latent infection (15). The latent infection is characterized by an overall lack of lytic gene expression, with the exception of the latency-associated transcripts (LATs) (16). During latency, the latent viral genome is maintained as a chromatinized circular episome that doesn't integrate into the host's genome (17). It has been proposed that histone modifications and epigenetic regulation

are one determinant in the switch between productive and latent infection and control reactivation from latency (18). In addition, expression of LATs assists in maintaining latency by enhancing the survival of the infected neurons (19-22). Currently, the LATs appear to be in involved in the expression of non-coding micro-RNA (miRNA) during latency (23).

In response to stressful conditions like UV irradiation or immunosuppression (24, 25), the latent viral genome in neurons initiates a productive infection, known as reactivation, and the virus spreads anterograde to the primary site of lytic infection. Besides LATs, the viral factors VP16 (26, 27) and ICP0 (28) are important for enhancing HSV-1 reactivation from latency.

1.5. The ocular mouse model for acute infection and latency

Mice are one of several animal models that have been used extensively to study HSV-1 acute replication, latency, and reactivation *in vivo*. Although mice are not the natural host of HSV-1, they recapitulate many aspects of acute infection, latency, and reactivation in humans. In addition, mice have been used in studies to test HSV-1 drugs. Moreover, many transgenic mouse strains are readily available, which have been used to study parts of the HSV-1 life cycle (reviewed in (29)). As will be described in this thesis, we used the mouse ocular model of HSV-1 infection to study acute infection, latency, and explant-induced reactivation from latency. In this model system, mice are infected ocularly with HSV-1, and samples are either collected early (up to 9 days post-infection) to examine acute replication, or late (28-30 days post-infection) to study latency and reactivation.

1.6. ICP0

ICP0 or infected cell protein 0 is a 775 amino acid (AA) IE protein expressed by HSV-1. ICP0's role in viral replication became apparent when ICP0 deletion mutants showed reduced growth in cell culture (30). Later studies showed that ICP0 is required for an efficient establishment of latency and efficient reactivation (31, 32). Cell culture experiments showed that ICP0 transactivates all categories of viral genes (IE, E, and L) (33), dissociates components of the subnuclear structure known as nuclear domain (ND) 10 (34-38), and directs the degradation of kinetochore proteins, interrupting the cell cycle (39-41). ICP0 was shown to contain a RING-finger, which is a structural motif found in many E3 ubiquitin (Ub) ligases. This observation led to studies that showed ICP0 colocalizes with polyubiquitin chains, and this activity is dependent on its RING finger (42). Later studies showed that ICP0 is capable of ubiquitinating different cellular targets *in vitro* and in cell culture; targets include p53 (43) and ubiquitin specific protease 7 (USP-7) (44). The RING-finger domain of ICP0 has been shown to be important for efficient acute viral replication, highlighting the importance of its E3 ubiquitin ligase activity in viral replication. In addition, ICP0 assists HSV-1 in counteracting other intrinsic and innate host defenses that include the DNA damage response (45-49), chromatinization or repression of the viral genome (50-54), and the activation and establishment of the interferon response (55-59). These activities of ICP0 require, to a great extent, its RING-finger domain and components of the ubiquitin-proteasome pathway.

1.6.1. **ICP0 and ND10s**

The nuclear domain 10 (ND10) is a subnuclear organelle that is formed by many proteins, with promyelocytic leukemia protein (PML) being a major organizer of ND10 assembly and the recruitment of other ND10 proteins. ND10 modulates several cellular biological processes including proliferation, senescence, apoptosis, and DNA damage (60-64). ND10 possesses intrinsic antiviral properties that target both DNA viruses and RNA viruses (65-67). Several ND10 constituent proteins, including PML, Sp100, hDaxx, and ATRX have been shown to limit HSV-1 replication (68-70); however, this effect has been shown to be counteracted by ICP0. Specifically, ICP0's E3 ubiquitin ligase activity promotes the disruption of ND10 by mediating the proteolysis (directly or indirectly) of SUMO-conjugated isoforms of PML and Sp100 (37, 38, 71-76) or by dissociating the ND10 components, hDaxx and ATRX (77). This disruption of ND10 ultimately stimulates viral transcription. ICP0-mediated disruption of ND10 occurs in the context of acute viral replication of different cell lines and in the absence of other viral factors, indicating that ICP0 alone is sufficient to disrupt ND10s.

1.6.2. **ICP0 is required for efficient lytic infection and reactivation from latency**

Mutants lacking ICP0 are defective in viral replication in cell culture, unless cells are infected with high multiplicities of infection (MOI) of viral particles. Interestingly, a loss in ICP0 expression promotes the silencing of viral gene expression, leading to a quiescent infection, and this phenotype can be reversed by the exogenous expression of ICP0 (53, 78). *In vivo* studies have shown that ICP0 is essential for efficient acute replication in the eyes and TG of mice. Even when equivalent latent infections can be established with wild-type HSV-1 and ICP0-null mutant viruses, an ICP0-null mutant is

also impaired for reactivation from latency (28). Overall, these cell culture and *in vivo* studies indicate that ICP0 stimulates lytic infection and its absence promotes a dormant or latent infection. ICP0's reversal of HSV-1 genome silencing is associated not only with ND10 disruption but also its ability to diminish the deposition or accumulation of repressive histone markers on viral DNA (50). Moreover, ICP0 interacts with histone deacetylases (HDACs), resulting in their relocalization in cells (79). Lastly, a C-terminal domain in ICP0 binds to RE1-silencing transcription factor corepressor (CoREST) leading to disruption of the repressor complex REST/CoREST/ HDAC1/2/LSD1, an activity which was shown to inhibit silencing of the viral genome (54, 80).

1.6.3. **ICP0 and USP-7**

The ubiquitin specific protease 7 (USP-7), also known as herpes-associated ubiquitin specific protease (HAUSP), is a 135-KDa cellular protein that was initially found to interact with the C-terminus of ICP0 (81, 82). USP-7 partially colocalizes with ND10, a phenotype which is enhanced in the presence of ICP0 (83). Interrupting ICP0 and USP-7 binding has been shown to reduce the transactivation activity of ICP0 and diminish viral plaque formation without affecting ND10 disruption (84). Interestingly, this interaction has been shown to stabilize ICP0 protein levels early during viral infection, (85) but later in the viral life cycle, ICP0 directs the ubiquitination and degradation of USP-7 (44) and ICP0 phosphorylation appears to play a role in this process (86). Furthermore, ICP0 has been shown to recruit USP-7 to the cytoplasm (87). Cytoplasmic USP-7 has been shown to interfere with (toll like receptor) TLR signaling, leading to the inhibition of NF-kB signaling (87).

1.6.4. **ICP0 and phosphorylation**

It has been known for some time that ICP0 is modified by phosphorylation (88); however, the exact function phosphorylation plays in regulating ICP0 activities is largely unknown. The observation that specific cellular kinase inhibitors impair the transactivating activity of ICP0 suggested a potential link between phosphorylation and this key activity of ICP0 (89). Three regions of ICP0 phosphorylation were identified by tandem mass spectrometric analysis and were named regions I, II, and III (90). To examine the importance of these phosphorylated regions for the activities of ICP0, the phospho-acceptor sites in each of these regions were mutated to alanine, blocking their phosphorylation, to create the mutations Phos 1, 2, and 3 (90). In transient expression assays, these phosphorylation mutations affected several properties of ICP0. Specifically, clustered mutation of the four phosphorylation sites in region I (Phos 1) impaired the ability of ICP0 to dissociate two ND10-associated proteins, PML and Sp100 from ND10, reduced its E3 Ub ligase activity, diminished its transactivation activity, and impaired HSV-1 acute replication in cell culture (91). Phos 2 was only defective in its ability to dissociate Sp100 from ND10. Phos 3, on the other hand, only showed different subcellular localization compared to wild type ICP0 and impaired the transactivating activity of ICP0 when expressed at high levels. These cell culture studies identified region I as having the greatest impact on ICP0 functions and HSV-1 replication (91, 92).

One of my thesis projects was to characterize the role these phosphorylated regions of ICP0 play in acute *in vivo* replication and reactivation from latency (Chapter 2). This study identified regions I and II of ICP0 as being important for acute viral

replication and reactivation from latency. A second part of this study was to map which specific sites in region I regulate the activities of ICP0, as Phos 1 was mutated for 4 phosphorylation sites. To address this question, individual and one double-phosphorylation knockout from region I were generated and tested in cell culture and the HSV mouse ocular model of infection. I determined that the residue at serine 224 modulate the majority of ICP0 functions in region I (Chapter 3).

1.7. Isolation of the mutant virus, KOS-NA

During the course of generating the Phos 3 mutant, we isolated a KOS mutant, termed KOS-NA (neuro-attenuated) that was severely impaired for acute replication in the eyes and trigeminal ganglia (TG) of mice, significantly reduced in its ability to establish latency, and was reduced in reactivation from latency by explantation. Given the severe attenuation of KOS-NA in mice, we hypothesized that KOS-NA contained a secondary set of mutations in one or more key viral genes that regulate HSV-1 pathogenesis. We then proposed that these secondary mutations will provide insights into HSV-1 pathogenesis and may prove useful in developing a vaccine against HSV-1 infection. To understand the genetic basis for KOS-NA's *in vivo* phenotypes, we sequenced the KOS-NA genome relative to wild type parental viral strain KOS (93). We discovered nonsynonymous mutations in both the ICP4 IE gene and Glycoprotein I (gI) L gene. Interestingly, the KOS-NA genome contained two nonsynonmyous mutations (AA 393, L to P and AA 950, R to H), in the UL39 gene, which encodes the large subunit of ribonucleatide reductase, also known as ICP6. ICP6 is a part of an enzyme complex that converts ribonucleotides to deoxyribonucleotides (94, 95). Although this

gene is not essential for viral growth in dividing cell lines, it is important for viral replication in quiescent cells such as neurons (96, 97). Several published studies have shown that UL39 mutants are severely impaired for viral replication, establishment of latency, and/or reactivation in mouse models of HSV-1 replication (98, 99). Given the parallels between the *in vivo* replication phenotypes of published UL39 mutants and KOS-NA, we proposed that the two mutated codons in ICP6 of KOS-NA are responsible for its attenuated phenotypes. To test this possibility, we rescued the UL39 mutated gene within the KOS-NA genome with a wild type copy of *UL39*, and introduced the KOS-NA UL39 mutations into the wild type genome. The acute replication of both viruses was examined in eyes and TG of mice. Results from these experiments indicate that AA 393 and/or 950 of ICP6 are essential for high levels of acute replication in the eyes and TG of mice, which facilitates an efficient latent infection (Chapter 4).

1.8. ICP22

Of the five IE proteins, infected cell protein 22 (ICP22) is the least studied, and its functions during viral replication are not fully understood. The basis for this lack of knowledge is partially due to an early report that showed ICP22 is dispensable for HSV-1 replication in African green monkey kidney (Vero) cells (100). Additional studies demonstrated that ICP22 is required for efficient replication in select cell lines, including primary human and rodent cells, which are designated as restrictive cells (101, 102). ICP22 is encoded by the US1 gene and is a 420 AA protein that is post-translationally modified by phosphorylation. These phosphorylation events during viral infection result in the detection of multiple ICP22 bands by western blots. Genetic studies have shown

that the phosphorylation of ICP22 is primarily mediated through the viral encoded kinase, UL13 (103-105).

A role for ICP22 in viral replication *in vivo* became evident when ICP22 mutant viruses were shown to be neuro-attenuated following intracerebral inoculation in mice and limited for acute ocular and ganglionic replication, which impaired the establishment of latency (102, 106). Diminished acute infection of ICP22 mutants was proposed to be attributed to two main factors: reduction in L viral protein expression and alterations in extracellular virion composition. In restrictive cells, early events of the viral life cycle were shown to be unaffected with ICP22 mutants (102, 107). On the other hand, expression of a subset of L viral proteins, including US11, UL38, UL41, and glycoprotein C, were markedly reduced (101, 108). Virions of the ICP22 truncation mutant, 22/*n*199, were shown to be markedly different from wild type HSV-1 virions. Differences in virion protein composition for the mutant were observed with glycoprotein C and a subset of tegument proteins. It was hypothesized that this difference in the virion composition enhances viral clearance or reduces virion stability (106).

Another function reported for ICP22 is its ability to alter the phosphorylation status of the C-terminus of the large subunit of the host RNA polymerase II (107, 109, 110). Although the significance of this function in viral replication is not clear, it has been proposed that the altered modification of RNA polymerase II either enhances HSV-1 genome transcription or suppresses cellular transcription (111).

1.8.1. **ICP22 and VICE domains**

Recently, ICP22 was shown to be required for the formation of the viral induced-chaperone enriched (VICE) domains (112). Those domains were initially described to form in response to viral infection (113, 114) and contain many cellular chaperone proteins that include Hsc70, Hsp70, and Hsp90, polyubiquitinated proteins, components of the proteasome, and the viral portal protein UL6. These proteins colocalize with ICP22 in the nucleus adjacent to viral replication compartments (RC) (113). Consequently, VICE domains are thought to have a role in nuclear protein quality control in viral infection (115). Notably, an ICP22 null mutant and several ICP22 truncation mutants were not able to induce the formation of VICE domains in several cell lines. Furthermore, the expression of ICP22 alone is sufficient to induce the formation of VICE domains.

1.8.2. **U_S1.5**

Analyzing the functions of ICP22 has been complicated by the co-expression of an in-frame N-terminally truncated form, termed U_S1.5 (116). The U_S1.5 protein was initially proposed to be the product of a transcript, which was distinct from that of ICP22, and its translation was reported to initiate at the methionine (M) codon 147 of the ICP22 open reading frame (ORF) (116). When the expression of U_S1.5 was examined in another study, a second transcript encoded by the *U_S1* gene was not detected (117). In this same report, the ICP22 ORF was mutated, and it was established that expression or translation of U_S1.5 protein originated from the M codon at position 90 in the ICP22 ORF and not at M147 as previously reported (117).

None of the studies conducted to characterize ICP22 have separated its functions from those of $U_S1.5$. Although viral mutants have been made to express only the $U_S1.5$ protein, these were engineered based on the previously reported initiation codon (i.e., M147) of $U_S1.5$ (118, 119). As a part of my thesis, we wanted to examine if the functions of ICP22 could be separated from those of $U_S1.5$. To test this possibility, I made mutant viruses that either express ICP22 by mutating M90, the $U_S1.5$ initiation codon into alanine (M90A), or only express $U_S1.5$, by introducing stop codons upstream of M90 (3Xstop). As described in Chapter 5, I tested these mutant viruses for acute replication and establishment of latency in the mouse ocular model and viral replication and VICE domain formation in cell culture-based assays. Moreover, I examined the inhibitory effect of both proteins on the transactivated gene expression of the HSV-1 IE protein, ICP0, and whether they contributed to the plating efficiency of HSV-1 in the presence and absence of type I interferon (IFN-β). My data indicate that although both ICP22 and $U_S1.5$ are able to enhance the maximum expression of the late viral proteins vhs and gC and inhibit ICP0-mediated gene expression in cell culture, only ICP22 is required for efficient acute viral replication and the establishment of latency *in vivo*, and the formation of VICE domains. Additionally, my data demonstrate a new function for ICP22 in counteracting the antiviral effects of IFN-β.

1.9. HSV-1 and CDK-5/p35

A previous study from our laboratory showed that wild-type HSV-1 acute replication, latency and reactivation were impaired in the eyes and trigeminal ganglia (TG) of p35 knockout mice, a binding and activating partner of CDK-5 (120).

Furthermore, when we tried to identify cellular kinases that could potentially phosphorylate ICP0 using multiple kinase prediction programs, CDK-5 was listed as a potential kinase that could phosphorylate S224 and S371 in regions I and II of ICP0, respectively. These observations led me to study the relationship between HSV-1 acute infection in neurons and CDK-5 and p35.

CDK-5 is a neuronal factor that is highly active in post-mitotic neurons and is required for neuronal survival during stress (121, 122). In contrast to other cyclin-dependent kinases, CDK-5 is not required for the cell cycle progression and in fact represses the re-entry of post-mitotic neurons into the cell cycle (123). CDK-5 regulates many neuronal processes, including neuronal differentiation and the formation of synapses (reviewed in (124)). A unique feature of CDK-5 is that it does not require cyclins for its activation. Instead, one of its binding partners, p35, was found associated with CDK-5 in brain extracts, and another, p39, was identified based on its similarity to p35; these binding partners can activate its kinase activity and modulate its subcellular localization (125-128). These activators have very limited amino acid similarity with cyclins (129), suggesting that the activation of CDK-5 by p35 or p39 is mechanistically different from other cell cycle-associated CDKs. So far, it is not clear if p35 and p39 confer different substrate specificity for CDK-5. p39 has been shown to be capable of compensating for some, but not all, of the functions of p35, and p35 can compensate for the absence of p39, as $p39^{-/-}$ mice have no apparent neuronal phenotypes that are different than wild-type mice (130). The activity of CDK-5 directly correlates with the level of its major activator, p35 (131), which is found predominantly in neurons. This

likely explains why CDK-5 is highly active in neurons, although it is constitutively expressed in many cell types (125, 132).

CDK-5 has been shown to play important roles in both neuronal survival and death. Inactivation of CDK-5 has been shown to trigger neuronal death (133-136). On the other hand, the survival activity of CDK-5 is evident when neurons are stressed, and several studies showed that CDK-5 counteracts DNA damage-induced neuronal apoptosis (137-141). Interestingly, CDK-5 hyperactivity, which is observed when CDK-5 couples with p25, an N-terminal truncated form of p35 catalyzed by the protease calpain (124, 142), is associated with neuronal death and neurodegenerative diseases (reviewed in (124)).

Chapter 6 examines the effect HSV-1 acute infection of neurons has on p35 and CDK-5. I observed that viral infection upregulates p35 protein levels and changes the localization of CDK-5 from the nucleus to the cytoplasm. Consequently, I hypothesized that p35 upregulation supports viral infection, as it will stabilize and enhance the pro-survival activities of CDK-5 in response to the stress triggered via HSV-1 infection. While HSV-1 infection triggers DNA damage response in non-neuronal cells in culture (143-145), a previous study indicated that HSV-1 does not trigger a DNA damage response in cultured neurons (144). My goal was to determine if components of the DNA damage response were altered or activated in neurons by HSV-1 during acute infection *in vivo*. HSV-1 positive neurons showed extensive γH2AX staining, a marker of the DNA damage response. Interestingly, when I looked at poly ADP-ribose polymerase-1 (PARP-1), a downstream DNA damage response marker shown to be activated in response to HSV-1 (49), PARP-1 localization changed from nuclear staining

in uninfected neurons to cytoplasmic in HSV-1-positive neurons. Consequently, I propose a model in which HSV-1 infection activates components of the cellular DNA damage response during acute infection of neurons. This activation, in turn, increases p35 protein levels and the cytoplasmic localization of CDK-5 stimulates neuronal survival or anti-apoptotic signaling (Chapter 6).

Chapter 2

Herpes Simplex Virus Type 1 ICP0 Phosphorylation Site Mutants are Attenuated for Viral Replication and Impaired for Explant-Induced Reactivation

This chapter is modified from the published article: J Virol. 2011 Dec;85(23):12631-7

Co-authors

Thornton W. Thompson, Anna S. Kushnir, Steve D. Haenchen, Adam M. Bayless, Joshua G. Hilliard, Malen A. Link, Lisa A. Pitcher, Emma Loveday, Priscilla A. Schaffer

2.1 Abstract

In cell culture experiments, phosphorylation appears to be a critical regulator of the herpes simplex virus type 1 (HSV-1) immediate-early (IE) protein, ICP0, which is an E3 ubiquitin ligase that transactivates viral gene expression. Three major regions of phosphorylation in ICP0 (amino acids 224-232, 365-371, and 508-518) have been identified, and mutant viruses that block phosphorylation sites within each region (termed Phos 1, 2, and 3) have been constructed. Previous studies indicated that replication of Phos 1 is significantly reduced compared to wild-type virus in cell culture (C. Boutell, *et al.*, J. Virol. 82:10647-56, 2008). To determine the effects these phosphorylation site mutations have on the viral life cycle *in vivo*, mice were ocularly infected with wild-type HSV-1, the Phos mutants, or their marker-rescue counterparts. Subsequently, viral replication, establishment of latency, and viral explant-induced

reactivation of these viruses were examined. Relative to wild-type virus, Phos 1 eye titers were reduced as much as 7- and 18-fold on days 1 and 5 post-infection, respectively. Phos 2 eye titers, on the other hand were reduced by 6-fold on day 1 post-infection. Phos 1 and 2 trigeminal ganglia titers were reduced as much as 16- and 20-fold, respectively, on day 5 post-infection. Additionally, the reactivation efficiencies of Phos 1 and 2 were impaired relative to wild-type HSV-1, although both viruses established wild-type levels of latency *in vivo*. The acute replication, latency, and reactivation phenotypes of Phos 3 were similar to wild-type HSV-1. We conclude from these studies that phosphorylation is likely a key modulator of ICP0's biological activity in a mouse ocular model of HSV-1.

2.2 Materials and Methods

Cell Lines and Viruses: Vero cells (African green monkey kidney cell line) and L7 (Vero cells that contain the ICP0 gene) were cultured in Dulbecco's modified Eagle's medium (DMEM) supplemented with fetal bovine serum (FBS), 100 µg/ml penicillin, 100 units/ml streptomycin, and 2mM L-Glutamine as previously described (146, 147), except 5% FBS was used in our experiments. The wild-type HSV-1 (strain KOS), 7134 (an ICP0-null mutant virus), Phos 1, 2, and 3, and their respective marker-rescue viruses (Phos 1, 2, and 3 MR) were propagated and titered as previously described (91, 147, 148).

Ocular Infection of Mice: CD-1 out-bred female mice (6-7 weeks old) were obtained from Charles Rivers Laboratories (Shrewsbury, MA) and cared for according to *Guide for the Care and Use of Laboratory Animals* (149), and the protocol for their use was approved by University of Kansas Institutional Animal Care and Use Committee. Mice were infected as previously described (150). Briefly, mice were anesthetized by intraperitoneal injection with ketamine (100 mg/kg of body weight) and xylazine (6.6 mg/kg of body weight). Corneas were scarified with a 26-gauge needle and infected with one of 8 viruses (KOS, 7134, Phos 1, Phos 2, Phos 3, Phos 1 MR, Phos 2 MR, or Phos 3 MR) at 2 x 10^5 PFU of virus per eye in 3 µl medium.

Determination of Viral Titers in Eyes and Trigeminal Ganglia (TG): On indicated days 0-9 post-infection, eye swabs and TG samples were collected. For eye swabs, a sterile cotton-tipped swab was moistened with Vero cell medium. Tear film

was collected by swabbing each eye, placing the swab in 500 µl growth medium. For TG samples, the mice were euthanized by CO_2 asphyxiation, and the TG were removed and placed in microfuge tubes with 500 µl 1% FBS growth medium and 100 µl of 1 mm glass beads. These samples were homogenized using a Mini-Beadbeater 8 (BioSpec, Bartlesville, OK). In all cases, the wild-type and MR viruses were titered on Vero cells, and mutant viruses were titered on L7 cells. Statistical analyses for acute viral titers were performed using the Student's *t* -test.

Latent Viral Genome Loads in TG: At 30 days post-infection, latently infected TG were collected, and DNA was isolated from each TG as reported by Halford, et al. (151). PCR primers for the HSV-1 UL50 gene (152) and the mouse adipsin gene (153) were used to amplify viral DNA sequences and as a loading control for cellular DNA, respectively. Real time PCR samples were performed in a total volume of 25 µl containing FastStart SYBR Green Master (Rox) (Roche, Indianapolis, IN) and primers [300 nM] in an ABI Prism 7500 real-time PCR system (Applied Biosystems, Foster City, CA). UL50 PCR samples contained 125 ng of DNA per reaction, adipsin PCR samples contained 10 ng of DNA per reaction, and all samples were analyzed in duplicate or triplicate. Standard curves for each PCR condition were carried out as described (153) to quantify the relative amount of viral DNA present in each sample relative to adipsin, using the $2^{(\Delta\Delta Ct)}$ method (154). One-way ANOVA was used to determine statistically significant differences in latent viral DNA loads.

Viral Explant-Induced Reactivation Studies: Thirty days post-infection, latently infected mice were sacrificed, each trigeminal ganglion was collected and cut into 8 approximately equal pieces, and all 8 pieces were cultured in a well in 24-well plates (155), with each well containing Vero cells in 1.5 ml of Vero cell medium. The cultures were sampled daily (150 µl per sample) up to 16 days for the presence of infectious virus by cytopathic effect on Vero cell monolayers (for KOS and Phos 1, 2, and 3 MR) or L7 cell monolayers (for 7134 and Phos 1, 2, and 3). Vero cell medium (300 µl/well) was added to each explant culture every other day. After taking samples on day 10 post-explantation, cultures were heat-shocked at 43º C for 3 h to provide an added stimulus for reactivation. Statistically significant differences for viral reactivation were determined using the Fisher's Exact Test. The mortality of mice ocularly infected with all viruses ranged from 0-19%.

2.3 Results

Mutations in Phos 1 and 2 impair viral replication in the eyes. We have previously shown that cluster mutations in one of three phosphorylated regions of ICP0 (Fig. 2.1) altered several properties of the protein and at least one ICP0 phosphorylation mutant (Phos 1) was impaired for viral replication in cell culture (90, 91). To determine whether the relative replication efficiencies of the Phos mutant viruses were altered *in vivo,* we used the mouse ocular model of HSV latency and reactivation. Initially, to examine acute replication at the periphery, CD-1 mice were infected with 2×10^5 PFU of virus per eye, and eye swabs were taken up to 9 days post-infection. Viral titers were determined by standard plaque assay. Viral replication for wild type HSV-1 (KOS) was

biphasic in the eye, peaking on days 1 and 5 post-infection, which has been observed in other studies (156, 157); this increase in ocular replication on day 5 is likely attributed to viral spread from the TG back to the eye (158). As shown in Fig. 2.2A, the replication of Phos 1 was reduced relative to KOS, on days 1 and 5 post-infection, with a 7-fold reduction (P=0.047) on day 1 and an 18-fold reduction (P=0.01) on day 5 (Fig. 2.2A). Interestingly, Phos 2 replication was only diminished 6-fold (P=0.039) on day 1 post-infection. In contrast to the first two mutants, the replication of Phos 3 was comparable to KOS on all days tested (Fig. 2.2A). In the case of Phos 1 and 2, their replication was not as reduced as that of the ICP0 null mutant, 7134, which reached a 64-fold decrease on day 5 post-infection. As expected, the marker-rescue (MR) viruses (Phos 1 MR, Phos 2 MR, and Phos 3 MR) replicated at levels similar to KOS (Fig. 2.2B). Collectively, these data indicate that the mutations in Phos 1 and 2 impair viral replication in the eyes.

Phos 1 and 2 are diminished for acute replication in the trigeminal ganglia (TG). To determine if the Phos mutations affected productive infection in the sensory neurons, viral replication of the Phos mutant viruses was monitored in the TG of ocularly infected mice. For TG titers on days 3 and 5 post-infection, Phos 1 replication was diminished 7-fold (P=0.01) and 16-fold (P=0.00009), respectively, compared to KOS (Fig. 2.3A). In the case of Phos 2, viral titers were reduced 18-fold day 3 post-infection (P=0.04) and 20-fold day 5 post-infection. (P=0.0002) (Fig. 2.3A). Decreases in the TG viral titers of Phos 1 and Phos 2, however, did not approach those of 7134, which were reduced as much as ~2000-fold days 3-7 post-infection. The acute replication of Phos

3, however, showed no significant difference when compared with the wild-type virus (Fig. 2.3A). Titers of the Phos MR viruses were comparable to KOS (Fig. 2.3B). Our results show that the Phos 1 and 2 mutations impair acute viral replication in the TG, whereas the Phos 3 mutation does not influence the viral growth in the TG.

The Phos mutants are not impaired in establishing a latent infection. To quantify the amount of viral DNA present in latently infected neurons, TG were collected 30 days post-infection and assayed for the presence of HSV-1 DNA by real time PCR. As shown in Fig. 2.4, the relative amounts of latent viral DNA present in TG were comparable to KOS for all of the Phos mutants. 7134 was the only virus that showed a significant reduction (11-fold, $P<0.05$) in viral DNA levels relative to KOS, and this reduction corresponded with previously published studies (28, 151). As expected, there were no appreciable differences in the latent viral genome loads among Phos 1 MR, Phos 2 MR, Phos 3 MR, and KOS.

Phos 1 and 2 show reduced efficiencies of explant-induced reactivation from latency. The efficiencies and kinetics of explant-induced reactivation from latency were established for all viral groups by collecting latently infected TG 30 days post-infection and culturing them *ex vivo*. Samples were examined daily for cytopathic effect, which indicates reactivation of virus from latent TG, and the total percentage of reactivating samples per virus was determined. In our initial set of studies, we examined the rates of reactivation for KOS, 7134, and the Phos mutants. KOS began to reactivate on day 3 post-explant (p.e.) at 66% and reached 100% reactivation by day

5 p.e. (Fig. 2.5A). Compared with KOS, Phos 1 and 2 reactivated at reduced rates of 33% (*P*=0.0003) and 50% (*P*=0.0009) respectively, on day 5 p.e. (Fig. 2.5A). Phos 3 reactivated efficiently achieving 85% (*P*=0.15) reactivation efficiency on day 5 p.e., which was comparable to KOS (Fig. 2.5A). 7134 reactivated on day 10 p.e. and after heat shock reached its highest levels (58.8%) on day 16 p.e. (Fig. 2.5A). Notably, the reactivation phenotypes of Phos 1 and 2 were intermediate to those of KOS and 7134. In a second set of studies, we examined the reactivation efficiencies of the Phos mutants relative to their MR viruses. The MR viruses behaved as expected, rapidly reactivating from days 2-5 p.e., eventually reaching efficiencies of 87-92% by day 5 p.e. (Fig. 2.5B). In contrast, Phos 1 reached a peak efficiency of 48% by day 11 p.e. (*P*=0.0002) and Phos 2 peaked at 68% by day 11 p.e. (*P*=0.01) (fig. 2.5B). Phos 3 reactivation rate resembled its MR virus with a rate of 85% on day 5 p.e., and reached 100% at the end of the study (Fig. 2.5B). These explant-induced reactivation studies show that the frequencies and kinetics of reactivation are altered for two of the Phos mutants, with Phos 1 showing the greatest deficiency followed by Phos 2.

2.4 Discussion

In this study, we have shown that two ICP0 phosphorylation site mutants are impaired for acute replication and explant-induced reactivation using the mouse ocular model of HSV infection. Specifically, Phos 1 and Phos 2 were impaired for acute ocular and neuronal replication and explant- induced reactivation from latency. Interestingly, all Phos mutants established latency at wild type levels, even though the levels of Phos 1 and 2 acute replication in the TG were intermediate to wild type HSV-1 and the ICP0

null mutant, 7134. Given that the degree of acute viral replication in the TG correlates with the establishment of latency (159, 160), the decreases in Phos 1 and 2 acute neuronal replication were, nonetheless, sufficient to allow these viruses to establish efficient latent infections. The life cycle of Phos 3 in mice mirrored wild type HSV-1 in our experiments, indicating that phosphorylation of residues in region III of ICP0 (Fig. 2.1A) is not required for productive infection and explant-induced reactivation in mice. Of the Phos mutants examined, Phos 1 was the only mutant to show replication deficiencies in cell culture (90, 91) and *in vivo*, as demonstrated in this report. Notably, Phos 2 had no obvious viral growth defects in cell culture (90, 91); however, decreased levels of viral replication and explant-induced reactivation observed with Phos 2 only became apparent when tested in the mouse ocular model, highlighting the importance of characterizing our mutants *in vivo*. While we tested only one viral dose in this study, it is possible that the replication, latency, and/or reactivation phenotypes of Phos 1, 2, and 3 may be greater or become evident when infecting mice at lower input doses (<2 x 10^5 PFU/eye). Overall, our results suggest that phosphorylation plays an important role in the biology of ICP0 to enhance HSV-1 acute replication *in vivo* and reactivation *ex vivo*. Studies are being conducted to identify the mechanisms responsible for the *in vivo* phenotypes of Phos 1 and Phos 2.

For Phos 1, its mutation lies in the proline-rich transactivation domain and is adjacent to the RING-finger domain of ICP0 (Fig. 2.1). We have previously shown that Phos 1 is impaired for ICP0's E3 ubiquitin ligase activity, dispersal of ND10-associated proteins, and transactivator function, in the absence of other viral factors, and has enhanced protein stability during viral infection (91). Thus, defects in Phos 1 auto-

ubiquitination and its ubiquitination of other cellular target proteins are likely contributors to its reduced levels of acute replication and reactivation. The delay and reduced efficiency of explant-induced reactivation observed with Phos 1 could also be linked to alterations in viral chromatinization and apoptosis. ICP0 is known to enhance viral gene expression during reactivation, which is associated with a decrease in the chromatinization of the viral genome (51, 53). Indeed, unlike wild-type strains of HSV-1, a RING-finger mutant of ICP0, which is impaired for ICP0's E3 ubiquitin ligase activity, was unable to induce viral gene expression in quiescently-infected cultures (78). Because Phos 1 is defective or diminished for ubiquitin conjugation, Phos 1 may not be as proficient as wild-type ICP0 in altering the structure of viral chromatin to promote viral transcription and replication. Lastly, ICP0 has been shown to ubiquitinate the tumor suppressor protein, p53 and limit apoptosis in virally-infected cells upon DNA damage (43). Thus, Phos 1 may not efficiently mediate the degradation of p53 or other anti-apoptotic targets during reactivation, potentially increasing apoptotic signaling, thereby reducing the levels and kinetics of reactivation. Clearly, the impairment of these activities does not impede Phos 1's ability to establish an efficient latent infection, which is similar to that of KOS.

The Phos 2 mutation, which is also located in a proline-rich transactivation domain of ICP0 (Fig. 2.1), has a minor defect in ocular shedding and is significantly defective in neuronal replication and explant-induced reactivation from latency. These results indicate that phosphorylated residues in region II of ICP0 are important for efficient viral replication, especially in sensory neurons. One potential explanation for Phos 2's attenuation *in vivo* is its ability to differentially affect the dissociation of cellular

proteins from ND10. The Phos 2 mutant form of ICP0 is unable to dissociate PML from ND10 but is able to dissociate Sp100 from ND10 in a cell type dependent manner (91). Thus, the inability of Phos 2 to alter the subcellular localization of PML, which is a part of the host's antiviral response, could diminish its viral replication. Related to its ND10-disrupting activity, ICP0 has been described to contain a SUMO interacting motif (SIM) in region II (161). A SIM facilitate interactions with SUMO isoforms or SUMO-conjugated proteins (reviewed in (162, 163)). A recent publication showed that phosphorylation of SIM domains in at least three cellular proteins, which includes PML, significantly enhances their interaction with SUMO isoforms (164). Thus, in the case of Phos 2, blocking phosphorylation in region II may impede this putative SUMO-binding activity, affecting its interaction with SUMO-conjugated proteins (such as PML) or specific SUMO isoforms. Indeed, in a preliminary experiment, when we incubated bacterially expressed GST-tagged SUMO-1 or SUMO-2 with Phos 2 infected Hep-2 cells, we noticed a significant reduction in the interaction between SUMO-2 and Phos 2 compared to the wild type interaction (Figure 2.6). Lastly, the Phos 2 mutation lies within a region that contains Src homology 3 (SH3) binding motifs, which allow for interaction with a subset of Src kinase family members and other SH3 containing proteins (165, 166). These kinases and factors play important roles in cell signaling. It has been suggested that the interaction between these factors and ICP0 perturbs normal cell signaling. Thus, Phos 2 might interrupt these interactions in neurons, impairing acute replication and explant-induced reactivation.

Of the three Phos mutants, only mutations in Phos 3 did not influence the replication of HSV-1 *in vivo*, similar to our previously published results in cell culture (90,

91). While mutations in Phos 3 appear to affect its subcellular localization and transactivating activity when expressed in transient transfection assays (90), our results indicate that the phenotypes observed with Phos 3 in cell-based assays do not impact acute infection and latency *in vivo*, and explant-induced reactivation. How phosphorylation of region III in ICP0 contributes to HSV replication remains to be determined.

It has been demonstrated that phosphorylation state of ICP0 is altered during the course of the viral replication cycle (89, 167-170), suggesting that differential phosphorylation of ICP0 might activate or inhibit one or more specific functions of this key viral regulatory protein. Consequently, the identity of specific phosphorylation sites in regions I and II of ICP0, the potential kinases that phosphorylate these sites, and their temporal regulation and roles in ICP0's functions will likely elucidate new mechanisms in the switch between the lytic and latent infections of HSV-1.

Contribution to this work:

I constructed isolates for Phos 3 virus and Phos 3MR virus, and I reproduced all the *in vivo* data including acute replication, latency (RT PCR assays were done by Adam Payless), and reactivation (originally done by the Schaffer lab) assays. I did the cell culture experiment shown in Figure 2.6. I analyzed all the new data and performed all statistical analyses.

2.5 **Figures and Figure legends**

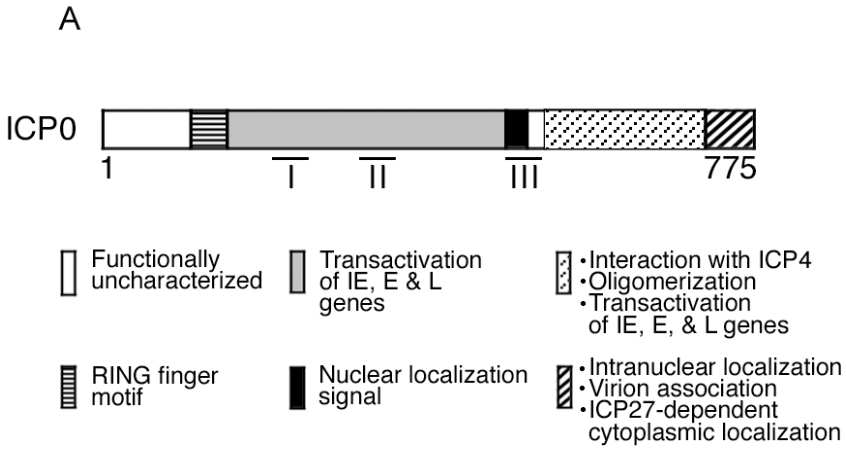

B

Region		Peptide Sequence	
I	222	ALSPTHPEPTTDEDDDDLDD/ADYVPPAPR	
1	222	AL<u>A</u>P<u>A</u>HPEP<u>AA</u>DEDDDDLDD/ADYVPPAPR	
II	356	ANNRDPIVISDSPPASPHRPPAAPMPGSAPR	
2	356	ANNRDPIVI<u>A</u>D<u>A</u>PPA<u>A</u>PHRPPAAPMPGSAPR	
III	505	RRGSGQENPSPQSTRPPLAPAGAK	528
3	505	RRG<u>A</u>GQENP<u>A</u>PQ<u>AA</u>RPPLAPAGAK	528

Figure 2.1. Location of ICP0 functional domains, phosphorylation sites, and phosphorylation site mutants. A. The 775 amino acids of ICP0 and the location of its major functional domains. The regions of ICP0 phosphorylation are indicated by bars below its structure. B. Location of the mutated phosphorylation sites for each Phos mutant. The serines (S) or threonines (T) identified within regions I, II, and III substitution into alanines (A) in Phos 1, Phos 2, and Phos 3 are underlined. Phos 1 is mutated at S224, T226, T231, and T232. Phos 2 is mutated at S365, S367, and S371.

Phos 3 is mutated at S508, S514, S517, and T518. This figure was modified from Davido, *et al.* (90) and Boutell, *et al.* (91).

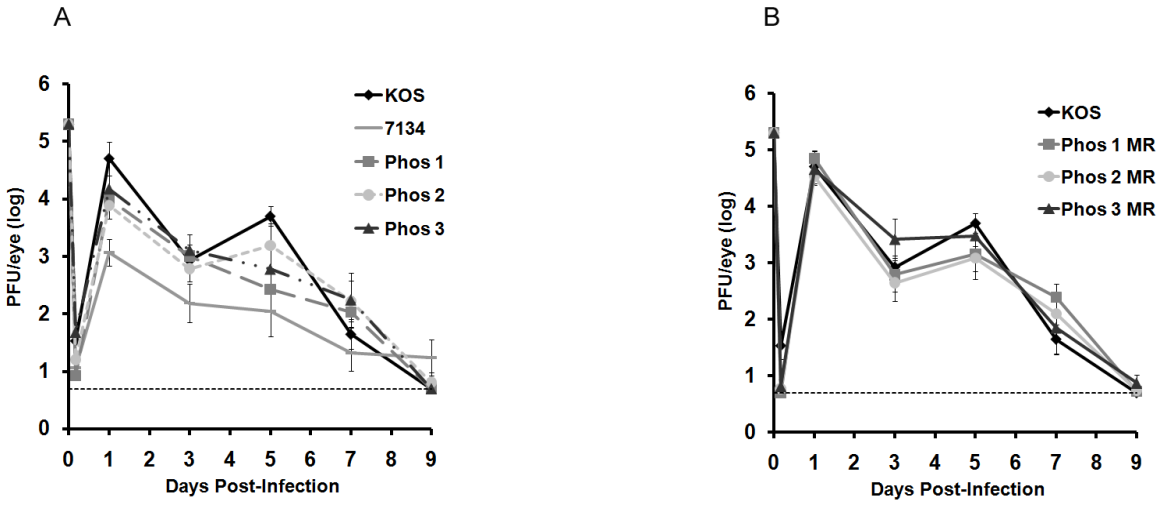

Figure 2.2. Viral titers of eye swabs taken at days 1, 3, 5, 7, and 9 post-infection. Mice were infected with 2 x 10^5 PFU per eye, and tear film was collected from each eye on the aforementioned days. The amount of infectious virus collected in each sample was determined by plaque assay. Results shown are logarithmic means (n=10 eyes per group), with the error bars indicating the standard error of the mean (SEM). The horizontal dotted lines represent the lower limit of detection. The experiments were performed simultaneously for all viral groups, but the results are separated for ease of interpretation. (A) KOS, 7134, Phos 1, Phos 2, and Phos 3 titers. (B) KOS and Phos 1 MR, Phos 2 MR, and Phos 3 MR titers.

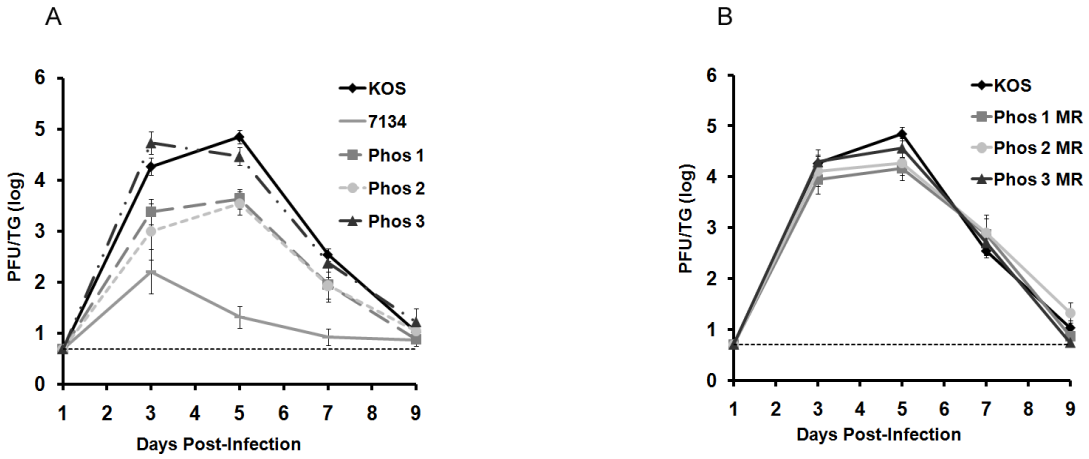

Figure 2.3. Viral titers of TG collected on days 1, 3, 5, 7, and 9 post-infection. Mice were infected with 2 x 10^5 PFU per eye, and TG were collected on the indicated days. TG were then homogenized and the amount of infectious virus present was determined by plaque assay. Results shown are logarithmic means (n=10 TG per group), with the error bars indicating the SEM. The horizontal dotted lines represent the lower limit of detection. The experiments were performed simultaneously for all groups, but the results are separated for ease of interpretation. (A) KOS, 7134, Phos 1, Phos 2, and Phos 3 titers. (B) KOS, Phos 1 MR, Phos 2 MR, and Phos 3 MR titers.

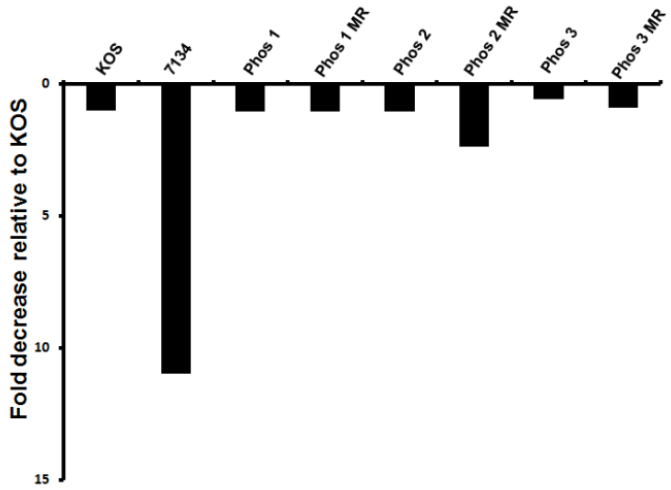

Figure 2.4. Viral genome loads in latent TG. Mice were infected with 2 x 10^5 PFU per eye, and TG were collected 30 days post-infection, with the exception of one set of KOS samples taken 21 days post-infection. DNA was extracted from latent TG, and the amount of HSV-1 DNA present was determined by real time PCR (n=4-10 TG per group). The graph shown is the relative fold reduction in viral DNA levels for each virus compared to KOS by the $2^{(\Delta\Delta Ct)}$ method for the basis of comparison, and the viral DNA level for KOS was given the value of 1. Mock-infected samples were below the limit of detection (data not shown).

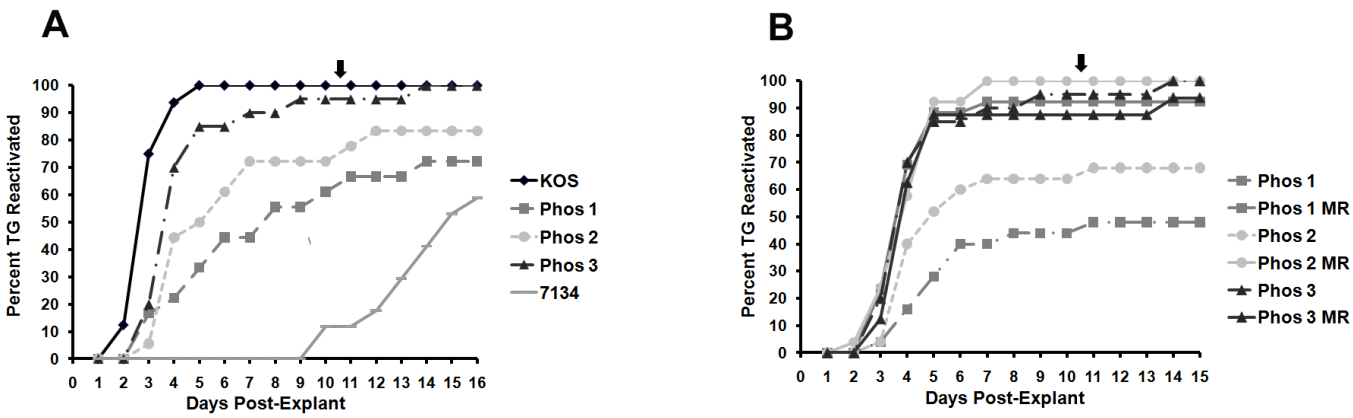

Figure 2.5. Virus explant-induced reactivation from latent TG**.** Mice were infected with 2 x 10^5 PFU per eye. On day 30 post-infection, TG were collected and explanted onto Vero cells. The time required for each virus to reactivate from the latent TG was determined by assaying the culture medium daily for the presence of infectious virus. Each time point represents the cumulative percentage of samples that reactivated (n=19-20 TG per group). Two groups of experiments are shown. (A) KOS, 7134, and phosphorylation site mutants. (B) Phosphorylation site mutants and MR viruses. The arrows at the top of both graphs indicate that after day 10, samples were heat shocked at 43ºC for 3h.

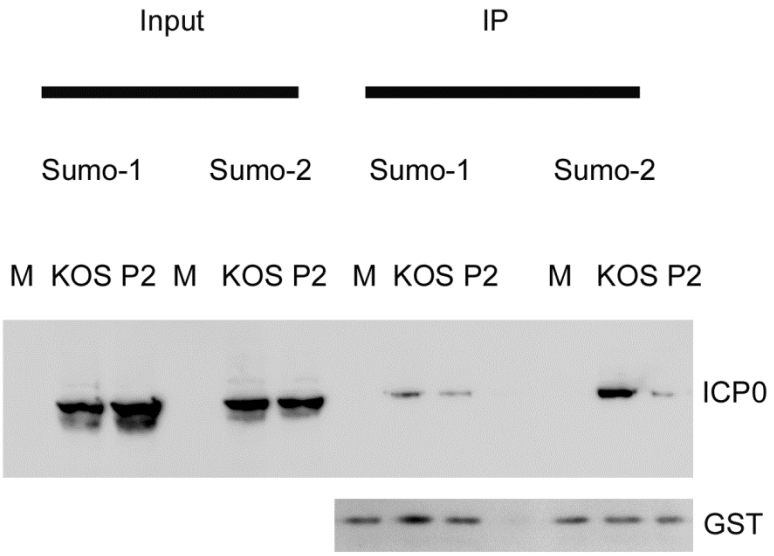

Figure 2.6. Phos 2 interaction with Sumo-1 and Sumo-2. Hep-2 cells were infected at MOI of 5 with KOS or Phos 2 for 6 hours. Extracts were incubated with 1 µg bacterially expressed, GST-tagged, Sumo-1 or Sumo-2 and Glutathione magnetic beads overnight. ICP0 levels pulled down with each sample were determined by western blot.

Chapter 3

N-terminal phosphorylation sites of herpes simplex virus 1 ICP0 differentially regulate its activities and enhance viral replication.

This chapter is modified from the published article: **J Virol. 2013 Feb;87(4):2109-19.**

Co-author

Thornton W. Thompson

3.1 Abstract

The herpes simplex virus type 1 (HSV-1) infected cell protein 0 (ICP0) is an immediate early phospho-protein that transactivates viral gene expression. Evidence suggests that phosphorylation regulates the functions of ICP0 and three regions (termed I, II, and III) in the protein are known to be phosphorylated. Mutation of the putative phosphorylation sites within region I, termed Phos 1, which lies in the N-terminal portion of ICP0, impairs the E3 Ub ligase and ND10-disrupting activities of ICP0 in cell culture and diminishes viral replication. To identify the specific phosphorylation site(s) or residues responsible for the phenotypes observed with Phos 1, Specifically, serine 224 and threonine 226, which have been shown to be phosphorylated in cell culture by tandem mass spectrometric analyses (M.C. Smith, W.S. Lane, and D.J. Davido, unpublished data; M.S. Chaurushiya, A. Aslanian, and M.D. Weitzman, unpublished data), as well as the potentially phosphorylated threonines 231 and 232. individual potentially phosphorylated residues within region I were

mutated to alanine (S224A, T226A, T231A, and T232A), as well as one double mutant (S224A/T226A). Tissue culture studies demonstrated that the S224A, S224A/T226A, T231A, and T232A mutations were unable to dissociate the cellular protein, PML, from ND10s, whereas the S224A/T226A mutation was defective in its ability to dissociate the cellular protein, Sp100, from ND10s. Additionally, S224A and S224A/T226A mutations were impaired for ICP0's transactivation activity. The S224A and S224A/T226A mutant forms were more stable than wild type ICP0, suggesting that their ability to auto-ubiquitinate was limited. Moreover, one ICP0 ubiquitination target, USP7, was also more stable after infection with these two mutants. Lastly, the S224A and S224A/T226A mutant viruses were reduced for viral replication in cell culture and *in vivo*. Our data indicate that of the four serines and threonines identified in region I, serine 224 has the greatest impact on ICP0 functions and viral replication. Interestingly, a combined mutation of this site with the threonine 226 site further reduced the transactivation activity of ICP0 and impaired its ability to dissociate Sp100 from ND10. Our results strongly suggest a model in which specific amino acids in region I can differentially regulate ICP0 activities that are subsequently required for efficient viral replication.

3.2 Materials and Methods

Cells and viruses. Vero, Hep-2, and HeLa cells were obtained from the American Type Culture Collection (ATCC) and grown in Dulbecco's modified Eagle's medium (DMEM) supplemented with 5% fetal bovine serum (FBS), 2 mM L-glutamine, 100 µg/ml penicillin, and 100 U/ml streptomycin as previously described (171). L7 cells, a Vero cell line stably transfected with HSV-1 ICP0 gene, were grown in the same medium as Vero cells and used to titer all the ICP0 mutant viruses, including the ICP0 null mutant, 7134 (32). The wild type strain KOS (passage 11) and marker rescue (MR) viruses were titered on Vero cells.

Construction of region I phosphorylation mutations. The plasmid, pAlter-1 + ICP0, was used to make all region I mutations using the pAlter Site-directed Mutagenesis Kit according to the manufacturer's protocol (Promega). Primers (IDT) used for the mutagenesis are: S224A (5'-GGGCCCTGTCGCCCAC-3'), T226A (5'-GTCGCCCACCCACCC-3'), S224A/T226A (5'-GGGCCCTGTCGCCCACCCACCC-3'), T231A (5'-CTGAGCCGGCCACGGA-3'), T232A (5'-CTGAGCCCACCGCGGA-3'), where the underlined text is the mutated codon or codons. Each primer was constructed such that a restriction enzyme site was created or eliminated. Mutations were identified by restriction enzyme digest analyses and were confirmed by DNA sequencing. The double mutant was made as these sites are phosphorylated in HSV-1 ICP0 and are conserved between HSV-1 and HSV-2 (M.C. Smith and D.J. Davido, unpublished data).

Generation of ICP0 phosphorylation mutant viruses. Region I mutant viruses were created by marker transfer. Briefly, Vero cells were plated on 60 mm dishes at $4x10^5$ cells per plate and 24 h later, cells were co-transfected with 1 µg of 7134 viral DNA and 2.5 µg of pAlter-1 expressing mutant forms of ICP0 digested with EcoR1 and HindIII. Transfections were done using Fugene 6 or Fugene HD (Roche) at a ratio of 3:1 (µl transfection reagent : µg DNA) according to the manufacturer's recommendations. Mutants were identified by blue/white selection. White plaques were picked and purified in at least 3 rounds in the presence of X-gal. Insertion of region I mutations were initially identified by PCR and restriction enzyme digestions (Figure 3.3) and confirmed by restriction enzyme digestion and Southern blot analyses. Marker rescue viruses, were generated by co-transfecting the mutant viral genomic DNA with pAlter-1+ ICP0 plasmid digested with EcoRI and HindIII. Rescuants were identified by PCR amplification of region I and restriction enzyme and/or Southern blot analyses. All the marker rescue viruses were plaque purified at least 3 times.

Immunofluorescence studies. i) ND10 and ICP0 staining. Hep-2 cells were plated on glass coverslips in 12-well plates for 24 h ($5x10^4$ per well). Cells were then transfected with 1 µg of plasmid DNA with Fugene 6 or Fugene HD using a 3:1 dilution ratio as described above. Sixteen to eighteen h post-transfection, cells were fixed with 5% formaldehyde and 2% sucrose in phosphate buffered saline (PBS) for 5 min, washed with PBS, and permeabilized in 0.5% NP-40 and 10% sucrose in PBS for 15 min at 4ºC. Cells were washed and blocked with PBS-FB (1% fetal bovine serum + 1% bovine serum albumin + 0.05% sodium azide) for 1 h at 37ºC. The primary antibodies

used were: ICP0 mouse monoclonal (11060 sc-53070, Santa Cruz Biotechnology) diluted 1:500 and PML rabbit polyclonal (A301-167A, Bethyl Laboratories) diluted 1:100 or Sp100 rabbit polyclonal (AB1380, Chemicon International) diluted1:100. Cells were incubated in primary antibodies for 30 min at 37ºC then washed at least 3 times. Each secondary antibody was added for 30 min at 37ºC. The secondary antibodies used were: donkey anti-rabbit dy594 (Jackson Immunoresearch, cat. no. 711-515-152) diluted 1:1000 and donkey anti-mouse dy488 (Jackson Immunoresearch, cat. no 715-295-151) diluted 1:1000. Cells were then washed 3 times with PBS, mounted with Prolonged Antifade Kit (Invitrogen) and examined with immunofluorescence microscopy (Nikon Eclipse TE-2000-U4).

ii) Subcellular localization of ICP0. HeLa and Hep-2 cells were infected at an MOI of 4 with KOS, 7134, Phos1, or each region I phosphorylation mutant for 4 and 8 h and fixed, permeabilized, and stained for ICP0 as described above.

iii) PIAS-1 localization. Hep-2 cells were plated ($5x10^4$ per well) on glass coverslips in a 24-well plate for 24 h. The cells were then transfected with 0.5 µg of plasmid DNA using Fugene HD at a 3:1 diluting ratio. Sixteen h post-transfection, samples were fixed with 4% formaldehyde in PBS for 15 min and blocked for 1 h in 5% normal goat serum and 0.2% Triton X-100 diluted in PBS. The ICP0 mouse monoclonal (11060, sc-53070, Santa Cruz Biotechnology) was diluted 1:500 and the PIAS-1 primary rabbit polyclonal antibody, kindly provided by Dr. Yoshi Azuma, was diluted 1:200 and the staining proceeded as described in the ND10 and ICP0 staining section.

Luciferase assays. Vero, Hep-2, or HeLa cells were plated at $5x10^4$ cells per well in 24 well-plates for 24 h. Cells were co-transfected with 50 ng of the reporter plasmid (VP16 promoter- luciferase construct) (172) alone or with 100 ng of pAlter-1 (empty plasmid), pAlter-1+ICP0, or pAlter-1 expressing each of region I site mutation and salmon sperm DNA was added for a total of 1 µg per well. Transfections were performed according to the manufacturer's protocol using Fugene HD or X-tremeGENE 9 at a ratio of 3:1. Cells were transfected for 48 h, wells were washed with PBS, and each well was then harvested in 100 µL of 1X passive lysis buffer (PLB; cat. no E1941, Promega) by rocking at room temperature for 15 min. Samples were harvested in a microfuge tube, vortexed for 30 sec, and briefly centrifuged at room temperature. Twenty micro liters of each sample was used for each assay. Luciferase assays were conducted using the Promega Luciferase Assay System 1000 (cat. no E4550): 100 µL of luciferase assay reagent was added per sample and a 2-sec delay before a10-sec read (Biotec Synergy, HT multicode microplate reader). Light units are displayed as percentages normalized to the wild type value and statistical analyses were performed using the Mann-Whitney *U* test.

Western blot and immunoprecipitation analyses. i) ICP0 stability: $1x10^5$ HeLa or Hep-2 cells were plated per well of a 12-well plate. Twenty four hours post-plating, cells were infected at an MOI of 2 for each virus in triplicate wells. Samples were harvested at 4, 6, and 8 h post-infection in 50 µL 1X Laemmeli buffer (100ºC) supplemented with 1X protease inhibitors (Leupeptin 1µg/mL, Aprotinin 1µg/mL, PMSF 1mM) and 1X phosphatase inhibitor cocktail (Sigma, cat. no. P2850) with the 6 and 8 h

samples treated with 100 μg/ml of cycloheximide (CHX) at the 4 h time point. Samples were heated at 95ºC for 5 min, vortexed, and centrifuged. Ten μl/sample was loaded on a 6% SDS PAGE gel, and ran at 120V for 1 h. Proteins were transferred to nitrocellulose membranes using a semidry transfer unit (GE Health Care, cat. no. TE77). Each membrane was blocked in 2% nonfat dried milk in TBS and 0.05% Tween-20 (TBS-T) for 1 h at room temperature and then cut into two parts to probe for ICP0 and β-Actin. To detect ICP0, the mouse monoclonal antibody 11060 (Santa Cruz Biotechnology, cat. no. sc-53070) was diluted 1:1000 in 2% nonfat dried milk in TBS-T overnight at 4ºC. β-Actin was detected with a rabbit polyclonal antibody (Santa Cruz Biotechnology, cat. no. sc-1616) diluted 1:1000 in 2% nonfat dried milk in TBS-T). The membranes were washed 3 times in TBS-T, and secondary antibodies were added: peroxidase conjugated goat antirabbit (Jackson Immunoresearch, cat. no 111-035-144) diluted 1:1000 and peroxidase conjugated goat antimouse (Jackson Immunoresearch cat. no. 205-035-108) diluted 1:1000 at room temperature for 1 h. Membranes were washed 3 times in TBS-T and developed using SuperSignal West Pico chemiluminescent substrate (Thermo Fisher Scientific, cat. no. 34087). Pictures captured with a Kodak 4000R image station, and the band intensities were measured by densitometry.

ii) USP-7 levels. Hep-2 or HeLa cells were infected and samples were processed as described in the ICP0 stability experiment except that the cells were not treated with cycloheximide. Samples were separated on 10% SDS PAGE gels and membranes were blocked in 5% BSA in TBS containing 0.1% Tween-20 for 1 h at room temperature. Probing for USP-7 was performed using the rabbit monoclonal antibody

HAUSP (Cell Signaling cat. no.4833) diluted 1:1000 in 5% BSA in TBS containing 0.1% Tween at 4º C overnight.

iii) PIAS-1 protein levels. Infection of Hep-2 or HeLa cells, sample processing, and transfer of proteins to membranes were performed as described in the USP-7 studies, except blocking was done in 5% milk in TBS with 0.1% Tween-20 for 1 h at room temperature. The PIAS-1 primary rabbit polyclonal antibody used was kindly provided by Dr. Yoshi Azuma and diluted at 1:500.

iv) USP-7 interaction studies. Hep-2 or HeLa cells were plated in 60 mm dishes at $5x10^5$ cells per plate. Twenty four hours later, the cells were mock infected or infected with KOS or Phos1 at MOI of 5 for 4 h. Plates were washed once with PBS and cells were harvested in 100 µL of a buffer containing 100 mM Tris-HcL pH 8, 50 mM NaCl, 10% glycerol, 20 mM β-mercaptoethanol, and 1% Nonidet P-40 with protease and phosphatase inhibitors as described above. Samples were sonicated at 100 W for 30 sec, incubated on ice for 30 min, and centrifuged at 15K rpm for 10 min at 4ºC. 50 µL protein G Dynabeads (Invitrogen, cat. no.77149610) were incubated, after aspirating the beads buffer, with 200 µL of PBS with 0.05% Tween-20 and 4 µL of an ICP0 rabbit polyclonal antibody (Pacific Immunology) by rotating for 1 h at room temperature. Beads bound to the antibody were washed with PBS and 0.05% Tween-20 and incubated with the sample lysates, rocking at 4ºC overnight. The beads were then washed twice with PBS-Tween and transferred to new tubes. Fifty microliters of 1X Laemmeli buffer (100ºC) with protease and phosphatase inhibitors were added to each sample and samples were boiled for 5 min, vortexed, boiled again, and vortexed twice for 1 min

each. Western blot analyses were performed as described in the USP-7 section and band intensities were measured by densitometry.

De novo viral replication assays. The assays were done as previously described (91). Briefly, Vero cells were plated in 12-well plates ($1x10^5$ cells per well) for 24 h. Two hours before transfection, fresh Vero cells medium was added to each well. Transfections were done in duplicate using 125 ng infectious viral DNA and 625 ng salmon sperm DNA per well, diluted in OPTIMEM (Invitrogen). Fugene 6 or Fugene HD was used for transfections at a 3:1 ratio (µl transfection reagent : µg DNA). The transfection mix was added to each well which contained 0.5 ml OPTIMEM for 5 h at 37ºC, and replaced with fresh Vero cells medium. Samples were harvested 48 h later. Wild type virus was titered on Vero cells, and all ICP0 mutants were titered on L7 cells. The replication of KOS was given 100% value and all the mutant viruses replication was normalized to KOS. Statistical analyses were performed using the Mann-Whitney *U* test.

Acute viral replication in trigeminal ganglia (TG) and eyes. Infections were done as previously published (92). Briefly, CD-1 outbred female mice (6-7 weeks old) were purchased from Charles Rivers Laboratories (Shrewsbury, MA) and cared for according to Guide for the Care and Use of Laboratory Animals (173). The protocol for using these mice is approved by the University of Kansas Institutional Animal Care and Use Committee. Mice were anesthetized by intraperitoneal injection of ketamine (75-100 mg/kg of body weight) and xylazine (10 mg/kg of body weight). Corneas of mice were scarified with a 26-gauge needle and infected with KOS, 7134, Phos 1, S224A, T226A, S224A/T226A, T231A, T232A, or each marker rescue virus at $2x10^5$ PFU of

virus per eye in 3-5 µl medium. To determine the acute titers in the trigeminal ganglia, the mice were euthanized by CO_2 asphyxiation at day 5 post-infection, and TG were removed and placed in microfuge tubes containing 500 µl 1% FBS growth medium and 100 µl of 1 mm glass beads. Samples were homogenized with a Mini-Beadbeater 8 (BioSpec). To determine the acute titers in the eyes, the mice eyes were swabbed using cotton tipped swabs at day 5 post-infection, and the swabs were placed in microfuge tubes containing 500 µl of 5% FBS growth medium. The wild type and rescuants viruses were titered on Vero cells, and all ICP0 mutant viruses were titered on L7 cells. Statistical analyses were performed using the Student's *t*-test.

3.3 **Results**

Dissociation of two ND10 components are differentially regulated by distinct phosphorylation sites in region I of ICP0. In a previous study, we showed that Phos 1 is unable to dissociate PML and Sp100 from ND10 relative to the wild type ICP0 in transient transfection assays (91). To determine which sites in the Phos 1 mutant form of ICP0 mediate the dissociation of these two proteins, we transfected Hep-2 cells with plasmids that express each region I phosphorylation site mutation or the double mutation (see Fig. 3.1), and the localization of ICP0 and PML or ICP0 and Sp100 were examined by immunofluorescence. As shown in Fig. 3.2A, wild type ICP0 did not colocalize with PML, dispersing it from ND10. Of the region I mutant forms that were examined, only T226A behaved like the wild type ICP0. As previously reported (91), Phos 1 was unable to efficiently dissociate PML from ND10 (Fig. 3.2A and 3.2C). All other region I phosphorylation site mutant forms of ICP0 (S224A, S224A/T226A,

T231A, and T232A) were as impaired as Phos 1 in dispersing PML from ND10. Of these mutants, T232A colocalized with PML, but PML staining appeared to be less intense than the mock transfected cells, indicating that this mutant form of ICP0 may retain a degree of PML dissociating activity. For Sp100, all region I phosphorylation site mutants were capable of dissociating Sp100 from ND10 similar to wild type ICP0, with the exception of the double mutant S224A/T226A, which behaved like Phos1 and was unable to disperse Sp100 (Fig. 3.2B and 3.2D). Our data show that different phosphorylation residues in region I of ICP0 regulate the dissociation of PML from ND10 compared to the dissociation of Sp100 in Hep-2 cells.

The transactivation activity of ICP0 is regulated by serine 224. A previous report indicated that Phos 1 is reduced for ICP0's transactivation activity in cell culture (90). To test the transactivation activity of region I phosphorylation site mutant forms of ICP0, Vero cells were transfected with HSV-1 VP16 promoter-luciferase reporter construct either alone or in combination with a plasmid expressing wild type ICP0 or each region I mutation. Forty-eight hours post-transfection, cells were lysed and assayed for luciferase activity, with the wild type ICP0 given a value of 100%. As expected, Phos 1 was unable to efficiently induce the expression of the VP16 promoter, and its induction ability was at 16% the level of the wild type ICP0 (P= 0.029) (Fig. 3.3). Of all the mutations that were tested, only S224A and S224A/T226A showed a significant decrease in transactivation activity, with levels that were 43% (P=0.02) and 17% (P=0.02) of wild type ICP0, respectively. T226A, T231A, and T232A were not impaired for inducing the VP16 promoter. Thus, S224 contributes to ICP0's

transactivation activity in combination with T226 to enable the maximal transactivation function of ICP0. Similar results were observed in two other cell lines (HeLa and Hep-2 cells, data not shown).

Construction of region I mutant viruses. In order to characterize the role region I sites have in the context of lytic replication, our region I mutations were introduced into the viral genomes as described in the Materials and Methods section, to create mutant viruses . The ICP0 null mutant, 7134, was used to make each mutant by marker transfer. For each mutant, a marker rescue virus was made to ensure that any observed phenotype is not due to secondary mutations in the viral genome. Insertion of restriction digestion sites when making each mutant helped us identify mutant viruses either by Southern blot analysis or PCR (Fig. 3.4).

De novo replication of S224A and S224A/T226A mutant viruses is reduced. Phos 1 was shown to be impaired for *de novo* replication in tissue culture (91), consequently, we wanted to determine which region I site(s) is/are responsible for this phenotype. To initially answer this question, we examined *de novo* replication of region I mutant viruses, as ICP0 significantly enhances viral replication in this assay (10). Vero cells were transfected with infectious viral DNA from wild type HSV-1 (strain KOS), the ICP0 null mutant, 7134, or each phosphorylation site mutant. In the absence of the HSV IE transactivator VP16, ICP0 transactivating activity is required for high levels of *de novo* replication (32). As expected, 7134 viral replication was reduced by 10^5-fold relative to KOS, similar to a previous report (91). Phos 1 mutant showed a decrease of

14-fold, and of region I phosphorylation site mutants, only S224A and S224A/T226A showed significant reductions of 9-fold and 16-fold, respectively (P=0.009 for both), relative to KOS (Table. 3.1). Taken together, our data indicate that the S224 is required for efficient *de novo* viral replication.

Serine 224 regulates the E3 ubiquitin ligase activity of ICP0. i) ICP0 protein stability. The Phos 1 mutant form of ICP0 was previously shown to have greater stability than wild type ICP0 (91), indicative of alterations in ICP0's E3 ubiquitin ligase activity. To identify sites in region I that contribute to Phos 1's stability, we infected HeLa cells in triplicate with KOS, Phos 1, or each region I mutant. After 4 hours of infection, one well was harvested, and the remaining two wells were blocked with the protein synthesis inhibitor, cycloheximide, for additional 2 and 4 hours and subsequently harvested. ICP0 and actin protein levels were examined by western blot. As shown in Fig. 3.5, Phos 1, S224A, and S224A/T226A were more stable than the wild type ICP0. The phenotype observed with these three mutants suggests that S224 controls the auto-ubiquitination of ICP0. Similar results were observed in Hep-2 cells (H. H. Mostafa and D. J. Davido, unpublished data).

ii) USP-7 levels. To confirm that mutations in Phos1, S224A, and S224A/T226A impaired ICP0's E3 ubiquitin ligase activity, we examined the protein levels of another target of ICP0 ubiquitination, USP-7. In this experiment, HeLa cells were mock infected or infected with KOS, 7134, Phos 1, S224A, or S224A/T226A for 4, 6, and 8 hours. The cells were then harvested, and the protein levels of USP-7, ICP0, and actin were determined by western blot. As was previously reported for wild type HSV-1 infections

(44), KOS infection resulted in a reduction in the USP-7 protein levels (Fig. 3.6). In contrast, USP-7 protein levels over time were comparable in mock, 7134, Phos 1, S224A, and S224A/T226A infected cells (Fig. 3.6). As it has been shown before that the interaction between ICP0 and USP-7 mediates stabilization of ICP0 early during lytic infection (85), we wanted to address the possibility that the higher stability of the Phos1 mutant form and/or the higher stability of USP-7 following Phos 1 infection may be due to alterations in the interaction between Phos 1 and USP-7. For this experiment, we took KOS- or Phos 1-infected cell extracts from HeLa cells 4 hours post-infection and determined the extent that USP-7 co-immunprecipitated with ICP0 in these extracts. When accounting for the amount of Phos 1 that was immunoprecipitated, our data show that Phos 1 pulled down USP-7 to similar extent as wild type ICP0 (Fig. 3.7). Consequently, this data does not support the hypothesis that an increase in Phos 1 stability is mediated by an increase in its interaction with USP-7. Similar results were obtained from Hep-2 cells (H. H. Mostafa and D. J. Davido, unpublished data). Taken together, our results support the conclusion that the three mutants: Phos 1, S224A, and S224A/T226A, have impaired E3 ubiquitin ligase activity and indicate that S224 regulates this activity of ICP0.

The subcellular localization of region I phosphorylation mutants is similar to the wild type ICP0: to examine the possibility that these mutant forms of ICP0 may be altered in their subcellular localization altering the activities of ICP0, HeLa and Hep-2 cells were infected with the KOS, Phos 1, and each of region I phosphorylation site mutants. The localization of ICP0 was determined at 4 and 8 hours post-infection. All

the mutants showed similar localization patterns to wild type ICP0 in the two cell lines tested, with primarily nuclear localization at 4 hours post-infection and both nuclear and cytoplasmic localization at 8 hours post-infection (Fig. 3.8).

Serine 224 is required for efficient acute viral replication in mice trigeminal ganglia (TG). We previously showed that Phos1 replication in the trigeminal ganglia during the acute phase of infection was significantly reduced relative to the wild type KOS, with the maximal decrease observed at day 5 post-infection (92). To test which residues in region I are required for efficient *in vivo* replication, CD-1 mice were infected with KOS, Phos1, each region I phosphorylation site mutant, and its marker rescue virus. Five days post-infection, mice were swabbed and then were sacrificed, TG were explanted, and the acute viral replication was monitored by standard plaque assay. Acute replication in the eyes on day 5 showed only a slight reduction in the acute replication of the S224A mutant (5-fold, P=0.005) and Phos 1 (11-fold, P=0.00012), whereas all the other region I mutants replicated to levels of wild type HSV-1 (H.H. Mostafa and D.J. Davido, unpublished data). For productive infection of the trigeminal ganglia, as expected, 7134 and Phos 1 were significantly reduced (650-fold, $P=1.2x10^{-18}$ and 11-fold, $P=2x10^{-6}$, respectively) in their replication relative to KOS (Fig. 3.9A). S224A and S224A/T226A replication were reduced by 48-fold ($P=1.9x10^{-11}$) and 15-fold ($P=1.8x10^{-8}$), respectively, whereas the replication of T226A, T231A, and T232A (Fig. 3.9A) and the marker rescue viruses (Fig. 3.9B) was similar to KOS. Our results demonstrate that S224 enhances productive infection in the TG of mice.

3.4 Discussion

Phosphorylation is a post-translational modification that regulates the activities of many viral proteins (174, 175). ICP0 has been shown to be heavily phosphorylated (88) and previous studies from our lab strongly support the hypothesis that phosphorylation regulates its activities (90-92). Because putative phosphorylation sites of Region I in ICP0 have been shown to play an important role in regulating its activities and viral replication, we performed mutagenesis of specific site or sites in this region to identify residues that are required for the activities of ICP0. Specifically, Region I has been shown to be phosphorylated at one or two residues (90), and it has been recently determined by our lab and other investigators that S224 and T226 sites are phosphorylated. Characterization of these mutations in the absence of other viral factors indicates that S224 phosphorylation is important for efficient PML dissociation from ND10 (Fig. 3.2A and 3.2C), and it appears that the phosphorylation of either S224 or T226 is sufficient for efficient Sp100 dissociation (Fig. 3.2B and 3.2D). Interestingly, T231 and T232 also play an important role in the dissociation of PML (Fig. 3.2A and 3.2C) but neither is required for Sp100 dissociation (Fig. 3.2B and 3.2D), suggesting a potential structural role for these residues in dissociating PML from ND10. S224 is also required for optimal levels of ICP0-mediated transactivation activity in luciferase reporter assays (Fig. 3.3). In the context of viral infections, we showed that the S224 is important for an efficient E3 ubiquitin ligase activity (Figs. 3.5 and 3.6), and for viral replication both in tissue culture (Table 3.1) and in mice trigeminal ganglia (Fig. 3.9A). Our data highlights that S224, which is in close proximity to the RING-finger motif of ICP0 (Fig. 3.1), as the residue in region I which has the major impact on ICP0's activities.

To understand the mechanism by which phosphorylation regulates ICP0's functions, particularly its E3 Ub ligase activity, we propose the hypothetical model shown in Figure 3.10. As a RING-finger-containing E3 ubiquitin ligase, ICP0 acts as a scaffold, binding both the E2 ubiquitin conjugating (Ubc) enzyme and it substrates, thereby facilitating the ubiquitin-chain transfer and conferring substrate specificity. Given that phosphorylation regulates the action of many E3 ubiquitin ligases, activating (176, 177) or inactivating them (178), it is possible that the E3 Ub ligase activity of ICP0 is regulated by phosphorylation, enhancing its contact with a particular substrate or E2 enzyme (Fig. 3.10A). Our data demonstrate that Phos 1 is not detectably altered in its interaction with USP-7 compared to wild type ICP0 (Fig. 3.7). Although this does not exclude the possibility that phosphorylation in region I can affect the binding of ICP0 to other target substrates, it suggests the other possibility that phosphorylation promotes ICP0's interaction with a particular E2 Ubc enzyme. In a preliminary experiment, we examined the colocalization between wild type ICP0 or Phos 1 with the E2 enzyme, UbcH5a. UbcH5a has been shown to be one of two E2 Ubcs of ICP0 that direct ubiquitination of selected ICP0 targets *in vitro* and in cell culture (43, 179, 180). Our initial results show that where there was extensive colocalization between wild type ICP0 and UbcH5a, whereas Phos 1 did not extensively colocalize with UbcH5a (Fig. 3.11). This suggests that Phos 1 may be impaired in its interaction with UbcH5a compared to the wild type ICP0. When we tested the colocalization of region I phosphorylation site mutations and UbcH5a, the S224A and the S224A/T226A mutants behaved like Phos 1 and showed reduced colocalization with the flag tagged UbcH5a (Fig 3.12A and B). This suggests that the S224 site might be required for an efficient

interaction with the E2 enzyme UbcH5a. Ongoing studies will determine the extent region I plays in facilitating ICP0's interaction with the E2 Ubc enzymes, such as UbcH5a and will specifically test the role of S224 site in facilitating such interaction. The increased stability of Phos 1 may also be attributed to alterations in its interactions with the E2 enzymes or the cellular E3 ubiquitin ligase, SIAH-1. In the latter case, the binding of SIAH-1 to ICP0 has been shown to decrease the stability of ICP0 (181). This raises the question of whether the Phos 1 mutant form of ICP0 is diminished for SIAH-1-binding, resulting in a more stable protein. This argument is supported by a recent publication showing that ICP0's binding to another cellular E3 ubiquitin ligase, RNF8, is dependent on ICP0 phosphorylation (182). Interestingly, the phosphorylation of ICP0 at an N-terminal residue specifically directed the degradation of RNF8, whereas the degradation of other ICP0 targets was unaffected. In addition, it is unclear whether ICP0 induces its own ubiquitination intramolecularly or intermolecularly, as it contains a dimerization domain and was shown to multimerize (183). Auto-ubiquitination has also been observed with the ICP0 orthologue from varicella zoster virus, ORF61 (37, 38, 72, 74-76). Thus, the relationship between phosphorylation and SIAH-1 binding and ICP0 auto-ubiquitination remain to be determined (Fig. 3.10B).

The impairment of PML and Sp100 dissociation was observed with Phos 1 and other region I phosphorylation site mutations in the absence of other viral factors in transient transfection assays (Fig. 3.2 and (91)) but not during the course of viral infection (H.H. Mostafa and D.J. Davido, unpublished data and (91)). These results indicate that other viral factors and/or the level of their expression likely compensate for region I Phosphorylation mutation's defect to dissociate these two ND10-associated

proteins, which is linked to their degradation. On the other hand, although it has been shown before that the dispersal of PML and Sp100 mediated by ICP0 is dependent on the E2 enzyme UbcH5a in cell culture (179), ICP0 was unable to ubiquitinate SUMOylated PML *in vitro* (180). This latter result suggests that other factors are required for the ubiquitination of PML, and potentially Sp100, mediated by ICP0. Our data show that the individual phosphorylation mutants differ in their regulation of PML versus Sp100. A similar result was observed in a previous study from our laboratory in which another ICP0 phosphorylation mutant, Phos 2, could dissociate Sp100 but not PML from ND10 (91) in transient transfection assays. For our region I mutant forms of ICP0, we hypothesize that distinct cellular factors regulate PML's dissociation compared to that of Sp100. In an attempt to determine what factors could potentially contribute to ICP0's directed PML dissociation, we looked at PIAS-1 staining pattern, protein levels, and interaction with ICP0 after transient transfection and infection. The E3 SUMO-ligase PIAS-1 has recently been shown to regulate the degradation of PML (184), and its loss results in increased PML stability. Our studies showed that the expression of wild type ICP0 or Phos 1 did not influence the staining of PIAS-1 in transient assays (Fig. 3.13A) or PIAS-1 protein levels during infection (Fig. 3.13B). We did not detect interactions between the ICP0 and PIAS-1 by co-immunoprecipitation assays (data not shown). We propose that the dissociation of PML directed by ICP0 is not dependent on interacting with PIAS-1.

Many questions remain as to how phosphorylation regulates the activities of ICP0. For example, how does phosphorylation of ICP0 differentially regulate its activities during acute infection *in vivo*? And what are the kinases that contribute to

ICP0's phosphorylation? Previous work has shown that the phosphorylation status of ICP0 is altered along the course of the viral replication (88, 168) and that its phosphorylation status is dependent on the viral kinase UL13 (185) and cellular cyclin-dependent kinases (cdks) (89). Ongoing work in our lab is aimed at identifying the kinases that phosphorylate and control the activities of ICP0

Contribution to this work:

I performed and analyzed the data for all of the experiments presented in this chapter, constructed the T226A and T226A MR viruses, and generated second isolates for most region I phosphorylation mutants.

3.6 **Tables**

Virus	Viral titer as a relative % to KOS	Fold difference relative to KOS
KOS	100	
7134	0.0002	$\downarrow 5x10^5$
Phos 1	6.9	↓14.5
S224A	11.1	↓9.05
T226A	79.9	↓1.25
S224A/T226A	6.2	↓16.1
T231A	128.2	↑0.78
T232A	130.3	↑0.77

Table 3.1. *De novo* replication of region I mutants. Vero cells were transfected with infectious viral DNA for Wt HSV-1 (strain KOS), an ICP0 null mutant (7134), and region I mutants. At 48 h post-transfection, cells were harvested and titered by standard plaque assay. The data are shown both as the percentage of replication relative to the wild type KOS and as a fold reduction relative to KOS. Mutants that were significantly reduced for viral replication relative to KOS were tested with two independent viral DNA preparations. The experiment was repeated five times, and the data presented are the mean values.

3.7 **Figures and Figure legends**

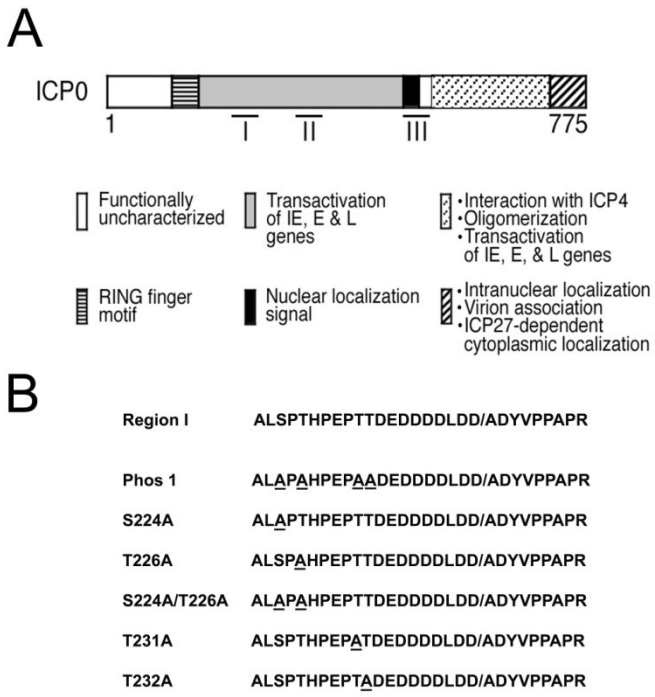

Figure 3.1. Region I phosphorylation site mutations. (A) ICP0 functional domains with three characterized phosphorylation regions (I, II, and III), adapted from (90) (B) The amino acid sequence of region I and each region I phosphorylation site mutant. All mutated residues are underlined. The slash mark in region I indicates the boundary between the second and third exons of ICP0.

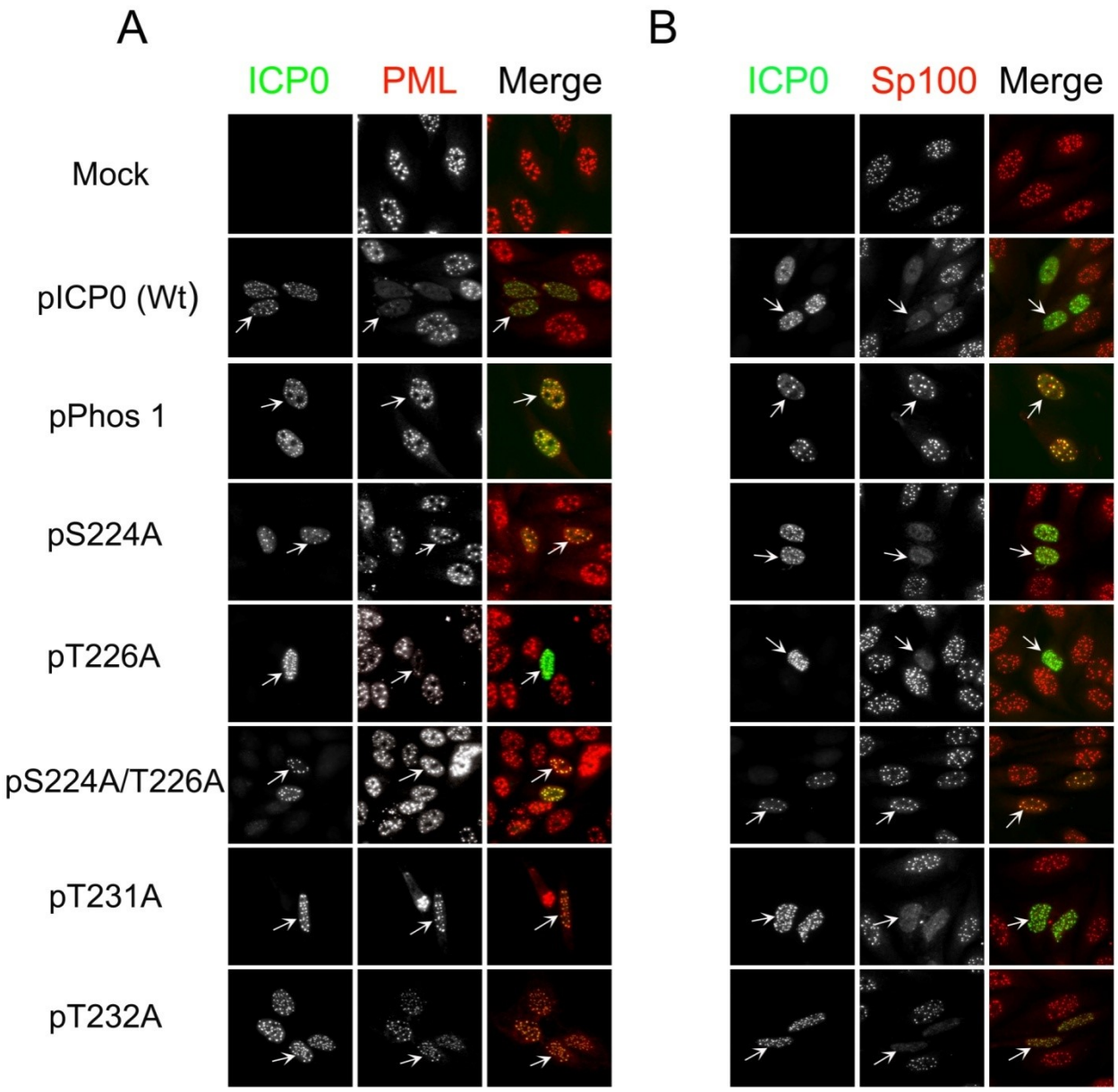
A
ICP0
PML
Merge
Mock
pICP0 (Wt)
pPhos 1
pS224A
pT226A
pS224A/T226A
pT231A
pT232A
B
ICP0
Sp100
Merge

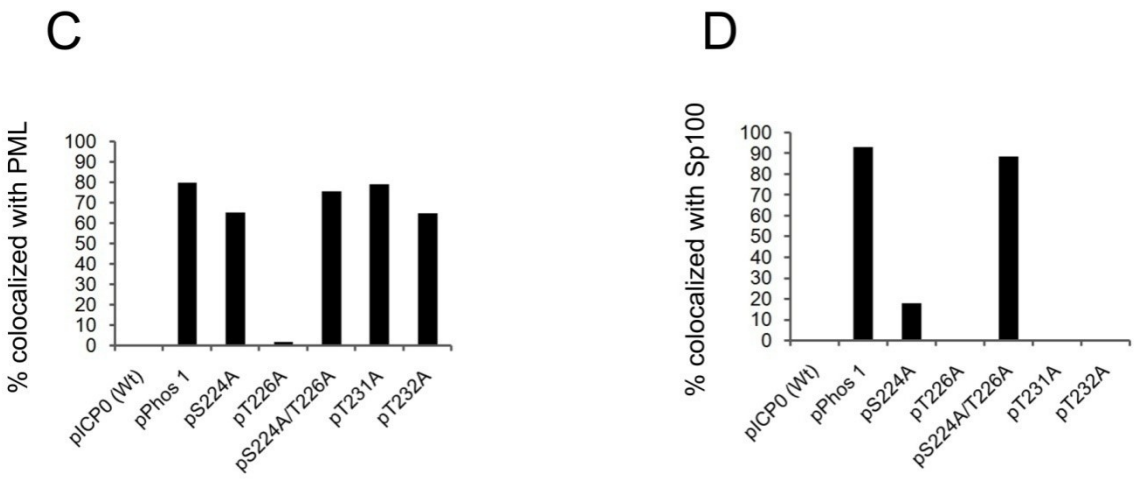

Figure 3.2. Region I phosphorylation site mutations and ND10 staining. A) Localization of PML and ICP0 or region I phosphorylation site mutant forms of ICP0. Hep-2 cells were transfected with plasmids expressing wild type (Wt) ICP0, Phos 1, each region I phosphorylation site mutation, and the double site mutation. Sixteen hours post-transfection, the cells were fixed and stained for ICP0 and PML and examined by fluorescence microscopy. B) Localization of Sp100 and ICP0 or region I mutant forms of ICP0. Hep-2 cells were transfected with plasmids expressing Wt ICP0, Phos 1, each region I phosphorylation site mutation, and the double site mutation. Sixteen hours post-transfection, the cells were fixed and stained for ICP0 and Sp100 and examined by fluorescence microscopy. . C) Graph indicating the percent of ICP0-expressing cells that colocalized with PML. D) Graph indicating the percent of ICP0-expressing cells that colocalized with Sp100. In both experiments, at least 100 ICP0-expressing cells were examined for each mutant form of ICP0.

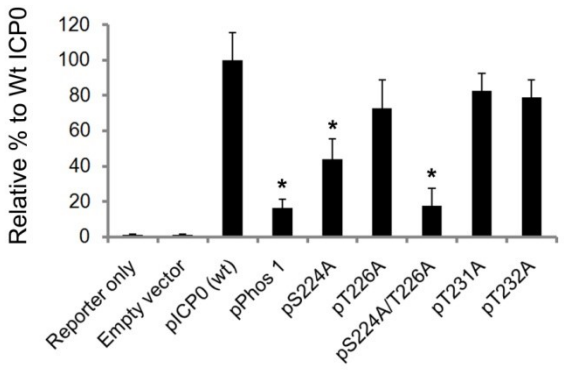

Figure 3.3. Transactivation activity of region I phosphorylation site mutations. Vero cells were transfected with an HSV-1 reporter plasmid (50 ng, pGL3-VP16) and a plasmid expressing Wt ICP0, Phos1, each of region I phosphorylation site mutation, or the double site mutation for 48 hours. Luciferase assays of cell extracts were performed to monitor ICP0's transactivating activity. * Mann-Whitney *U* test; $P < 0.05$. The error bars indicate the standard error of the mean (SEM) for all samples.

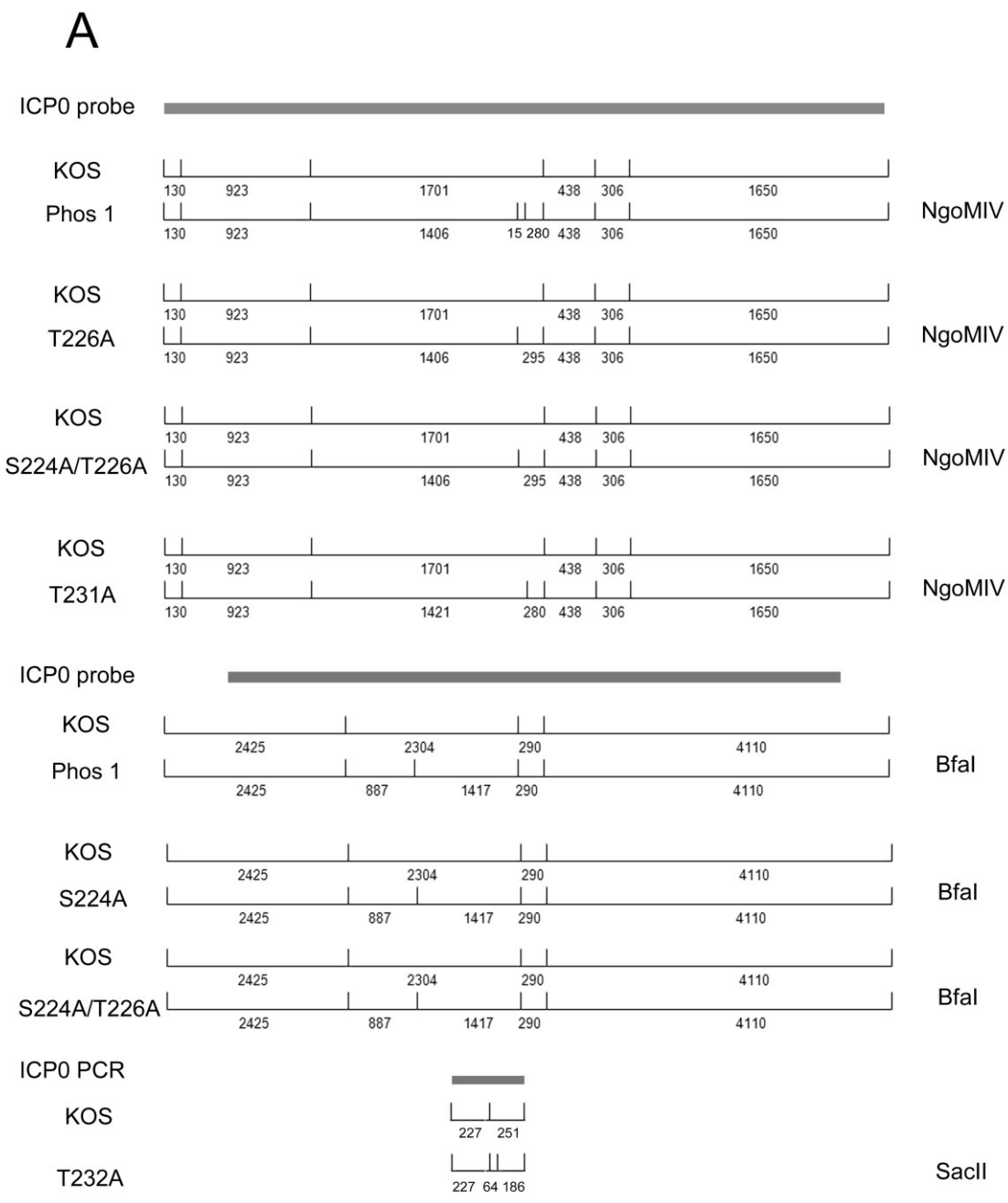
A
ICP0 probe
KOS
130 923 1701 438 306 1650
Phos 1
130 923 1406 15 280 438 306 1650
NgoMIV
KOS
130 923 1701 438 306 1650
T226A
130 923 1406 295 438 306 1650
NgoMIV
KOS
130 923 1701 438 306 1650
S224A/T226A
130 923 1406 295 438 306 1650
NgoMIV
KOS
130 923 1701 438 306 1650
T231A
130 923 1421 280 438 306 1650
NgoMIV
ICP0 probe
KOS
2425 2304 290 4110
Phos 1
2425 887 1417 290 4110
BfaI
KOS
2425 2304 290 4110
S224A
2425 887 1417 290 4110
BfaI
KOS
2425 2304 290 4110
S224A/T226A
2425 887 1417 290 4110
BfaI
ICP0 PCR
KOS
227 251
T232A
227 64 186
SacII
B
Kb
1 2 3 4 5 6 7 8 9
5
3
2
1.5
1
C
bp
1 2
300
200
100

Figure 3.4. Construction of region I ICP0 phosphorylation mutant viruses. Region I phosphorylation mutant viruses were constructed by marker transfer as described in the Materials and Methods section. A) The restriction enzyme digestion pattern with the fragment lengths (shown as base pairs) of KOS and region I phosphorylation mutants. Note that S224A/T226A contains both BfaI and NgoMIV sites. The restriction pattern shown for S232A mutant is from a PCR product. B) Southern blot, lanes 1-5, in order, are KOS, Phos 1, T226A, S224A/T226A, and T231A cut with NgoMIV. Lanes 6-9, in order, are KOS, Phos 1, S224A, and S224A/T226A cut with BfaI. C) 12% polyacrylamide gel of KOS (lane 1) and T232A (lane 2) PCR products digested with SacII.

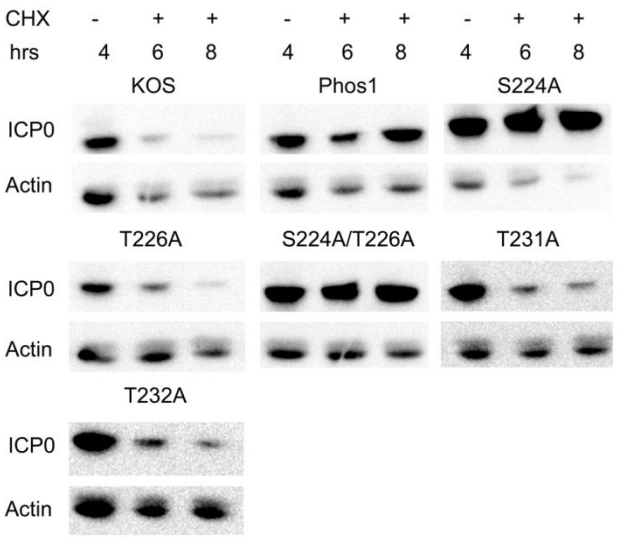

Figure 3.5. ICP0 stability of region I phosphorylation site mutants. HeLa cells were infected at an MOI of 2 with the indicated virus. Four hours post-infection, cells were harvested, and duplicate samples were treated with cycloheximide (CHX, 100 µg/ml) and harvested at 6 and 8 hours post-infection. ICP0 and actin levels were determined by western blot analyses.

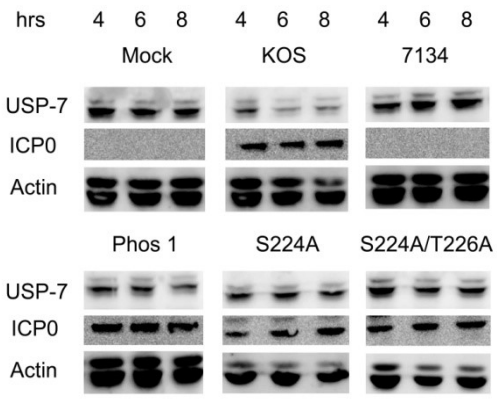

Figure 3.6. USP-7 degradation by region I phosphorylation site mutants. HeLa cells were mock infected or infected at an MOI of 2 with KOS, 7134, Phos 1, S224A, and S224A/T226A viruses for 4, 6, and 8 hours. ICP0, USP-7, and actin protein levels were determined by western blot analyses.

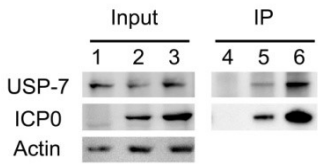

Figure 3.7. Interaction of ICP0 and Phos 1 with USP-7. HeLa cells were mock infected (lanes 1 and 4), infected with KOS (lanes 2 and 5), or Phos 1 (lanes 3 and 6). Four hours post-infection, ICP0 was immuno-precipitated, and the levels of ICP0 and USP-7 were analyzed by western blot.

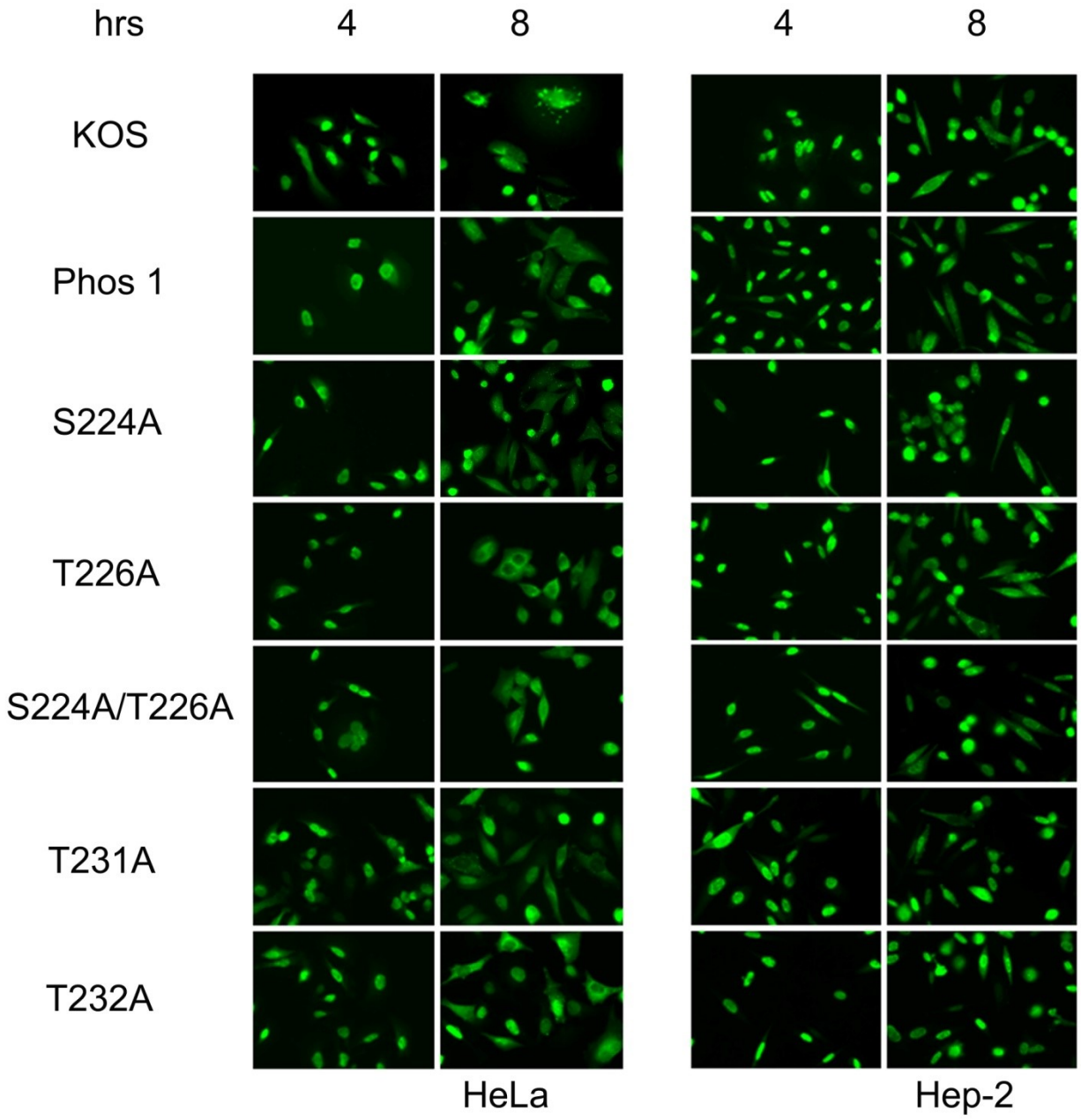

Figure 3.8.The subcellular localization of region I phosphorylation site mutants' ICP0 protein. HeLa and Hep-2 cells were infected with KOS or each region I phosphorylation mutant for 4 and 8 hours. The cells were fixed, stained for ICP0, and examined by fluorescence microscopy.

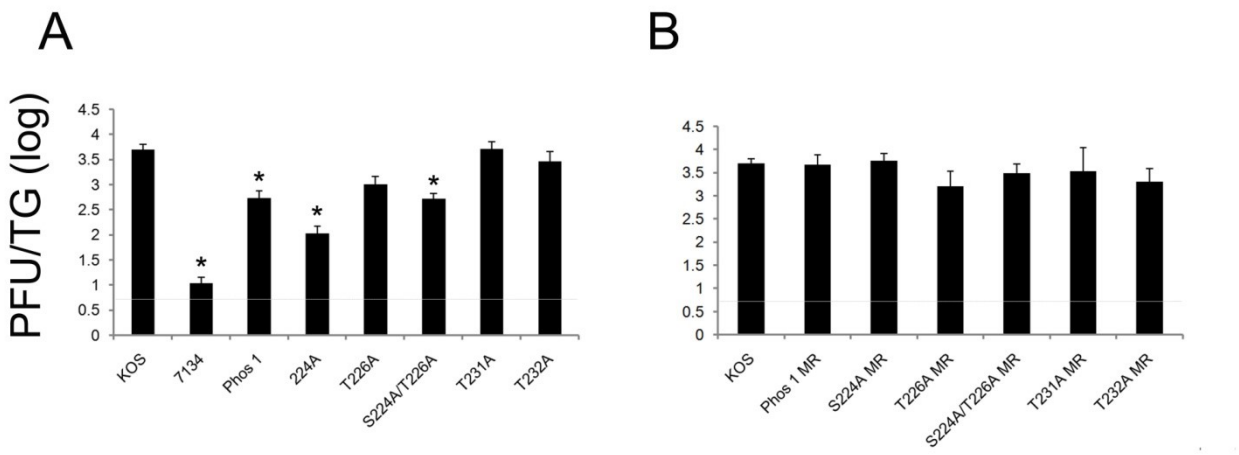

Figure 3.9. Acute replication of region I phosphorylation site mutants in trigeminal ganglia (TG) of mice at day 5 post-infection. CD-1 mice were infected with 2 x 10^5 PFU per eye. Five days post-infection, mice were sacrificed, and TG were removed and homogenized, and viral titers were determined by standard plaque assays. A) Replication of region I phosphorylation site mutants. B) Replication of region I phosphorylation mutants marker rescue viruses. * Student's *t* test P< 0.05. Error bars represent the SEM. The dashed line is the minimum limit of detection. *n*=8 mice/virus.

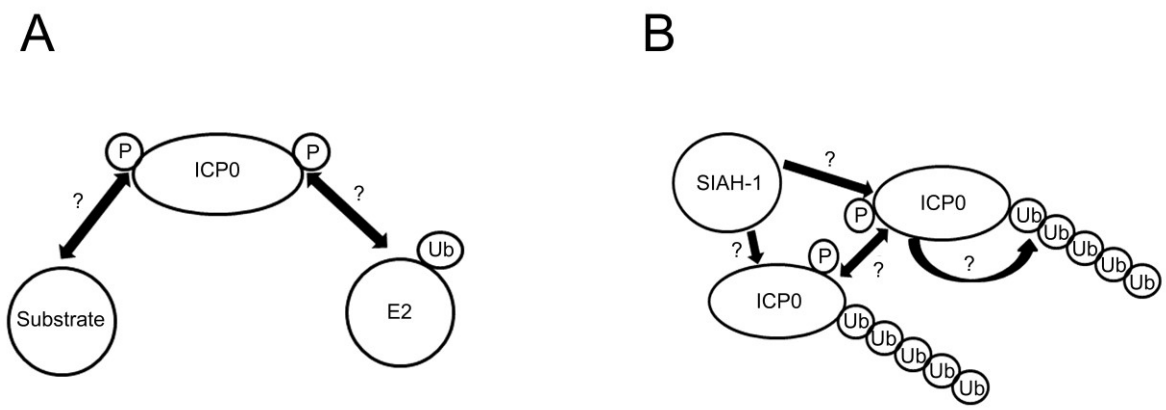

Figure 3.10. Hypothetical Models of how ICP0's E3 ubiquitin ligase activity is controlled by phosphorylation. A) Phosphorylation can either regulate ICP0's interaction with a target substrate or an E2 ubiquitin (Ub)-conjugating enzyme. B) ICP0's ubiquitination is regulated by phosphorylation that enhances the intra-molecular or inter-molecular auto-ubiquitination or binding to cellular E3 ubiquitin ligases, such as SIAH-1.

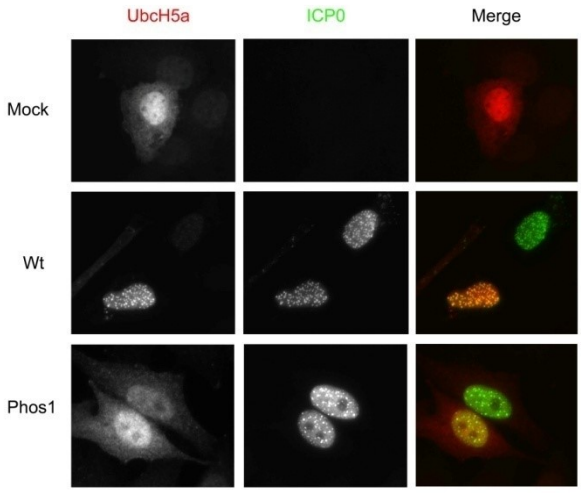

Figure 3.11. colocalization of ICP0 and Phos 1 with UbcH5a. Hep-2 cells were transfected with a flag tagged UbcH5a expressing plasmid and mock or co-transfected with a plasmid expressing wt ICP0 or Phos 1 . 24 hours post transfection, cells were fixed and stained for ICP0 and UbcH5a and examined by fluorescence microscopy. Around 50 cells expressing both ICP0 and UbcH5a were examined for both wt ICP0 and Phos 1 transfected cells.

A

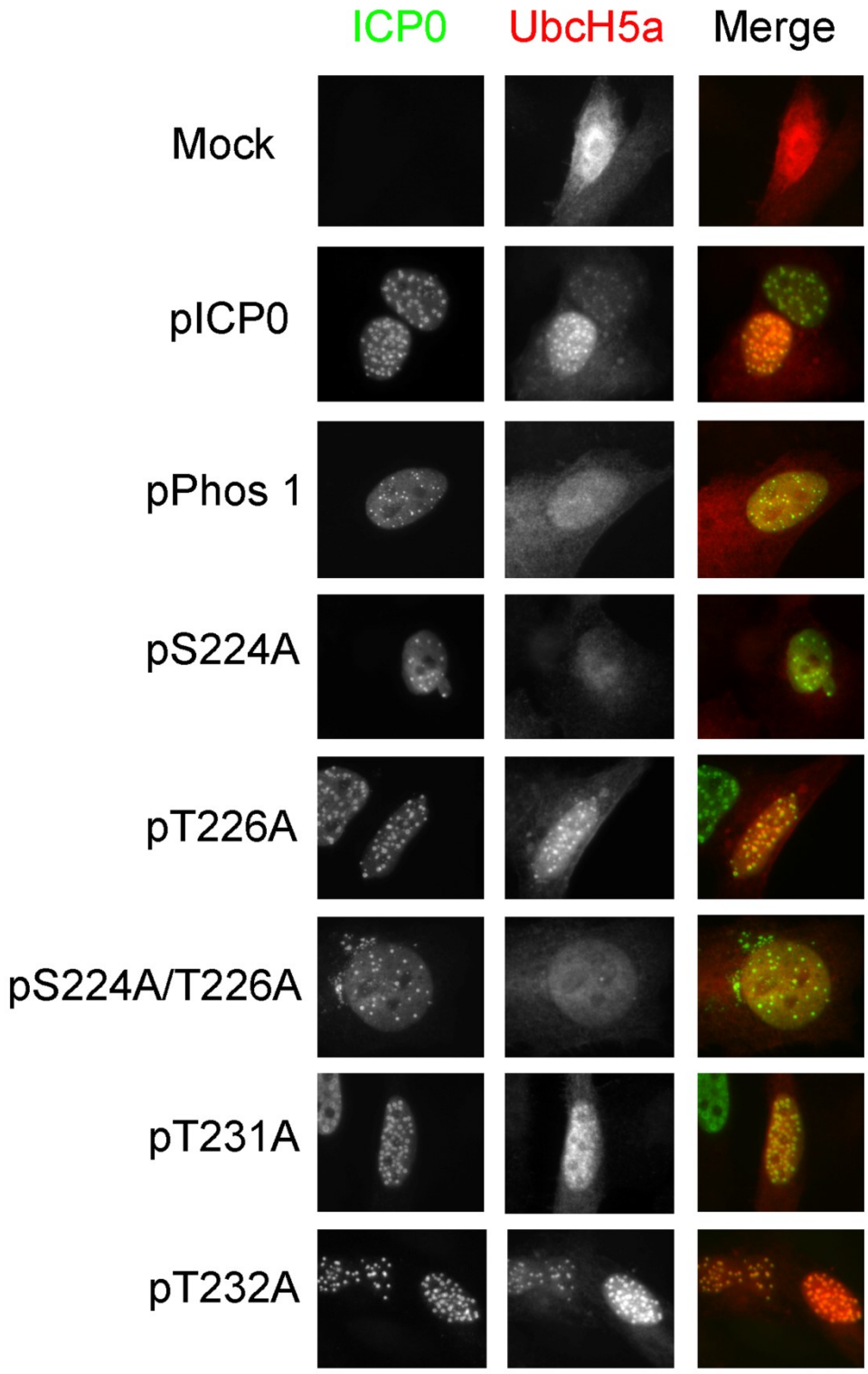
ICP0
UbcH5a
Merge
Mock
pICP0
pPhos 1
pS224A
pT226A
pS224A/T226A
pT231A
pT232A

B

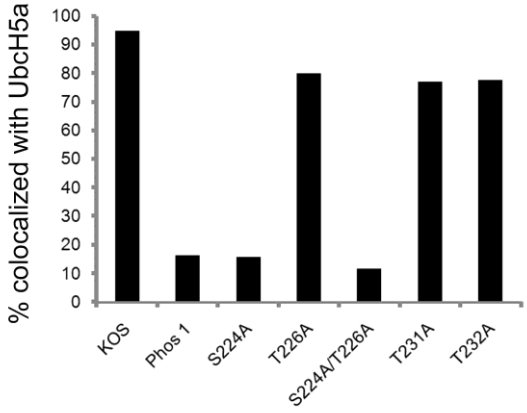

Figure 3.12. A) Region I phosphorylation site mutations and UbcH5a staining. Hep-2 cells were transfected with a flag tagged UbcH5a expressing plasmid and mock or co-transfected with a plasmid expressing wt ICP0, Phos 1, or each region I phosphorylation site mutation . 24 hours post transfection, cells were fixed and stained for ICP0 and UbcH5a and examined by fluorescence microscopy. B) Graph indicating the percent of ICP0-expressing cells that colocalized with UbcH5. Around 30 ICP0- and UbcH5a- coexpressing cells were examined for each mutant form of ICP0.

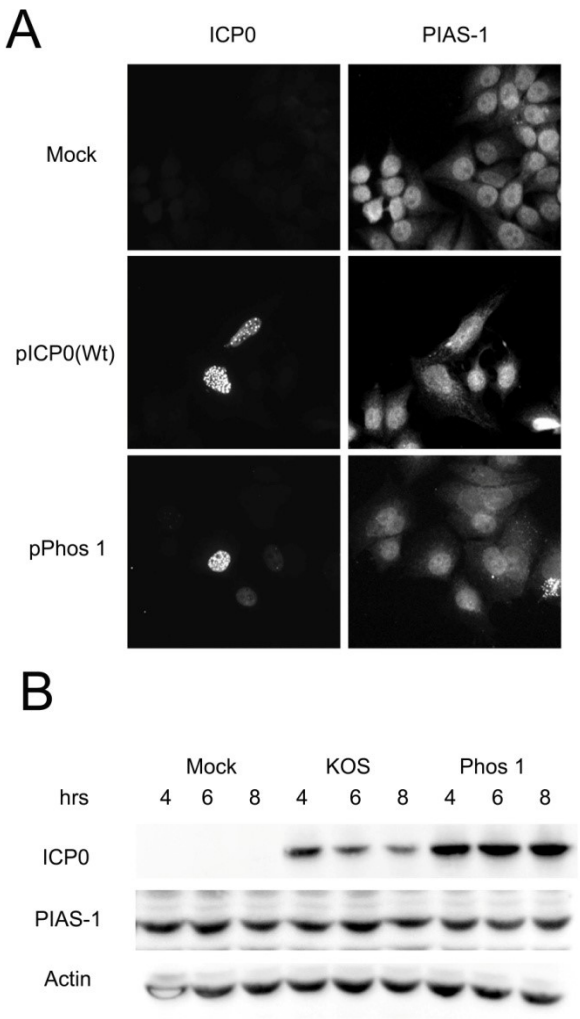

Figure 3.13. Localization of ICP0 with PIAS-1 and the effect of KOS and Phos 1 viral infection on PIAS-1 protein levels. A) Hep-2 cells were mock transfected or transfected with plasmids expressing Wt ICP0 and Phos 1. Sixteen hours post-transfection the cells were fixed and stained for ICP0 and PIAS-1 and examined by fluorescence microscopy, B) Hep-2 cells were mock infected or infected with KOS and Phos 1 at an MOI of 2 for 4, 6, and 8 hours. ICP0, PIAS-1, and actin protein levels were determined by western blot analyses

Chapter 4

Two Amino Acid Substitutions in Herpes Simplex Virus 1 ICP6 Impair Acute Viral Replication in Mice, Limiting The Establishment of Latency and Explant-Induced Reactivation.

Co-authors

Thornton W. Thompson, Steve D. Haenchen, Joshua G. Hilliard, Stuart J. Macdonald, Lynda A. Morrison

4.1. Abstract

In the process of generating HSV-1 phosphorylation mutants in the viral regulatory gene, infected cell protein 0 (ICP0), we also isolated a Phos 3 (refer to chapter 2) phosphorylation mutant which we termed KOS neuro-attenuated (KOS-NA) that was severely impaired for acute replication in the eyes and trigeminal ganglia (TG) of mice, significantly defective in establishing a latent infection, and reactivated poorly from explanted TG. Given the severe attenuation of KOS-NA relative to Phos 3 in mice, we hypothesized that KOS-NA contained a secondary set of mutations in one or more key viral genes that regulate HSV-1 pathogenesis. Notably, we postulated that these secondary mutations will provide insights into HSV-1 pathogenesis and would be useful in developing therapeutic interventions against HSV-1 (e.g., vaccine). To understand the genetic basis for KOS-NA's *in vivo* phenotypes, we sequenced its genome relative to its wild type parental virus, strain KOS (93). While we discovered two set of nonsynonymous mutations in the ICP4 and gI genes of the KOS-NA genome, we also identified two nonsynonmyous mutations (aa 393, L to P and aa 950, R to H), in the

UL39 gene, which encodes the large subunit of ribonucleatide reductase, also known as ICP6. ICP6 is a part of an enzyme complex that converts ribonucleotides to deoxyribonucleotides (94, 95). Although this gene is not essential for viral growth and replication in dividing cell lines, it is important for viral replication in quiescent cells such as neurons (96, 97), and several published studies have shown that *UL39* mutants are severely impaired for viral replication, establishment of latency, and/or reactivation in murine models of HSV-1 replication (98, 99). Given the parallels between the *in vivo* replication phenotypes of published *UL39* mutants and KOS-NA, we proposed that the two mutated codons in *UL39* of KOS-NA are responsible for its attenuated phenotypes.

To test this possibility, we rescued the UL39 mutated gene within the KOS-NA genome with a wild type copy of *UL39* (KOS-NAR), and we independently introduced the mutated copy of the *UL39* from the KOS-NA genome into the wild type KOS genome (UL39 L393P/R950H). The acute replication of both viruses was examined in eyes and TG of mice. Results from these experiments indicate that aa 393 and 950 of ICP6 are essential for high levels of acute replication in the eyes and TG of CD-1 mice, which facilitates the establishment of an efficient latent infection.

4.2. Materials and Methods

Cell Lines and Viruses. Vero cells and L7 (ICP0-containing Vero cells) were cultured in Dulbecco's modified Eagle's medium (DMEM) supplemented with 5% fetal bovine serum (FBS), 100 µg/ml penicillin, 100 units/ml streptomycin, and 2mM L-Glutamine. The wild-type HSV-1 strain KOS, 7134 (an ICP0-null mutant virus), KOS-NA, KOS-NA marker rescue (MR), UL39 L393P/R950H, and HrR3 R viruses were propagated and titered as previously described (186, 187).

High throughput sequencing of KOS-NA genome: We characterized the secondary mutations in the KOS-NA viral genome via whole genome sequencing as previously described for the wild type strain KOS (188). Briefly, genomic DNA from the strain was isolated from infected Vero cells, and used to construct a standard Illumina library. Following sequencing, the raw unpaired 42-bp reads were passed through the SolexaQA perlscripts to remove low quality reads (189), and aligned against both the *Rhesus macaque* and human genomes using Bowtie (190) to eliminate any reads derived from the Vero cell host. The remaining high-quality reads were *de novo* assembled with Velvet (191), and contigs >100-bp were assembled against the reference HSV-1 strain 17 syn+ genome using Seqman pro (DNASTAR, Inc.). The final KOS-NA genome is 152,011-bp, has 13 shorts gaps totalling 1,582-bp exclusively at variable number tandem repeat (VNTR) regions, and was sequenced to an average per-bp coverage of 3,104X.

We transferred annotation from the reference genome strain 17 syn+ using RATT (192), and confirmed the final KOS-NA annotation manually. To identify and

characterize nucleotide differences between KOS and KOS-NA we aligned the genomes using FSA (193) and applied a custom R script [www.r-project.org]. We identified 34 SNPs discriminating the strains, including 17 nonsynonymous changes residing in six genes, and 11 short (1-4bp) insertion-deletion events, all present outside of coding regions.

Construction of UL39 mutant and rescue viruses: KOS-NA contains mutations in ICP0 phosphorylation sites and was constructed as previously described in (86, 91, 92). To generate The UL39 L393P/R950H mutant, The UL39 gene was cloned out of the KOS-NA viral genome using BglII and KpnI sites and ligated into pSP72 using the same sites (pSP72:UL39). Vero cells were plated on 60 mm dishes at $4x10^5$ cells per plate. Twenty-four h post-plating, cells were co-transfected with 1 µg of viral DNA from HrR3 (96), which contains a *lacZ* insertion in *UL39*, and 2.5 µg pSP72:UL39 plasmid digested with BglII and KpnI. Transfections were performed using Fugene HD (Roche) at a ratio of 3:1 (µl of transfection reagent to µg of DNA) based on manufacturer recommendations. Mutants were identified by blue/white selection in the presence of X-gal. White plaques were isolated, and viral isolates containing the two mutated sites were screened with the PCR amplification refractory mutation system (ARMS) technique using the following primers: codon 393 site; WT (L393) primer (5'-CTGGACGTTCCTCCGGTACT -3'), P393mutant primer (5'-CTGGACGTTCCTCCGGTACC -3'), common primer (5'-TGGAAGACGGACTCCATGTAG -3');codon 950 site; WT (R950) primer (5'-CGTGTTTCATCATGCTCTAGC-3'), H950 mutant primer (5'-

CGTGTTTCATCATGCTCTAGT-3'), and common primer (5'-TGCACACGGCCTGCCTGAAGCT-3'). Candidates were confirmed by DNA sequencing. Correct insertion of the gene into the viral genome was confirmed by XhoI digest followed by Southern blot analysis (Data not shown). The KOS-NAR virus was generated by co-transfection of 1 µg of KOS-NA viral DNA and 2.5 µg of pKHF plasmid (96), which contains WT *UL39*, digested with EcoRI and XbaI. Plaques were picked randomly and screened with the PCR ARMS technique as described above. Confirmation of the rescue of the mutation was performed by PCR, followed by sequencing and Southern blot analyses using the restriction enzyme, BamHI (Heba H. Mostafa and David J.Davido, unpublished data). The HrR3R (rescue) virus was constructed by cotransfecting Vero cells with 1µg of HrR3 viral DNA and 2.5µg of pKHF plasmid digested with EcoRI and XbaI. Rescuants were identified by blue/white selection and confirmed by Southern blot analysis by digesting the viral DNA with XhoI (Data not shown).

Ocular Infection of Mice. CD-1 out-bred female mice (6-7 weeks old) were obtained from Charles Rivers Laboratories (Shrewsbury, MA), cared for according to Guide for the Care and Use of Laboratory Animals (194), and infected as previously described (92). Briefly, mice were anesthetized by intraperitoneal injection of ketamine (75-100 mg/kg of body weight) and xylazine (10 mg/kg of body weight). Corneas were scarified with a 26-gauge needle and were infected with (KOS, 7134, KOS-NA, KOS-NAR, UL39 L393P/R950H, or HrR3 R) at 2 x 10^5 PFU of virus per eye in 3-5 µl medium.

Determination of Viral Titers in Eyes and Trigeminal Ganglia (TG). Four hours and 1, 3, 5, 7, and/or 9 days post-infection (post infection), eye swabs and/or TG samples were collected. For eye swabs, tear film was collected by swabbing the eye with cotton-tipped swabs and placed in microfuge tubes containing 500 µl 5% FBS growth medium. For TG samples, the mice were sacrificed by CO_2 asphyxiation, and the TG were removed and placed in microfuge tubes with 500 µl growth medium and 100 µl of 1 mm beads. These samples were homogenized using a Mini-Beadbeater 8 (BioSpec, Bartlesville, OK). In all cases, the wild-type,UL39 L393P/R950H, and HrR3R viruses were titered on Vero cells, and KOS-NA and KOS-NAR viruses were titered on L7 cells. Statistical analyses were performed using student's *t* test.

Latent Viral Genome Loads in TG. At 28-30 days post infection, latently infected TG were collected, and DNA was isolated from each TG as previously reported (195). PCR primers for the HSV-1 UL50 gene and the mouse adipsin gene were used to amplify viral DNA and as a loading control for cellular DNA, respectively (92). Real time PCR samples were performed in a total volume of 25 µl containing FastStart SYBR Green Master (Rox) (Roche, Indianapolis, IN) and primers [300 nM] in an ABI Prism 7500 real-time PCR system (Applied Biosystems, Foster City, CA). UL50 PCR samples contained 125 ng of DNA per reaction, adipsin PCR samples contained 10 ng of DNA per reaction, and all samples were analyzed in duplicate or triplicate. Standard curves for each PCR condition were carried out as described before (92) to quantify the amount of viral DNA present in each sample relative to the adipsin gene using the $2^{-\Delta\Delta ct}$ method. Statistical analyses were performed using one-way ANOVA test.

Viral explant-induced reactivation studies. Days 28-30 post infection, latently infected mice were sacrificed, each TG was collected and cut into 8 pieces, and cultured on Vero cells in a well of 24-well plates. Each well contained 1.5 ml of Vero cells medium. The cultures were sampled daily for up to 16 days for the presence of infectious virus by cytopathic effect on Vero cells for KOS and on L7 cells for KOS-NA and 7134 infected samples. At day 10 post-explantation, cultures were heat-shocked at 43º C for 3 h as an additional stimulus for reactivation. Statistical analyses were performed using the Fisher's exact test.

Western blot and immunoprecipitation analyses. i) ICP6 and UL40 protein levels: $1x10^5$ Vero cells were plated per well of a 12-well plate. Twenty four hours post-plating, cells were infected at an MOI of 2 for each virus. Samples were harvested 24h post-infection in 50 µL 1X Laemmeli buffer (100ºC) supplemented with 1X protease inhibitors (Leupeptin 1µg/mL, Aprotinin 1µg/mL, PMSF 1mM). Samples were heated at 95ºC for 5 min, vortexed, centrifuged, and loaded on a 4-12% gradient gel (Invitrogen), and ran at 120V for 1 h. Proteins were transferred to nitrocellulose membranes using a semidry transfer unit (GE Health Care, cat. no. TE77). Each membrane was blocked in 5% bovine serum albumin (BSA) in TBS and 0.1% Tween-20 (TBS-T) for 1 h at room temperature.

Primary antibodies: ICP0: mouse monoclonal antibody 11060 (Santa Cruz Biotechnology, cat. no. sc-53070) diluted 1:1000. β-Actin: rabbit polyclonal antibody (Santa Cruz Biotechnology, cat. no. sc-1616) diluted 1:1000. ICP6: mouse monoclonal

antibody diluted 1:100. UL40: mouse monoclonal antibody kindly provided by Dr. Everett diluted 1:250

Primary antibodies were incubated overnight at 4°C then the membranes were washed 3 times in TBS-T, and secondary antibodies were added: peroxidase conjugated goat antirabbit (Jackson Immunoresearch) diluted 1:1000 and peroxidase conjugated goat antimouse (Jackson Immunoresearch) diluted 1:1000 at room temperature for 1 h. Membranes were washed 3 times in TBS-T and developed using SuperSignal West Pico chemiluminescent substrate (Thermo Fisher Scientific, cat. no. 34087). Pictures captured with a Kodak 4000R image station.

ii) ICP6 interaction studies. Vero cells were plated in 60 mm dishes at $5x10^5$ cells per plate. Twenty four hours later, the cells were mock infected or infected with KOS at MOI of 2 or KOS-NA at MOI of 5 for 24 h. Cells were harvested in 100 µL of a buffer containing 100 mM Tris-HcL pH 8, 50 mM NaCl, 10% glycerol, 20 mM β-mercaptoethanol, and 1% Nonidet P-40 with protease inhibitors as described above. Samples were sonicated at 100 W for 30 sec, incubated on ice for 30 min, and centrifuged at 15K rpm for 10 min at 4ºC. 50 µL protein G Dynabeads (Invitrogen) were incubated, after aspirating the beads buffer, with 200 µL of PBS with 0.05% Tween-20 and 5 µL of an ICP6 mouse monoclonal antibody (Kindly provided by Dr. Everett) by rotating for 1 h at room temperature. Beads bound to the antibody were washed with PBS and 0.05% Tween-20 and incubated with the sample lysates, rocking at 4ºC overnight. The beads were then washed twice with PBS-Tween and transferred to new tubes. Fifty microliters of 1X Laemmeli buffer (100ºC) with protease inhibitors were added to each sample and samples were boiled for 5 min, vortexed, boiled again, and

vortexed twice for 1 min each. Western blot analyses were performed as described in the previous section.

4.3. Results

Mutations in KOS-NA impair acute viral replication in the eyes and trigeminal ganglia (TG). We initially examined acute replication of KOS-NA at the periphery in ocular epithelia. For these experiments, CD-1 mice were infected with 2 x 10^5 PFU of wild type HSV-1 (KOS), the ICP0 null mutant, 7134, and KOS-NA per eye. 7134 was used as an attenuated virus control in these experiments. Eye swabs from mice were taken at days 1, 3, 5, 7, and 9 post infection. Viral titers were determined by standard plaque assay. As shown in Figure. 4.1A, the replication of KOS-NA on days 1 and 3 post infection was 79-fold (*t* test, p=0.015) and 25-fold (*t* test, p=0.006) lower than KOS, respectively. On day 5 post infection, no KOS-NA infectious virus was detected (1000-fold decrease compared to KOS, *t* test, p=3.9 x 10^{-5}), which was followed by 11-fold reduction on day 7 post infection. Interestingly, the replication of KOS-NA was more impaired than the ICP0-null virus, 7134, on days 3, 5, and 7 post infection. When acute replication in neurons of the TG was examined, KOS-NA showed no detectable replication for all the time points examined. Relative to KOS titers, these represented decreases of at least 3981-, 5011-, and 63-fold on days 3, 5, and 7 post infection (*t* test, p=1.4 X 10^{-5}, 3.5 X 10^{-9}, and 2.5 X 10^{-5}, respectively). 7134, as expected, was capable of replicating in TG neurons of CD-1 mice, albeit poorly (Figure. 4.1B)(92).

Mutations in KOS-NA reduced the establishment of latency. To quantify the relative amount of viral DNA present in latently infected neurons, TG were collected at days 28-30 post infection and assayed for the presence of HSV-1 DNA using quantitative real time PCR. As shown in Figure. 4.2, the amounts of latent viral DNA present in TG were significantly reduced for KOS-NA (64-fold, one way ANOVA, $p<0.05$) and 7134 (12-fold, one way ANOVA, $p<0.05$) relative to the level of KOS.

The efficiency of KOS-NA reactivation is reduced. To determine if the efficiency and kinetics of reactivation from latency were altered for KOS-NA, the latent TG of all viral groups were collected on days 28-30 post infection and subsequently cultured by explantation. Samples were examined daily for cytopathic effect to monitor reactivation, and the rate of reactivation and total percentage of reactivating samples were determined for KOS-NA and 7134 mutants relative to KOS. KOS began to reactivate on day 3 post-explant at 66% and reached 100% reactivation by day 5 post explant (Figure. 4.3). KOS-NA reactivation peaked at day 4 post explant, maintaining a reactivation efficiency of 8% throughout the study (Fisher's Exact Test, $p < 0.0001$) (Figure. 4.3). 7134 reactivated on day 10 post explant, and after heat shock reached its highest levels (73%) on day 16 post explant (Figure. 4.3). The defect in establishing an efficient latent infection and reactivation from latency with KOS-NA is likely attributed to its impaired acute replication phenotype in the eyes and TG as has been observed with other HSV-1 mutants (31, 160).

Whole genome sequencing of KOS-NA mutant. As our published ICP0 phosphorylation study showed (92), the ICP0 phosphorylation site mutant, Phos 3, was not impaired for acute replication in eyes or TG of mice, the establishment of latency, or reactivation. The differences in the pathogenesis between Phos 3 and KOS-NA strongly suggested that KOS-NA contained secondary mutations in its viral genome. To characterize the secondary mutations in KOS-NA responsible for its highly attenuated phenotypes, we sequenced its viral genome in the same manner as KOS (93). Consequently, the genomes of KOS-NA and KOS were aligned using fast statistical alignment (FSA) to identify nucleotide polymorphisms between these two viruses (99). The alignment of these genomes revealed that KOS-NA contained 5 nonsynonymous mutations in three genes; *UL39* which encodes ICP6, *US7* which encodes viral glycoprotein I, and *RS1* which encodes the viral transcriptional regulator, ICP4.

Construction of KOS-NAR, UL39 L393P/R950H, and HrR3 R viruses. Because the acute replication, latency, and explant reactivation capabilities of KOS-NA were remarkably similar to the UL39 mutant viruses in mice (98), we hypothesized that the amino acid substitutions, L393P and R950H, in the open reading frame of ICP6 were responsible for KOS-NA attenuated pathogenesis. To address this, we rescued the UL39 gene of the KOS-NA with a wild type copy, and we introduced the KOS-NA mutated UL39 gene into the genome of the HrR3 virus, an ICP6::lacZ insertion mutant (96). As a control, we also generated an HrR3 rescue (R) virus where we rescued the ICP6::lacZ gene with a wild type copy of *UL39*. We then tested these viruses for acute replication in mice eyes and trigeminal ganglia.

Mutations in the *UL39* are responsible for the reduced acute replication phenotype of KOS-NA. To establish that the mutations identified in the UL39 gene of KOS-NA virus resulted in its attenuated pathogenesis, we tested the acute replication potential of KOS-NAR and UL39 L393P/R950H in the eyes and TG of mice. As shown in Figure 4.4A, UL39 L393P/R950H replicated to comparable levels of KOS-NA and was reduced by 347-, 32-, and 501-fold relative to KOS at days 1, 3, and 5 post infection (*t* test, $p=5.5X10^{-7}$, $p=1.2X10^{-7}$, and $p=3.3X10^{-9}$), respectively. When the growth of the rescue viruses, KOS-NAR and HrR3 R, was examined in this set of experiments, they replicated to levels comparable to KOS (Figure 4.4A).

When the TG replication of these viruses was monitored in TG at day 5 post infection we couldn't detect any viral replication of UL39 L393P/R950H (1412 fold reduction relative to KOS, *t* test $p=6.7X10^{-15}$) (Figure 4.4B). Acute replication of KOS-NAR and HrR3 R was comparable to KOS (Figure 4.4B). Day 5 was picked to analyze the acute replication in TG as it showed the maximum fold reduction between KOS-NA and KOS (Figure 4.1B), however we also tested the acute replication phenotype of UL39 L393P/R950H in TG at day 3 post infection and we couldn't detect any viral replication at this time point either (Data not shown).

Mutations in the *UL39* lead to less ICP6 protein levels without affecting the interaction between the two subunits of the ribonucleotide reductase

To understand the mechanism by which mutations within the UL39 gene impact the functions of ICP6, we initially wanted to examine the ICP6 protein levels after KOS-NA infection versus KOS. As shown in figure 4.5A, the ICP6 protein levels after KOS-NA

infection were significantly reduced relative to those produced by KOS. The UL40 protein, levels on the other hand, produced by both viruses were comparable (Figure 4.5A). This indicates that mutations in aa393 and/or aa950 sites of ICP6 reduce the stability of ICP6 protein. Interestingly, when we tried to look at the interaction kinetics between ICP6 produced by KOS-NA with UL40 versus the wild type interaction kinetics by immuno-precipitating UL40, we were unable to pull down detectable amounts of UL40 protein. Furthermore, in one set of experiments we infected with KOS-NA at an MOI higher than KOS, trying to have more expressed ICP6/UL40. Under these conditions we could only detect a very faint UL40 band and a faint band of ICP6 after immuno-precipitating UL40, compared to KOS. This indicates that the reduced ICP6 protein levels in case of KOS-NA might be influencing the tertiary structure of UL40 and this is why it was difficult to pull it down with our antibody. On the other hand, apparently, the mutations in the KOS-NA UL39 gene are not affecting the interaction with UL40, indicated by the faint ICP6 band pulled down with UL40 (Figure 4.5B).

4.4. Discussion

In this study, we have isolated a virus which carries two nonsynonymous mutations L393P and R950H in the UL39 gene, which encodes for the large subunit of ribonucleotide reductase. KOS-NA containing these mutations is significantly reduced in its acute replication in mice eyes and TG, is greatly impaired in its ability to establish latency, and can poorly reactivate from a latent infection after explant-induced reactivation.

The HSV-1 ribonucleotide reductase belongs to class I of Ribonucleotide reductases that have a heterodimeric structure which is active in the α2β2 configuration (196-200), similar to mammalian and bacterial ribonucleotide reductases. The large subunit contains the catalytic and allosteric site, which confers substrate specificity. The smaller subunit on the other hand is responsible for generation of free radicals that are required for substrate activation (201). Viruses mutated in the UL39 gene have been shown to replicate normally in dividing cells at 37ºC, where the reductase activity is compensated by the cellular homolog. On the other hand, the viral reductase activity becomes important for viral DNA replication in neurons, non-dividing cells, or at elevated temperatures (e.g., 41ºC) (96). Of relevance to our study, this enzyme complex is essential for efficient *in vivo* acute replication, establishment of latency, and reactivation from latency (98). Characterization of ICP6 revealed that it is expressed early, before its small subunit partner, during viral infection in cell culture (202-205) and contains an extra N-terminal domain that is not required for HSV's ribonucleotide reductase activity (206). This N-terminal domain has been shown to possess anti-apoptotic (207, 208), chaperone-like (209), and protein kinase activities (210). Additionally, ICP6 has been shown to be a target of the HSV directed cytotoxic T lymphocytes, a function which was shown to be largely conferred by a single amino acid (211).

Previous studies showed that the N-terminal region of ICP6 is required for interdomain linking (212) and that the interaction with the smaller subunit of ribonucleotide reductase is conferred by its C-terminal region (213). Amino acid sequence alignment studies indicate that the 393 site is not conserved between strain

KOS and other HSV strains; syn17+ (HSV-1), McKrae (HSV-1) and HG52 (HSV-2). Like KOS-NA, a proline is encoded at amino acid 393 in these latter strains (Figure 5). This lack of conservation could exclude the 393 site from being responsible for the phenotypes observed with KOS-NA. On the other hand, the 950 site is conserved between all of the HSV-1 and HSV-2 strains we examined (i.e., KOS, syn17+, McKrae and HG52) (Figure 5) as well as VZV (214). Moreover, it was shown previously that a single aa mutation in the 961 site of HSV-1 ICP6 (215) reduced the ribonucleotide reductase activity of the enzyme (216). Although this site has been shown to be important for the two subunit interactions, it was previously concluded that this effect might be indirect because blocking this site using antisera didn't affect the interaction between the two subunits in the wild type virus (215). Consistent with this study, our interaction studies suggested that the R950H mutation doesn't interfere with the interaction between ICP6 and UL40 (Figure 4.5B) however, it is probably responsible for reduced ICP6 protein stability (Figure 4.5A). Of note, the 950 site is close to aa 960 to 963, a region which has been identified as block 10 and highly conserved between viral and cellular ribonucleotide reductases (214). Although The 950 site has been shown through our sequence alignment to be surrounded by highly conserved regions between HSV strains (Figure 4.5), these regions were less conserved when we aligned the protein with eukaryotic ribonucleotide reductase, CMV (data not shown), and VZV (214). Interestingly, R 950 was still conserved between all of them. This highlights the functional importance of this site and indicates that R 950 is the most likely cause of the KOS-NA phenotypes.

Because studies showed that lack of a US7 gene can also attenuate the acute viral replication in sensory ganglia and CNS of mice without having a great effect in cell culture (217), we tested the effect of introducing the KOS-NA *US7* mutation to the genome of our phosphorylation mutant, Phos 3. Our results didn't show any effect of introducing this mutation to the Phos 3 virus, which was able to acutely replicate efficiently both in mouse eyes and TG, comparable to the wild type KOS (data not shown).

Contribution to this work:

I assisted in identifying the KOS-NA mutations, constructed KOS-NAR, UL39 L393P/R950H, and HrR3R viruses, tested them *in vivo*, and conducted the cell culture western blot, and co-immunoprecipitation studies.

4.5 Figures and Figure legends

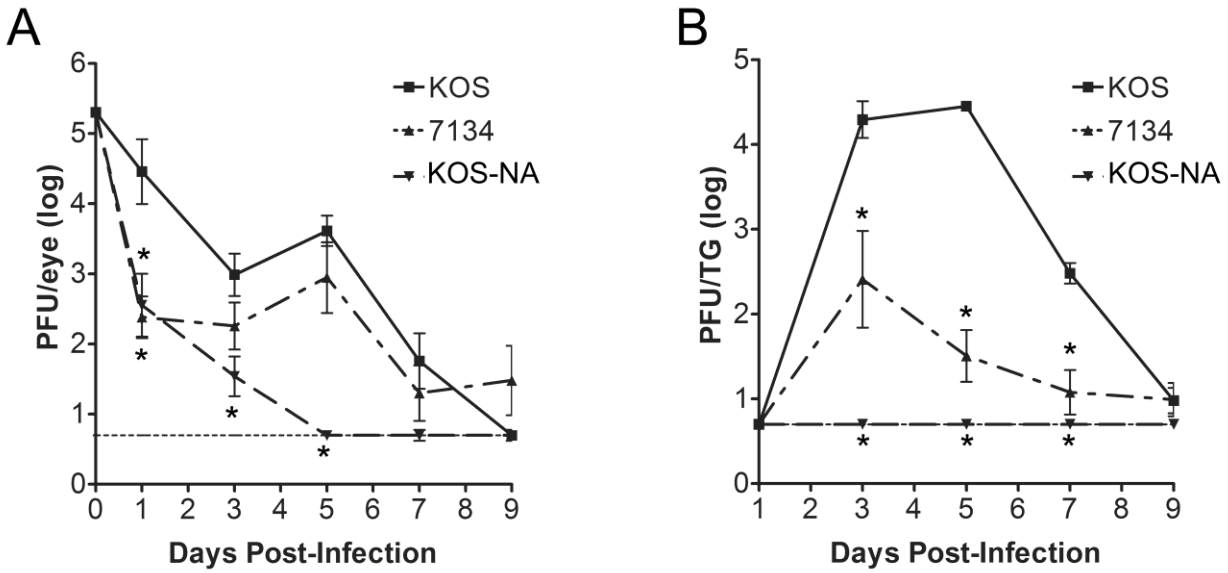

Figure 4.1**. Acute replication of KOS-NA**. A) Acute replication of KOS-NA in mice eyes. Mice were infected with 2 x 10^5 plaque forming units per eye, and tear film was collected from each eye on days 1,3,5,7, and 9. The amount of infectious virus collected in each sample was determined by plaque assay. B) Acute replication of KOS-NA in mice TG. Mice were infected as described above and TG were collected on the indicated days. TG were then homogenized and the amount of infectious virus present was determined by plaque assay. In both A and B results shown are logarithmic means (n=6 sample per group per time point), with the error bars indicating the SEM. The horizontal dotted lines represent the lower limit of detection.

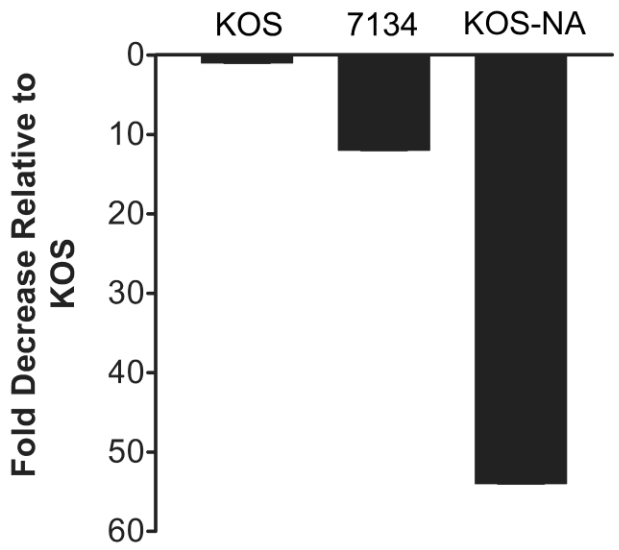

Figure 4.2**. Viral genomic loads in latent TG**. Mice were infected with 2 x 10^5 plaque forming units per eye, and TG were collected 28-30 days post infection. DNA was extracted from latent TG, and the amount of HSV-1 DNA present was quantified by real time PCR (n=4-10 TG per group). Results shown are the fold reduction compared to KOS.

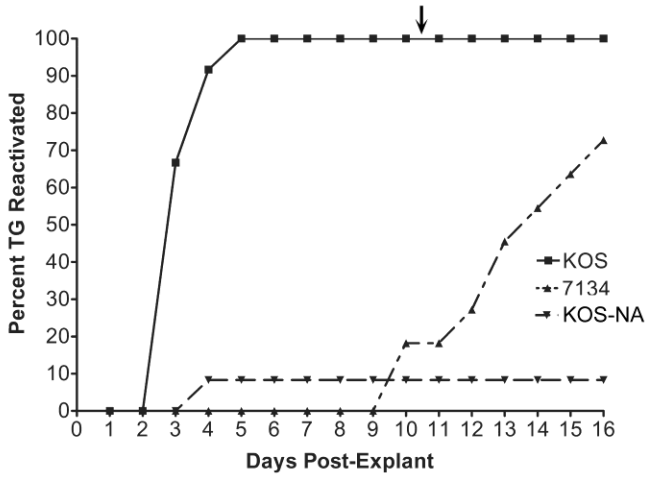

Figure 4.3. **Explant induced reactivation of KOS-NA.** Mice were infected with 2 x 10^5 plaque forming units per eye. On day 28-30 post infection, TG were collected and explanted onto Vero cells. The time required for each virus to reactivate from the latent TG was determined by assaying the culture medium daily for the presence of infectious virus. Each time point represents the cumulative percentage of samples that reactivated (n=19-20 TG per group). The arrow at the top of the graph indicates that after day 10, samples were heat shocked at 43ºC for 3h.

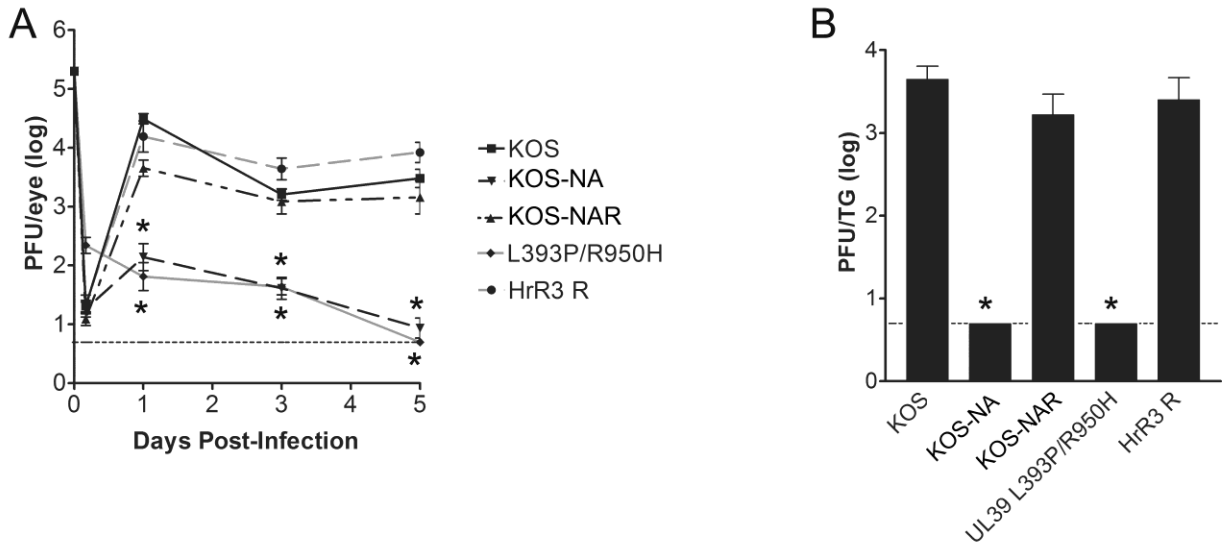

Figure 4.4. **Mutations in the UL39 gene are responsible for the reduced acute replication phenotype of KOS-NA**. A) Acute replication of KOS-NAR, UL39 L393P/R950H, and HrR3 R in mice eyes. Mice were infected with 2 x 10^5 plaque forming units per eye, and tear film was collected from each eye after 4 hours and days 1,3, and 5 post infection. The amount of infectious virus collected in each sample was determined by plaque assay. B) Acute replication of KOS-NAR, UL39 L393P/R950H, and HrR3 R in mice TG at day 5 post infection. Mice were infected as described above and TG were collected. TG were then homogenized and the amount of infectious virus present was determined by plaque assay. In both A and B results shown are logarithmic means and the error bars indicate the SEM (n=8 samples per group per time point). The horizontal dotted lines represent the lower limit of detection.

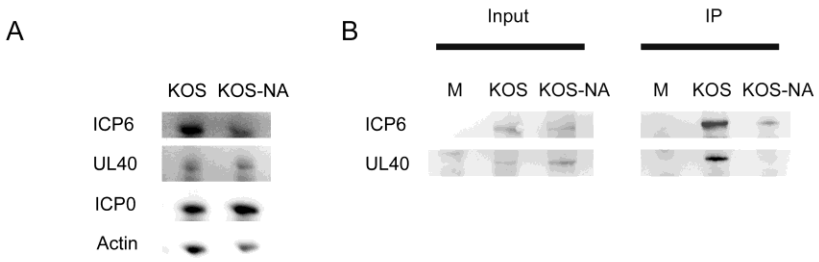

Figure 4.5. **KOS-NA ICP6 protein levels and interaction with UL40**. A) Vero cells were infected at MOI of 2 with KOS or KOS-NA for 24 hours. Infected monolayers were harvested and the indicated proteins were examined by western blot analyses. ICP0 was used as a loading control for infection B) Vero cells were mock infected or infected at MOI of 2 for KOS and 5 for KOS-NA for 24 hours. UL40 was immuno-precipitated and the levels of ICP6 and UL40 were analyzed by western blot.

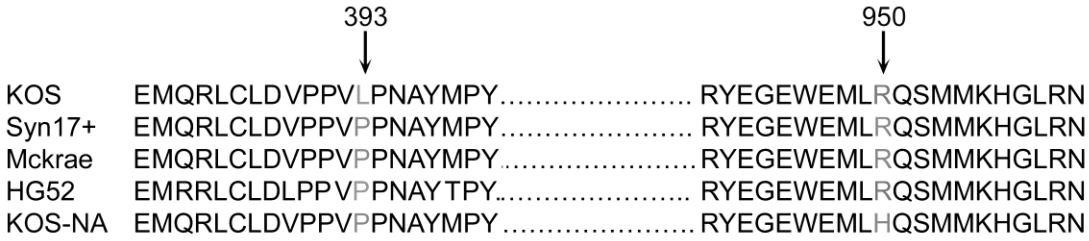

Figure 4.6. **Sequence alignment of KOS-NA to different HSV strains.**

Chapter 5

HSV-1 ICP22 but not $U_S1.5$ is Required for Efficient Acute Replication in Mice and VICE Domain Formation

This chapter is modified from the published article: J Virol. 2013 Dec; 87(24):13510-9

5.1 Abstract

The herpes simplex virus type 1 (HSV-1) immediate early protein, infected cell protein 22 (ICP22), is required for efficient replication in restrictive cells, viral induced chaperone enriched (VICE) domain formation, and normal expression of a subset of viral late proteins. Additionally, ICP22 is important for optimal acute viral replication *in vivo*. Previous studies have shown that *U_S1*, the gene that encodes ICP22, produces an in-frame, N-terminally truncated form of ICP22 known as $U_S1.5$. To date, studies conducted to characterize the functions of ICP22 have not separated its functions from that of $U_S1.5$. To determine the individual roles of ICP22 and $U_S1.5$, we made viral mutants that express either ICP22 (M90A) by mutating the $U_S1.5$ initiation codon, or $U_S1.5$ (3Xstop) by introducing stop codons upstream of the $U_S1.5$ start codon. Our studies showed that, in contrast to M90A, 3Xstop was unable to replicate efficiently in the eyes and trigeminal ganglia of mice during acute infection, efficiently establish a latent infection, induce VICE domain formation, and was only mildly reduced in its replication in restrictive HEL cells and MEFs. Both mutants enhanced the expression of the late viral proteins vhs and gC and inhibited viral gene expression mediated by HSV-

1 infected cell protein 0 (ICP0). When we tested our mutants' sensitivity to type I interferon (IFN-β) in restrictive cells, we noticed that the plating of the ICP22 null (d22) and 3Xstop mutants was reduced by adding IFN-β. Overall, our data suggest that $U_S1.5$ partially complements the functions of ICP22.

5.2 Materials and Methods.

Cells and viruses. Vero cells and HEL-299 cells were obtained from the American Type Culture Collection (ATCC). Vero cells were grown in Dulbecco's Modified Eagle's Medium (DMEM) supplemented with 5% fetal bovine serum (FBS), 2 mM L-glutamine, 100 µg/ml penicillin, and 100 U/ml streptomycin. HEL cells were grown in Minimum Essential Medium (MEM) Alpha supplemented with 10% FBS, L-glutamine, and antibiotics as described for Vero cells. CD-1 mouse embryonic fibroblasts (MEFs) (kindly provided by Dr. Kristi Neufeld) and 129 MEFs (prepared in our laboratory and the protocol is approved by the University of Kansas Institutional Animal Care and Use Committee) were grown in the same media as Vero cells, except the DMEM was supplemented with15% FBS. The wild-type HSV-1 strain KOS (passage 11) was used in our study. All the viruses were propagated and titered on Vero cells.

Construction of mutant and marker rescue (MR) viruses. To make our mutants in a KOS background, we initially made the ICP22 null mutant, d22, by marker transfer. For the construction of this virus, Vero cells were seeded on 60 mm dishes at $5x10^5$ cells/plate. Twenty-four hours later, cells were co-transfected with 1 µg KOS viral DNA and 2.5 µg of AgeI-linearized pUCNS:lacZ plasmid (218) (kindly provided by Dr Stephen Rice). Cells were transfected with Fugene HD (Roche) at a ratio of 3:1 (µl transfection reagent: µg DNA) according to the manufacturer's recommendations. Mutants were identified by blue/white selection in the presence of X-gal. Blue plaques were picked, and plaque purified at least three times. Correct insertion of the mutation was confirmed by BamHI digestion of viral DNA and Southern blot analyses (Figure

5.1B). To create the M90A and 3Xstop mutant viruses, pAlter-M90A and pAlter-3Xstop plasmids (kindly provided by Dr Priscilla Schaffer's lab) (117) were digested with EcoRI and KpnI and co-transfected with d22 viral DNA. White plaques were picked and purified at least three times. Correct insertion of M90A mutation was confirmed with BamHI and PciI digests and Southern blot analyses (Figure 5.1B). Correct insertion of 3Xstop mutation was confirmed with SacII digests and Southern blot analyses (Figure 5.1B). M90AMR and 3XstopMR viruses were made by co-transfecting the corresponding mutant viral DNA with the wild-type pAlter-ICP22 plasmid cut with EcoRI and KpnI. Plaques were picked randomly, and the rescuants were initially identified by PCR and restriction enzyme digestion analyses and rescue by the wild-type ICP22 sequences were confirmed by Southern blot analyses (data not shown).

Acute viral replication in mice. Infections were performed as previously described (92). Briefly, CD-1 outbred female mice (6-7 weeks old) were purchased from Charles Rivers Laboratories (Shrewsbury, MA) and cared for according to Guide for the Care and Use of Laboratory Animals (173). The protocol for using these mice is approved by the University of Kansas Institutional Animal Care and Use Committee. Mice were anesthetized by intraperitoneal injection of ketamine (75-100 mg/kg of body weight) and xylazine (10 mg/kg of body weight). Corneas of mice were scarified with a 26-gauge needle and infected with KOS, d22, M90A, 3Xstop, or each MR virus at $2x10^5$ PFU of virus per eye in 5 µL medium. To determine acute ocular titers, the eyes of infected mice were swabbed at 4 hours, days 1, 3, and 5 post-infection using moistened cotton tipped swabs, and placed in 500 µL of Vero cells growth medium. To determine

acute replication in the trigeminal ganglia, mice were euthanized by CO_2 asphyxiation at days 3 and 5 post-infection, and TG were removed and placed in 500 µL 1% FBS growth medium and 100 µL of 1 mm glass beads. Samples were homogenized with a Mini-beadbeater 8 (BioSpec). All viral samples were titered on Vero cells, and differences in viral titers were evaluated using the student's *t*-test.

Viral pathogenicity scoring. At day 8 post-infection, mice were scored for the appearance of gross lesions based on the following scoring system, 0: no signs of infection; 1: swollen eyelids; 2: less than 20% removal of hair around the eyes; 3: 20-70% removal of hair between the eyes; and 4: more than 70% removal of hair between the eyes. Statistical analyses were performed using the student's *t*-test.

Latent viral genome loads in TG. At day 28 post-infection, TG were collected, and DNA was isolated from each TG as previously described (195). PCR primers specific for the HSV-1 UL50 gene were used to measure viral DNA loads (152) and primers for mouse adipsin gene were used as a loading control (153). Real time PCR was performed in a total volume of 25 µL per sample of FastStart SYBR Green Master (Roche, Indianapolis, IN) and primers in a StepOnePlus Real-Time PCR System (Applied Biosystems). For UL50 PCR samples, 125 ng of DNA was used per reaction, and for adipsin PCR samples, 10 ng of DNA was used per reaction. All samples were analyzed in duplicate. Standard curves for each PCR condition were carried out as described (153) to quantify the amount of viral DNA present in each sample relative to

adipsin gene using the $2^{-\Delta\Delta ct}$ method (154). Statistical analyses were performed using the one-way ANOVA test.

Viral yield assays. HEL cells or MEFs were plated at $1x10^5$ cells per well in 12-well plate. Twenty-four hours later, cells were infected at MOI of 0.1 with each virus. One hour after addition of the virus, cells were washed with acid wash buffer for 1 minute to inactivate any unabsorbed virus, then washed with phosphate buffered saline (PBS), and supplemented with HEL or MEF growth medium. Twenty-four hours post-infection, cells were harvested, and viral yields were determined by standard plaque assays. For viral yield assays in the presence of IFN-β, the same protocol was followed as above, with the exception that HEL cells and MEFs were pretreated with human IFN-β (PBL InterferonSource, cat. no 11410-2) or mouse IFN-β (PBL InterferonSource, cat. no 12400-1), respectively, at 1000 units per mL for 16 hours before adding the virus. The same concentration of IFN-β was added to PBS washes and media during the course of infection.

Western blot analysis. HEL cells and MEFs were plated on 12-well plates at $1x10^5$ cells per well. Twenty-four hours post-plating, cells were infected at an MOI of 2 for each virus. Samples were harvested at 8 or 24 hours post-infection in 50 µL 1X Laemmeli buffer (100ºC) supplemented with 1X protease inhibitors (1µg/mL Leupeptin, 1µg/mL Aprotinin, 1mM PMSF). Samples were heated at 95ºC for 5 min, vortexed, and centrifuged. Ten µl per sample was resolved on a 6% SDS PAGE gel. Proteins were transferred to nitrocellulose membranes using a semidry transfer unit (GE Health Care,

cat. no. TE77). Each membrane was blocked in 5% bovine serum albumin (BSA) in 0.1% Tween-20 diluted in tris-buffered saline (TBS-T) for 1 h at room temperature. Primary antibodies used were: ICP22, a rabbit polyclonal antibody 413 produced by Bethyl laboratories (117) diluted 1:5000; β-Actin, a rabbit polyclonal antibody (Santa Cruz Biotechnology, cat. no. sc-1616) diluted 1:1000; vhs, a rabbit polyclonal antibody described in (219) diluted 1:100; and gC, a mouse monoclonal antibody (Santa Cruz Biotechnology, cat. no. sc-56982) diluted 1:250.The membranes were washed 3 times in TBS-T, and probed with: peroxidase conjugated goat antirabbit (Jackson Immunoresearch) diluted 1:1000 and peroxidase conjugated goat antimouse (Jackson Immunoresearch) diluted 1:1000 at room temperature for 1 h. Membranes were washed 3 times in TBS-T and developed using SuperSignal West Pico chemiluminescent substrate (Thermo Fisher Scientific). Images were captured with a Kodak 4000R image station, and the band intensities were measured by densitometry using ImageJ.

Immunofluorescence studies. HEL cells or Vero cells were plated on glass coverslips in 24-well plates for 24 h ($5x10^4$ per well). Cells were then infected at an MOI of 0.1. After 24 h of infection, cells were fixed with 4% formaldehyde in phosphate buffered saline (PBS) for 15 min at room temperature, washed with PBS, and blocked for 1 h in 5% normal goat serum and 0.2% Triton X-100 diluted in PBS at 37ºC. The primary antibodies used were: ICP22 rabbit Polyclonal 413 described in our western blot studies diluted 1:500 and Hsc-70 rat monoclonal (Stressgen, cat. no SPA-815) diluted 1:500.Cells were incubated in primary antibodies for 1 h at 37ºC and then washed at least 3 times. Each secondary antibody was added for 1 h at 37ºC. The

secondary antibodies used were: goat anti-rabbit dy488 (Jackson Immunoresearch) diluted 1:500 and goat anti-rat Alexaflour 568 (Invitrogen) diluted 1:1000. Cells were then washed 3 times with PBS, mounted with Prolonged Antifade Kit (Invitrogen) and examined with fluorescence microscopy (Nikon Eclipse TE-2000-U4).

Luciferase assays. Vero cells were plated at $5x10^4$ cells per well in 24-well plates for 24 h. Cells were co-transfected with 50 ng of the reporter plasmid (VP16 promoter- luciferase construct) (172) alone or with 100 ng of pAlter-1+ICP0 (pICP0), or pAlter-1 that expresses both ICP22 and $U_S1.5$ (pICP22), only ICP22 (pM90A) (117), or only $U_S1.5$ (p3Xstop) (117), all driven by their native promoters, or a combination of 100 ng of pICP0 and 100 ng of pICP22, pM90A, or p3Xstop. In all cases, salmon sperm DNA was added for a total of 1 µg per well. Transfections were performed according to the manufacturer's protocol using Fugene HD at a ratio of 3:1. Cells were transfected for 48 h, wells were washed with PBS, and each well was then harvested in 100 µL of 1X passive lysis buffer (PLB; cat. no E1941, Promega) by rocking at room temperature for 15 min. Samples were harvested in microfuge tubes, vortexed for 30 sec, and briefly centrifuged at room temperature. Fifty µL of each sample were then added to 50 µL luciferase assay buffer (125 mM sodium MES pH 7.8, 25 mM magnesium acetate, 2 mg of ATP per mL) as previously described (220). Luciferase assays were conducted using the Promega Luciferase Assay System 1000: 50 µL of 1 mM D-luciferin was added per sample and a 2-sec delay before a10-sec read (Biotec Synergy, HT multicode microplate reader). Light units are displayed as percentages normalized to the pICP0 values, and statistical analyses were performed using the Mann-Whitney *U* test.

Plaque reduction assays. HEL cells or MEFs were plated in 24-well plates at $5x10^4$ cells per well for 24 h. Cells were then mock-treated or pre-treated with human IFN-β as described above for viral yield assays. Sixteen hours later, cells were infected with a serially diluted KOS, d22, M90A, or 3Xstop. At 1 hour post-infection, cells were overlaid with 0.5% methylcellulose in the appropriate cell culture medium. Three days later, cells were fixed in 4% formaldehyde in PBS for 15 min at room temperature, washed with PBS, and stained for 1 hour at room temperature with an anti-HSV-1 antibody (Dako, cat. no. B0114) diluted 1:350 at room temperature with shaking. Plates were washed once with PBS, and incubated with horseradish peroxidase conjugated antibody (Jackson Immunoresearch) diluted 1:500 for 1 h at room temperature. Plates were washed once with PBS, and plaques were visualized using a peroxidase substrate kit, AEC (Vector Laboratories) according to the manufacturer's recommendations. Pictures were taken with a scanner, and the number of pixels within a given plaque (that represents its area) was measured by Adobe Photoshop. Twenty plaques were examined for each virus.

5.3 Results

Construction of ICP22 mutant viruses. In order to separate the functions of ICP22 and the $U_S1.5$ protein during viral infection, we constructed two mutant viruses. The M90A mutant (Figure 5.1A and B) was generated by homologous recombination as previously described (117), except we used an ICP22 deletion virus (d22) that we generated in a KOS background (Figure 5.1A, B, and C). M90A contains a methionine to alanine mutation in codon 90 of ICP22, which is the initiating codon for $U_S1.5$ (Figure

5.1A and B). Consequently, this mutant expresses ICP22 and not $U_S1.5$ (Figure 5.1C) (117).The 3Xstop mutant virus was generated similar to the M90A mutant virus. This mutant introduces 3 stop codons upstream to the initiation codon of $U_S1.5$ (Figure 5.1A and B) and expresses the $U_S1.5$ protein and not ICP22 (Figure 5.1C).

ICP22 but not $U_S1.5$ is required for efficient acute viral replication *in vivo*. Genetic studies have demonstrated the importance of ICP22 for acute replication *in vivo* when the productive replication of various ICP22 mutant viruses were examined in different animals models (102, 106, 221). In order to test the individual roles of ICP22 and the $U_S1.5$ protein during acute viral replication *in vivo*, we used a mouse ocular model of HSV-1 infection. The eyes of mice were infected with KOS, d22, M90A, or 3Xstop and in the case of M90A and 3Xstop, their corresponding marker rescue (MR) viruses. Eye swabs were taken at 4 hours and days 1, 3, and 5 post-infection to monitor ocular replication, or trigeminal ganglia homogenates were prepared on days 3 and 5 post-infection to monitor acute replication in neurons. As shown in Figure 5.2A, the M90A mutant virus replicated to levels comparable to that of KOS in the eyes of mice for all time points tested. In contrast, the replication of the 3Xstop mutant in the eyes was significantly reduced relative to KOS on day 1 (17-fold, *t* test p=0.01) and day 5 (184-fold, *t* test $p=6.8x10^{-7}$) post-infection. The replication of d22 in the eyes of mice was significantly reduced at days 1, 3, and 5 post-infection by 1722-, 255-, and 554-fold, respectively (*t* test $p=5.9x10^{-11}$, $1.7x10^{-19}$, and $6.5x10^{-18}$). The replication of M90AMR and 3XstopMR viruses in the eyes was comparable to KOS (Figure 5.2B). When acute replication of the M90A and 3Xstop mutants in TG was examined, only the 3Xstop

mutant showed decreased growth at day 3 (59-fold, *t* test $p=3.6x10^{-5}$, Figure 5.2C) and day 5 (429-fold, *t* test $p=2.3x10^{-10}$, Figure 5.2E). The M90A mutant replicated as efficiently as KOS on both days (Figure 5.2C and E). We were unable to detect progeny virus in the TG of d22-infected mice on days 3 and 5 post-infection (*t* test $p=6.7x10^{-16}$ and $3.3x10^{-18}$, Figure 5.2C and E). The M90AMR and 3XstopMR viruses replicated similar to KOS in TG on both days (Figure 5.2D and F). Thus, ICP22, not $U_S1.5$, is the major contributor to acute ocular and consequently neuronal replication.

ICP22 but not $U_S1.5$ is required for external pathological lesions in mice. We scored the pathological lesions caused by the ocular infection of mice with KOS, d22, M90A, 3Xstop, M90AMR, and 3XstopMR at day 8 post-infection. The severity of infection was ranked on a scale of 0-4 for each group, where "0" indicates no signs of infection and "4" indicates more than 70% loss of hair from between the eyes, which is the result of scratching or secondary inflammation. As shown in Figure 5.3, the 3Xstop mutant behaved like d22 in that it did not show any signs of disease, as both groups had pathology scores of 0 (Table 1, *t* test, $p=9x10^{-5}$). The M90A mutant, on the other hand, behaved similar to KOS and the MR viruses, where inoculated mice showed obvious signs of infection (Figure 5.3 and Table 5.1). Our data indicate that, in contrast to ICP22, the expression of $U_S1.5$ is insufficient to induce signs of viral pathogenesis in mice.

ICP22 is required for efficient establishment of latency. To examine the ability of our mutants to establish a latent infection, TG from infected mice were

collected 28 days post-infection, and viral DNA loads were determined using real time PCR. As shown in Figure 5.4, relative to KOS, the 3Xstop mutant was significantly reduced for viral DNA levels by 11.5 fold (one way ANOVA, $p<0.05$). The M90A mutant, on the other hand, was able to establish latency comparable to KOS and the MR viruses (Figure 5.4). The fold reduction of the d22 mutant was comparable to the mock-infected mice (≥568-fold, one way ANOVA, $p<0.05$, Data not shown). The defect in establishing an efficient latent infection with both d22 and 3Xstop is likely attributed to their impaired acute replication phenotypes in the eyes and TG as has been observed with other HSV-1 mutants (31, 160).

ICP22 or U_S1.5 is sufficient for HSV-1 replication in restrictive cells. It has been previously established that ICP22 is required for efficient viral growth in certain cell lines, which have been termed "restrictive" cell lines (102). In order to test the roles of ICP22 and U_S1.5 in viral replication in restrictive cells, we performed a viral yield assay in HEL cells (102). HEL cells were infected at an MOI of 0.1 with KOS, d22, M90A, or 3Xstop mutants. At 24 hours post-infection, cells and progeny virus were collected, and viral yields were determined with a standard plaque assay. As shown in Figure 5.5, the M90A mutant replicated to levels that were comparable to that of KOS; however, d22 replication was significantly reduced (83-fold, *t* test $p=2.5x10^{-7}$). Replication of the 3Xstop mutant was only modestly impaired relative to KOS (4.5-fold, *t* test $p=0.003$) (Figure 5.5). The replication of the 3Xstop mutant was also significantly reduced relative to the d22 mutant (18.4-fold, *t* test $p=5.5X10^{-8}$). Similar results were seen in mouse embryo fibroblasts (MEFs) of CD-1 mice strain (Data not shown). These data indicate

that ICP22 is sufficient to enhance viral growth in HEL and MEF cells; however, the U_S1.5 protein can, to a great extent, complement the function of full-length ICP22.

Both ICP22 and U_S1.5 enhance the expression of late viral proteins in cell culture. ICP22 has been demonstrated to enhance the expression of a subset of late viral proteins, including viral glycoprotein C (gC) and virion host shutoff (vhs) (101, 102, 107, 108). In order to test the individual roles of ICP22 and U_S1.5 in the expression of late viral proteins, we infected HEL cells with KOS, d22, M90A, and 3Xstop for 24 hours and examined vhs and gC protein levels by western blots. When compared to KOS-infected samples, the expression of gC and vhs was reduced in d22-infected cells but not in M90A- or 3Xstop-infected cells (Figure 5.6). Similar results were also observed at 12 hours post-infection (Data not shown). Our data show that both ICP22 and U_S1.5 are capable of stimulating late viral protein expression. Analogous results were observed in MEFs (CD-1 strain) and Vero cells (Data not shown).

U_S1.5 does not induce VICE domains. ICP22 has been shown to be required for the formation of VICE domains (112) during productive HSV-1 infection. To test the individual contributions of ICP22 and U_S1.5 in the formation of VICE domains, HEL cells were mock infected or infected with KOS, d22, M90A, or 3Xstop for 24 hours, and the localization of ICP22 and the VICE domain marker, Hsc70, were examined by immunofluorescence. Our experiments showed that the M90A mutant was able to form VICE domains that appeared identical to KOS (Figure 5.7A and B), in which ICP22 colocalized with Hsc70 in the nucleus. The 3Xstop mutant, however, was unable to

induce Hsc70 puncta (Figure 5.7A and B). Although the U_S1.5 protein localized to the nucleus, it failed to form the speckled pattern of ICP22 staining observed with KOS- and M90A-infected nuclei (Figure 5.7A). Notably, the staining pattern of Hsc70 in the presence of U_S1.5 localized to the nucleus, which was different from that of mock- and d22-infected cells (Figure 5.7A). This indicates that, although U_S1.5 fails to induce the formation of VICE domains, it is still capable of relocalizing Hsc70 to the nucleus. Similar results were observed in Vero cells (Data not shown).

M90A and 3Xstop inhibit ICP0-directed transactivation of an HSV promoter-luciferase reporter. The IE protein ICP0 is a promiscuous transactivator of all classes of HSV-1 genes (222). One published report demonstrated that ICP22 represses ICP0-transactivated expression of reporter genes in transient transfections (223), which could be directly through interfering with ICP0's transactivation activity, or indirectly by reducing ICP0's expression (224, 225). To investigate if this inhibitory function is carried out by ICP22, U_S1.5, or both, we performed a luciferase assay to test the effect of both proteins on ICP0-mediated gene expression. ICP0 expression led to the maximum activity of the VP16 promoter and was given the 100% value (Figure 5.8). Neither the pICP22 plasmid (which expresses both ICP22 and U_S1.5), pM90A, or p3Xstop was able to activate VP16 promoter. Combining pICP22, pM90A, or p3Xstop with pICP0 led to a significant inhibitory effect on ICP0's transactivation of the VP16 promoter (Mann Whitney *U*-test, p= 0.002). Our results demonstrate that ICP22 and U_S1.5 both have a significant and comparable inhibitory effect on the ICP0-directed transactivation in reporter gene experiments.

ICP22 but not U_S1.5 counteracts the effects of interferon-β (IFN-β) in restrictive cell lines. In order to understand the reduction in the ability of the 3Xstop mutant to replicate acutely *in vivo,* we wanted to test if there is a relationship between ICP22 or U_S1.5 and the type I IFN response. An earlier publication examined the plaquing of an ICP22 null mutant in IFN-treated Vero cells, a cell line permissive for ICP22 mutant replication (100), and concluded that ICP22 is not required to counteract an established type I IFN response (58). Consequently, we decided to perform plaque reduction assays in a restrictive cell line, HEL cells. Interestingly, we found a noticeable reduction in the number of plaques formed by d22 in the presence of IFN-β relative to KOS (Table 5.2). The overall size plaque size for d22 was smaller than that of KOS. Furthermore, the reduction in plaque size for d22 was further enhanced by IFN-β compared to KOS (46-fold vs. 10-fold, Figure 5.9). For M90A, the reduction in the number of plaques in the presence of IFN-β was comparable to KOS (Table 5.2), as well as the plaque sizes with and without IFN-β (9-fold). Interestingly, although the reduction in the number of plaques formed by 3Xstop after adding IFN-β were comparable to KOS (Table 5.2), the plaques appeared smaller than those of KOS only after adding IFN-β (37-fold versus 10-fold, Figure 5.9). In order to correlate this observation to the *in vivo* acute replication data, we decided to repeat the same experiment in CD-1 MEFs. Our results showed that the size of d22 and 3Xstop plaques was markedly smaller than the wild-type plaques, a phenotype that was enhanced in IFN-β-treated cells (34-fold and 21-fold, respectively, versus a 2-fold reduction with KOS, Figure 5.9). Consistent with these experiments, there was a reduction in the number of plaques for d22 and 3Xstop that exceeded the decreases observed for KOS

and M90A (Table 5.2). When we repeated the same experiments on MEFs of 129 strain, we observed an even further reduction in the number of plaques for d22 and 3Xstop (Table 5.2). To determine if the plaque reduction phenotype correlated with reductions in the viral replication, we performed yield assays in the absence or presence of IFN-β. As shown in Figure 5.10A, reductions in viral replication after the addition of IFN-β were similar for KOS, d22, M90A, and 3Xstop mutants (~50-fold decrease) on HEL cells and similar results were noticed on 129 MEFs (Data not shown). In CD-1 MEFs (Figure 5.10B), IFN-β further impaired d22 replication (140-fold compared to 6-fold reduction of KOS), while IFN-β only slightly reduced the growth of M90A and 3Xstop compared to KOS (19- and 27-fold respectively). These data indicate that ICP22 but not U_S1.5 is required for efficient plaquing in the restrictive cell lines, HEL and MEFs, in the presence of a pre-established interferon response and the degree of this requirement is cell type dependent.

5.4 Discussion

The HSV-1 genome contains ~90 genes, and with some exceptions, each gene encodes a single protein. The *U_S1* gene is one such exception, as it codes for two proteins: ICP22 and its N-terminally truncated form, U_S1.5 (116). To date, reports that have examined the functions of ICP22 have largely not separated its biological activities from those of U_S1.5. The goal of this study was to characterize the individual contributions of ICP22 and U_S1.5 in the HSV-1 life cycle by generating mutant viruses (i.e., M90A and 3Xstop) that can only express one of the two proteins. Our data show that the U_S1.5 protein is dispensable for acute replication in mice and for the induction

of VICE domains. Also, our data indicate that either protein can functionally enhance the expression of late viral proteins in cell culture and inhibit ICP0-mediated gene expression in transient transfection assays. Additionally, we identified a new role for ICP22 in enhancing viral plaquing in the presence of IFN-β, a function that was not fully compensated by $U_S1.5$ alone. Moreover, as the M90A mutant behaved like KOS in all of our assays, this indicates that the point mutation at M90 residue did not have any impact on the functional activities of ICP22.

We did observe that the expression of $U_S1.5$ alone (expressed from 3Xstop) was marginally reduced for viral replication in restrictive HEL and MEFs cells; however, its acute replication in the eyes and TG of mice was remarkably reduced relative to KOS. The diminished replication of 3Xstop in TG may be attributed to its reduced ocular replication (31), given that the acute TG titers of 3Xstop at days 3 and 5 followed a similar trend for replication in the eyes at days 1 and 5 post-infection (Figure 5.2A, C, and E). This impaired acute replication phenotype both in the eyes and TG likely explains its defect in establishing an efficient latent infection, as similar results have been observed with other mutants of HSV-1 (31, 160). This decrease in the establishment of latency by 3Xstop would be expected to negatively impact reactivation. For this reason, we did not perform *ex vivo* reactivation studies with this mutant.
The deficiency of the 3Xstop mutant in acute replication *in vivo* suggests that the $U_S1.5$ protein lacks a critical function of ICP22. What could this function be? A potential answer is that it is unable to induce VICE domains (Fig. 5.7A and B). Notably, our results provide a finer map of the region of ICP22 required for VICE domain formation, reducing it from the first 146 N-terminal residues as previously described (112) to the

first 89 N-terminal amino acids. Because the functional significance of VICE domains in the HSV-1 life cycle is not yet fully understood, it is possible that the requirement of VICE domains in viral growth could be cell type dependent and specifically required for *in vivo* replication. Thus, this defect in the VICE domains observed with the 3Xstop virus may contribute to its impaired acute replication *in vivo*. Additional studies will be needed to determine the role VICE domains play in HSV-1 replication and how ICP22 facilitates their formation. While VICE domain formation is affected in 3Xstop infected cells, U_S1.5 is expected to modify the C-terminus of the large subunit of the host RNA polymerase II based on ICP22 mapping studies from Steve Rice's laboratory, as residues 147-420 of ICP22 are sufficient to modify RNA Polymerase II (119). Although the mechanism by which ICP22 alters RNA Polymerase II to enhance viral gene expression is unknown, the expected presence of this activity in U_S1.5 may explain the intermediate levels of acute ocular and neuronal replication observed with 3Xstop in mice when compared to KOS and d22.

Although the 3Xstop mutant's expression levels of U_S1.5 protein might be lower than that of ICP22 expressed either from KOS or M90A (Figures 5.1C and 6), the protein is still able to fully carry out some functions of ICP22; these functions include enhancing late viral protein expression, inhibiting ICP0 transactivated gene expression, and largely enabling efficient viral replication in cell culture. Additionally, we also tested if overexpression of U_S1.5 using the HCMV promoter (117) might lead to VICE domain formation in transiently transfected HEL cells. In contrast to ICP22, we did not detect VICE domains in these experiments (data not shown). Thus, while it may be argued that

the expression levels of $U_S1.5$ dictates its ability to complement ICP22's functions, this latter experiment does not support this possibility.

Another plausible explanation for the impaired replication of 3Xstop mutant is related to the host's antiviral IFN response. Specifically, our results demonstrate that the 3Xstop and d22 mutants are hypersensitive to IFN-β in cell culture. Thus, we have identified a new function of ICP22, in that it counteracts the effects of this type I IFN. Interestingly, this phenotype correlated very well with the impaired replication phenotype in the restrictive cell lines HEL and MEFs of the CD-1 mice strain (Figures 5.5 and 5.10) and in MEFs of strain 129 and the neuronal cell line, SK-N-SH (data not shown). On the other hand, the hypersensitivity of both mutants to IFN-β was not detected in the permissive cell line, Vero cells ((58) and data not shown), which are known to have a defect in IFN signaling (226). This could explain, in part, the replication phenotypes of 3Xstop and d22 in mice. Because the decrease in the plaque sizes observed in plaque reduction assays (Figure 5.9) was not accompanied by a similar reduction in viral growth (Figure 5.10) after adding IFN-β, this raises the possibility that the observed phenotype is due to a defect in cell-to-cell spread rather than a defect in viral replication. Whether this function of ICP22 is mediated directly or indirectly through other viral factors will require more studies to address this question. In support of this hypothesis, we couldn't detect a complementation of d22 or 3Xstop replication on IFN-α/β receptors knockout mice derived MEFs (data not shown). What was intriguing is the effect of d22 mutant virus on the IFN-β promoter. When we infected the restrictive cell line HepaRG (data not shown) which stably expresses IFN-β promotor::luciferase construct with KOS, d22, or 3Xstop, we noticed that d22 could induce the IFN-β promoter about 3-fold more

than KOS (Figure 5.11). This observation indicates that ICP22 is required for interfering with the induction of IFN-β promoter during viral infection and strongly suggest that this phenotype is separate from the plaque reduction phenotype mechanistically because the 3Xstop couldn't induce the IFN-β promoter (Figure 5.11). Related to this possibility, the reduction in the levels of the late viral protein, vhs, might partially contribute to this phenotype in case of d22 mutant. vhs is an endoribonuclease that degrades viral and cellular mRNA and is capable of interfering with an interferon induced antiviral state (227). This mechanism is not applicable to the 3Xstop phenotype, which is able to enhance wild type levels of vhs protein (Figure 5.6). Additionally, there could be a potential association between the formation of VICE domains and the interferon response based on published reports that have linked the cellular chaperone machinery to type I IFN (228-230).

It is notable that the acute replication of the ICP22 null mutant, d22, was greatly reduced in the eyes relative to the 3Xstop mutant both at day 1 and at day 3. Consequently, d22 was unable to acutely replicate in TG or establish a detectable latent infection in our experiments. The absence of both ICP22 and $U_S1.5$ in d22 significantly attenuated lytic and latent infections in mice, which mirrors the *in vivo* phenotypes of other ICP22 mutants (106, 118, 221). Many of these mutants do not express optimal levels of late viral genes, including vhs, US11, and/or gC. As previously mentioned, it has been hypothesized that the expression of these late genes is dependent on VICE domain formation and/or the altered modification of the C-terminus of the host RNA polymerase II (231). Ultimately, this defect in late viral gene expression likely reduces d22 growth in mice. Additionally, a reduction in gC levels could thwart the ability of

HSV-1 to counteract complement-mediated neutralization (232-235), which might further contribute to the defective acute replication phenotype of d22 *in vivo*. Lastly, the composition of virions proteins in the ICP22 mutant, 22/*n*199, is altered, and this mutant replicates poorly in mice (106). It was hypothesized that 22/n199 virions are less stable than wild-type virions, and that this contributes to its *in vivo* phenotype. Consequently, it is plausible that the composition of d22 virions is similarly altered, and that this negatively impacts its replication.

Our results did not define a unique function for U_S1.5, or a defect in HSV-1 replication in its absence. This raises the question of why HSV-1 has evolved to express the U_S1.5 protein. One possibility might be that the viral requirement for U_S1.5 is conditional and is enhanced only under certain circumstances during the HSV-1 life cycle. Moreover, while U_S1.5 is not required for HSV-1 replication in our assays, a role for U_S1.5 in the HSV-1 life cycle may be apparent in other models systems or in its natural host, humans. Finally, since we find that many if not most of the known functions of ICP22 can be carried out by U_S1.5, we propose that U_S1.5 can serve as a biological "backup" for ICP22, should the ribosome readthrough be blocked at the translation initiation codon of ICP22.

5.6 Tables

Table 5.1.**Viral pathogenesis scoring of wild-type HSV-1 and ICP22 mutants.**

Virus	KOS	d22	M90A	M90AMR	3Xstop	3XstopMR
Score	2.5±0.5	0±0	2.5±0.5	2.33±0.47	0±0	2.5±0.5

Mice were infected per eye with each virus. Eight days post-infection, mice were scored for gross pathological lesions from 0 to 4, where 0 indicates no signs of infection and 4 indicates >70% removal of the hair between the eyes. n= 5-6 mice per virus, and statistical analyses were done using the Student's *t*-test. Scores are given ± the standard deviation.

Table 5.2. **Plaque reduction assays of KOS and ICP22 mutants in the absence and presence of IFN-β**.

Virus	Ratio –IFN-β/+IFN-β					
	HEL		MEFs (CD-1)		MEFs (129)	
	Expt. 1	Expt. 2	Expt. 1	Expt. 2	Expt. 1	Expt. 2
KOS	6.7	15	6.7	2	37.5	20
d22	50	133	45.5	20	1100	1400
M90A	6.7	6.2	4	6.7	27	35
3Xstop	20	13	14	20	125	175

HEL cells or MEFs cells were infected with serially diluted viruses in the absence or presence of 1000 U/mL of IFN-β. Three days post-infection, cells were fixed and immunostained for plaque formation. Plaques were counted for all samples, and the ratios of plaque numbers between untreated and treated plates were determined. The data shown are results from two independent experiments for each cell line.

6.7 **Figures and Figure legends**

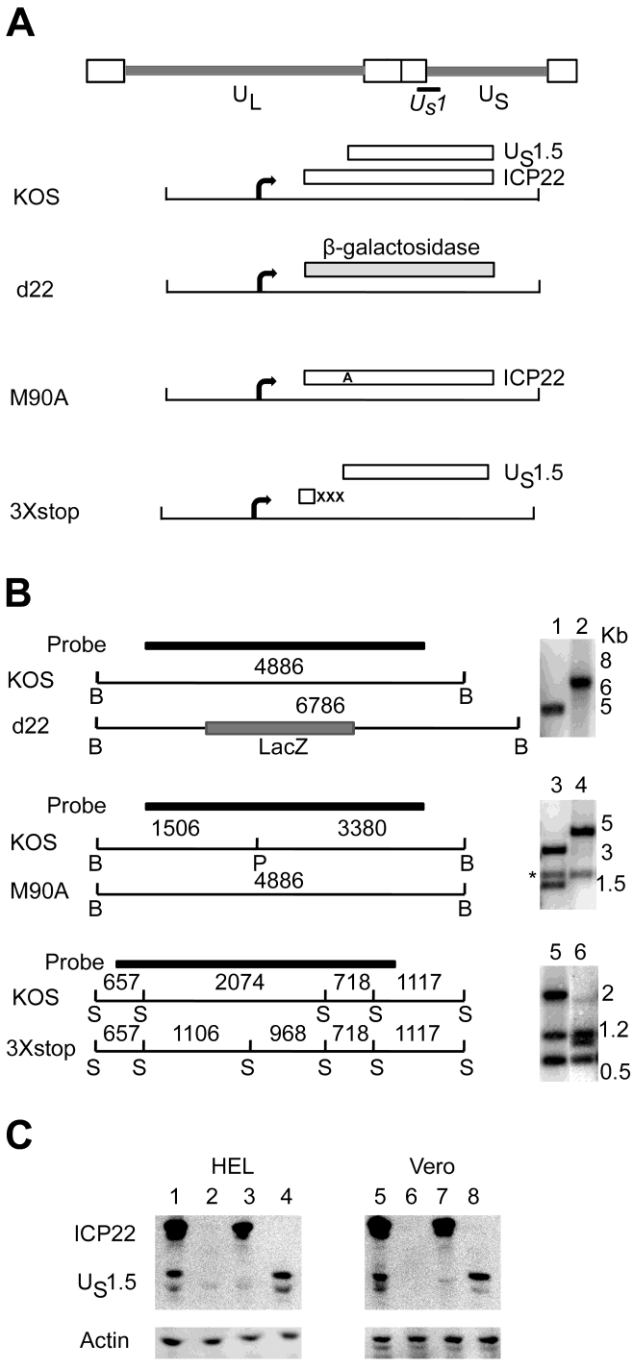

Figure 5.1. **Construction of ICP22 and U_S1.5 mutant viruses**. A) Diagram of the HSV-1 genome showing the *U_S1* gene, which encodes ICP22 and U_S1.5 protein. The open boxes denote the repeated sequences flanking the unique long (U_L) and unique short (U_S) segments. The ICP22-null mutant, d22 has the *lacZ* gene (which codes for β-galactosidase) inserted in place of the ICP22 ORF. M90A is mutated such that only ICP22, but not U_S1.5, is produced as the initiation codon of U_S1.5 is mutated to alanine. 3Xstop produces only U_S1.5, but not ICP22, as this mutant has 3 stop codons inserted upstream of the initiation codon of U_S1.5. B) The restriction enzyme digestion patterns with the fragment lengths (indicated in base pairs) on the left (B: BamHI, P: PciI, S: SacII) and Southern blots shown on the right. The M90A and 3Xstop mutations were designed to eliminate a PciI site or add a SacII site respectively. The lanes are: 1 and 2: KOS and d22, respectively, cut with BamHI; 3 and 4: KOS and M90A, respectively, cut with PciI; 5 and 6: KOS and 3Xstop, respectively, cut with SacII. The star in the second blot denotes a 1.9 kb BamHI fragment of the opposite U_S/R_S junction (119) C) ICP22 and U_S1.5 protein expression of KOS (lanes 1 and 5), d22 (lanes 2 and 6), M90A (lanes 3 and 7), and 3Xstop (lanes 4 and 8) mutant viruses 8 hours post-infection in HEL cells or Vero cells, as determined by western blot analyses.

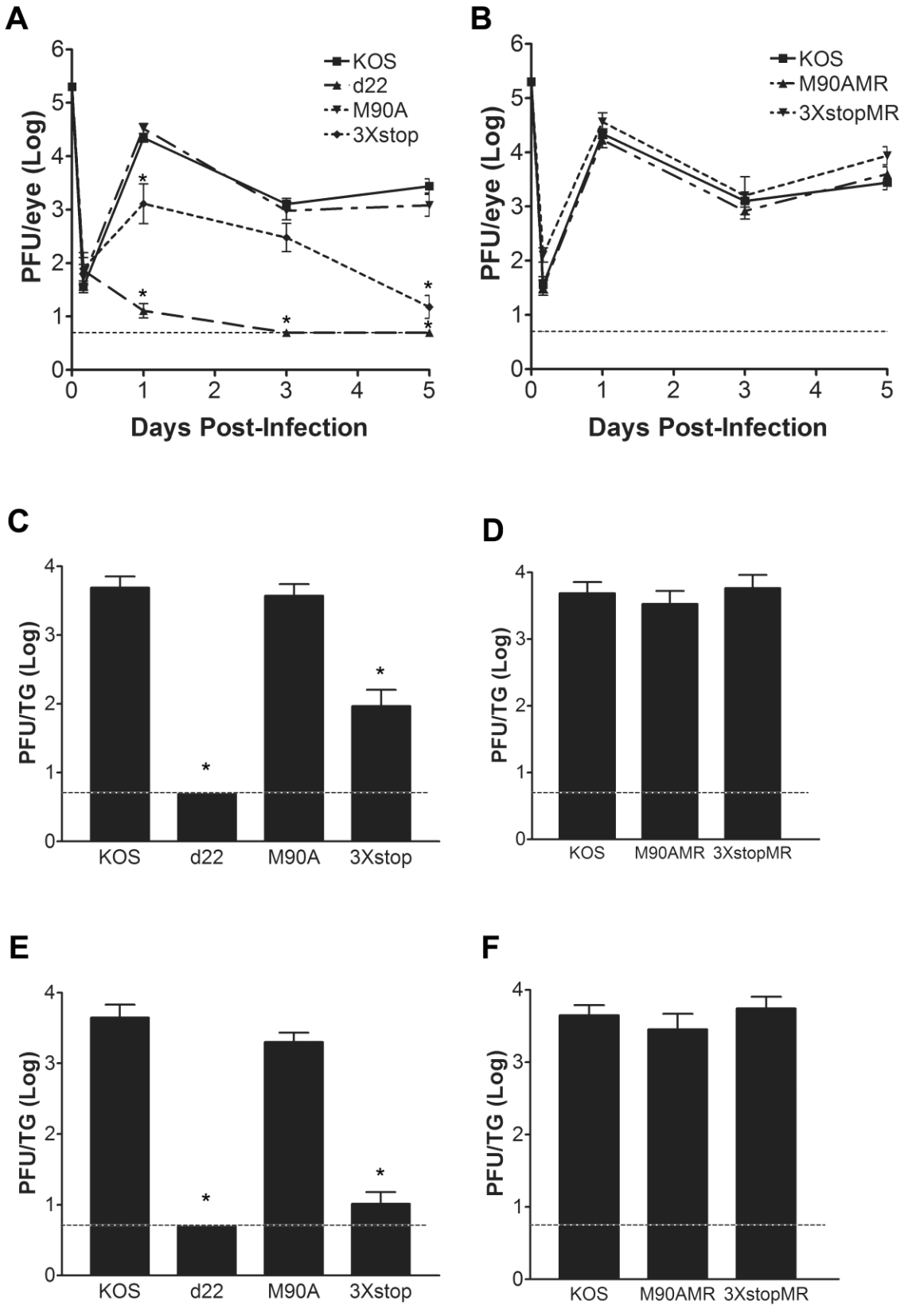
A
PFU/eye (Log)
Days Post-Infection
KOS
d22
M90A
3Xstop
B
PFU/eye (Log)
Days Post-Infection
KOS
M90AMR
3XstopMR
C
PFU/TG (Log)
KOS
d22
M90A
3Xstop
D
PFU/TG (Log)
KOS
M90AMR
3XstopMR
E
PFU/TG (Log)
KOS
d22
M90A
3Xstop
F
PFU/TG (Log)
KOS
M90AMR
3XstopMR

Figure 5.2. **Acute replication of M90A and 3Xstop mutants and MR viruses *in vivo*.** A and B) Acute ocular replication of M90A and 3Xstop mutants and MR viruses in mice. CD-1 mice were infected with $2x10^5$ PFU per eye. At the indicated times points, the eyes of mice were swabbed, and viral titers were determined by standard plaque assays. C - F) Acute TG replication of M90A and 3Xstop mutants and MR viruses in mice. CD-1 mice were infected with $2x10^5$ PFU per eye. On day 3 (C and D) or day 5 (E and F) post-infection, mice were sacrificed, TG were removed and homogenized, and viral titers were determined by standard plaque assays. * Student's *t*-test; $P< 0.05$ compared to KOS. Error bars represent the standard errors of the means (SEMs). In all cases, the dashed line is the limit of detection. n = 8 samples/virus/time point.

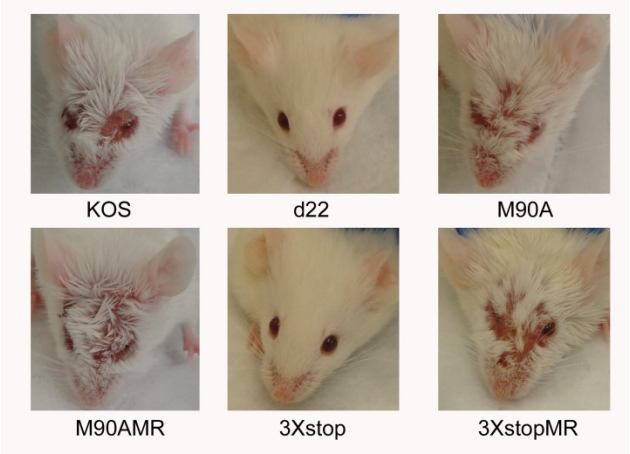

Figure 5.3. **Gross pathological effects of M90A and 3Xstop mutants and MR viruses**. CD-1 mice were infected with $2x10^5$ PFU per eye. Eight days post-infection, a representative picture from each group of mice infected with the designated virus was taken and is shown.

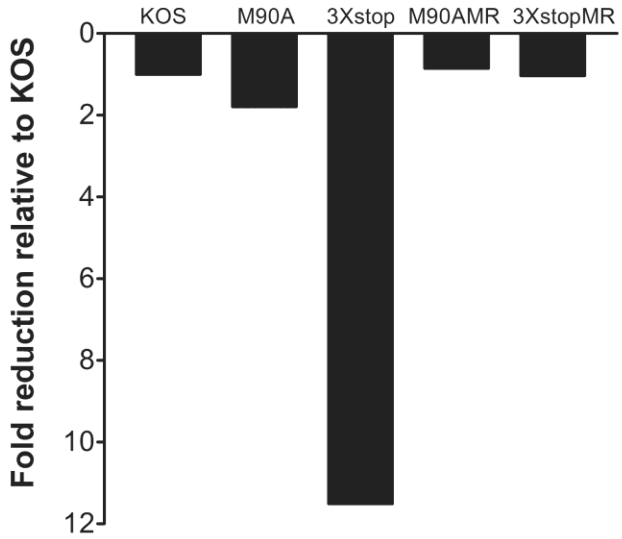

Figure 5.4. **Establishment of latency of M90A and 3Xstop mutants and MR viruses**. CD-1 mice were infected with $2x10^5$ PFU per eye. Twenty-eight days post-infection, mice were sacrificed, TG were removed, and genomic DNA was isolated from samples. The amount of HSV-1 DNA present in each sample was quantified by real time PCR (n=10-12 TG per group). Results shown are the fold reductions compared to KOS. NB. the d22 virus had a fold reduction comparable to the mock infected TG (≥568-fold, Data not shown).

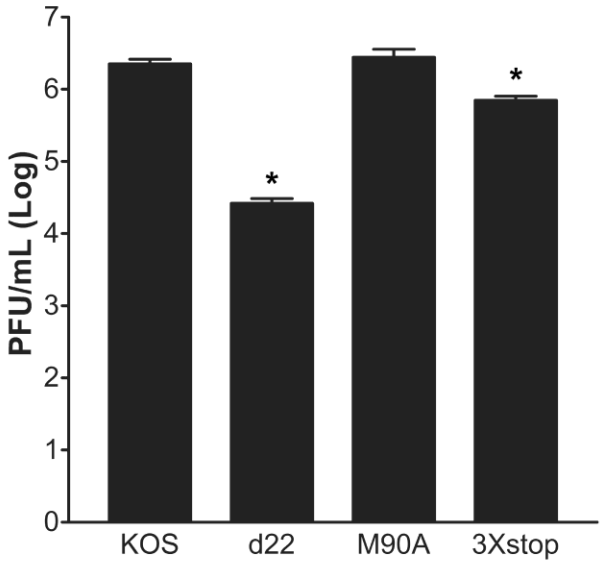

Figure 5.5. **Growth of M90A and 3Xstop mutant viruses on HEL cells**. HEL cells were infected at MOI of 0.1 with the indicated viruses. Twenty-four hours post-infection, cells were harvested, and viral titers were determined by a standard plaque assay. * Student's *t*-test; P< 0.05 compared to KOS. Error bars represent the standard errors of the means (SEMs).

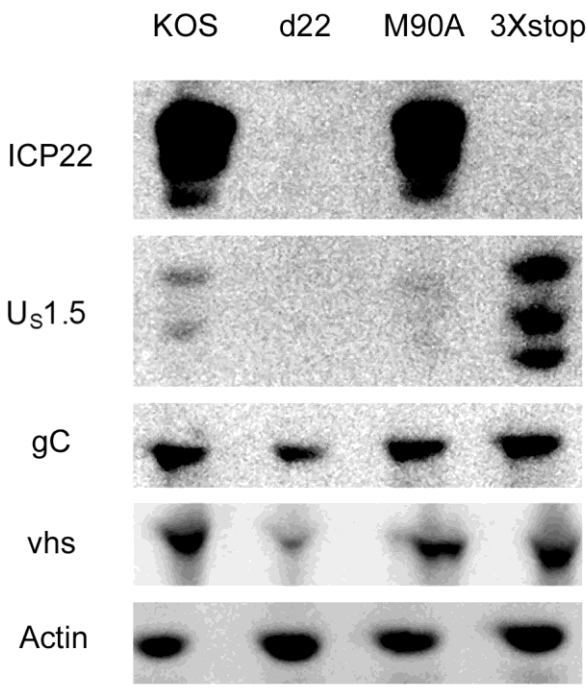

Figure 5.6. **Examination of late viral gene expression for M90A and 3Xstop mutant viruses**. HEL cells were infected at an MOI of 2 with the indicated viruses. Twenty-four hours post-infection, cells were harvested, and protein levels from cell extracts were determined by western blot analysis.

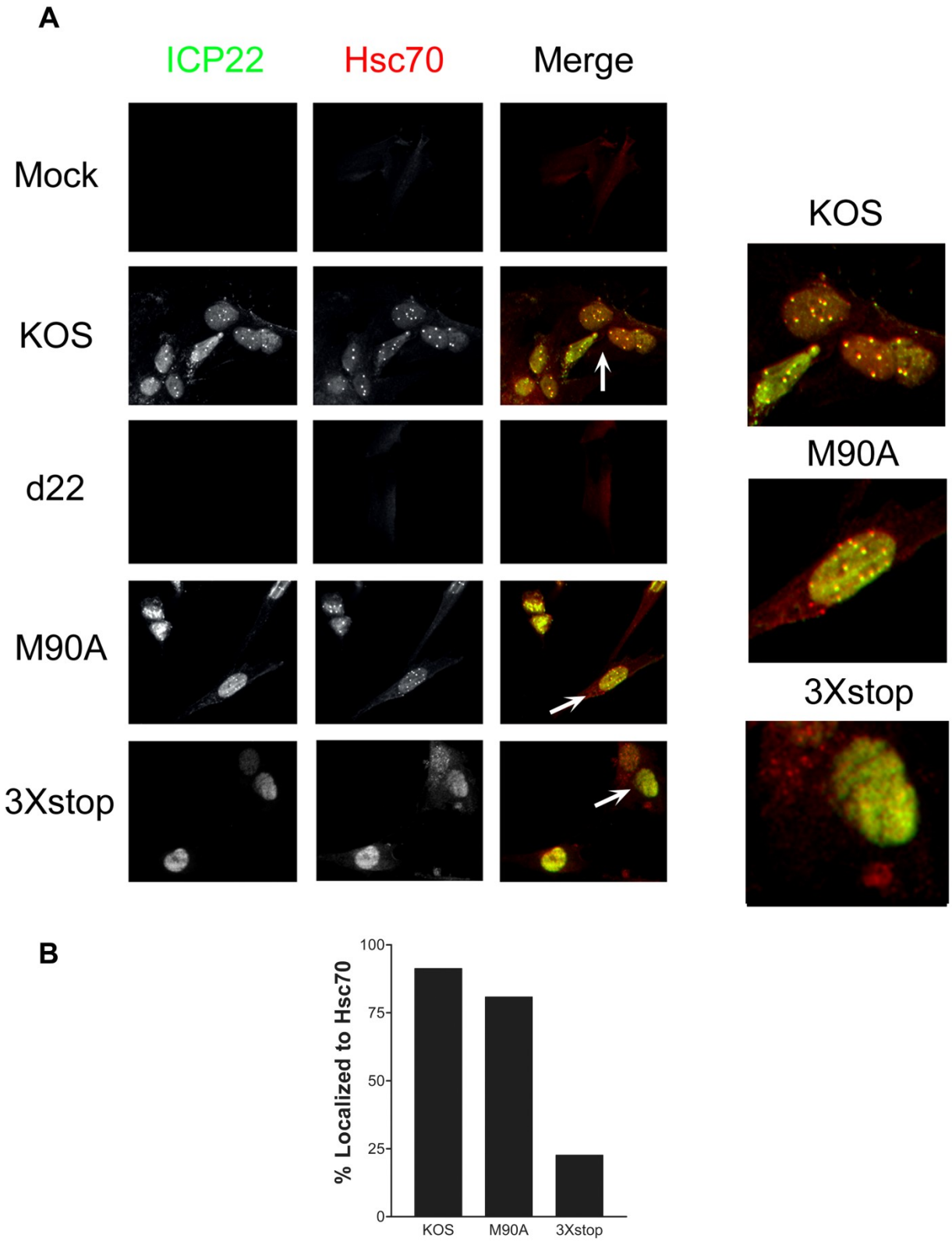
A
ICP22
Hsc70
Merge
Mock
KOS
d22
M90A
3Xstop
KOS
M90A
3Xstop
B
% Localized to Hsc70
100
75
50
25
0
KOS
M90A
3Xstop

Figure 5.7. **ICP22 but not U_S1.5, induces VICE domain formation.** A) HEL cells were mock infected or infected with the indicated viruses at an MOI of 0.1. Twenty-four hours post-infection, cells were fixed and stained for ICP22 and Hsc70 and examined by fluorescence microscopy. B) At least 100 cells that express ICP22 and/or US1.5 were examined for each virus, and the percentage of these cells that colocalized with Hsc70 is shown.

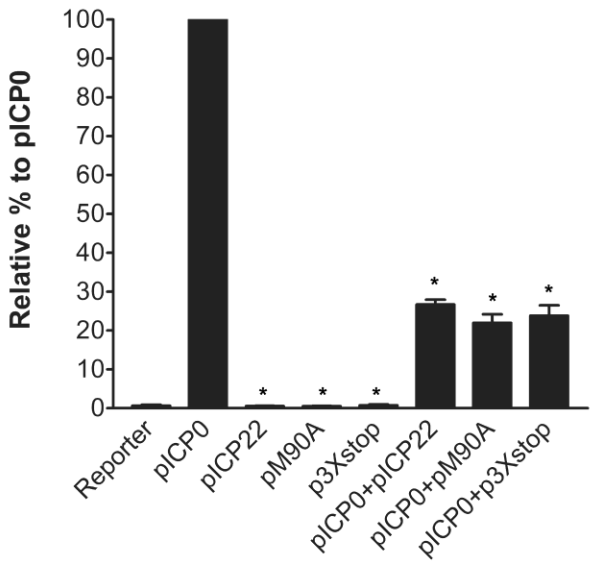

Figure 5.8. **Inhibition of ICP0's transactivated gene expression by vectors that express either ICP22 or U_S1.5**. Vero cells were transfected with an HSV-1 reporter plasmid (50 ng, pGL3-VP16) and a plasmid expressing Wt ICP0 (pICP0), both ICP22 and U_S1.5 (pICP22), ICP22 alone (pM90A), or U_S1.5 alone (p3Xstop) or a combination of pICP0 and pICP22, pM90A, or p3Xstop for 48 hours. Cell extracts were analyzed in luciferase assays to monitor ICP0's transactivating activity. * Mann-Whitney *U* test; $P < 0.05$ compared to pICP0. The error bars indicate the standard errors of the means (SEMs).

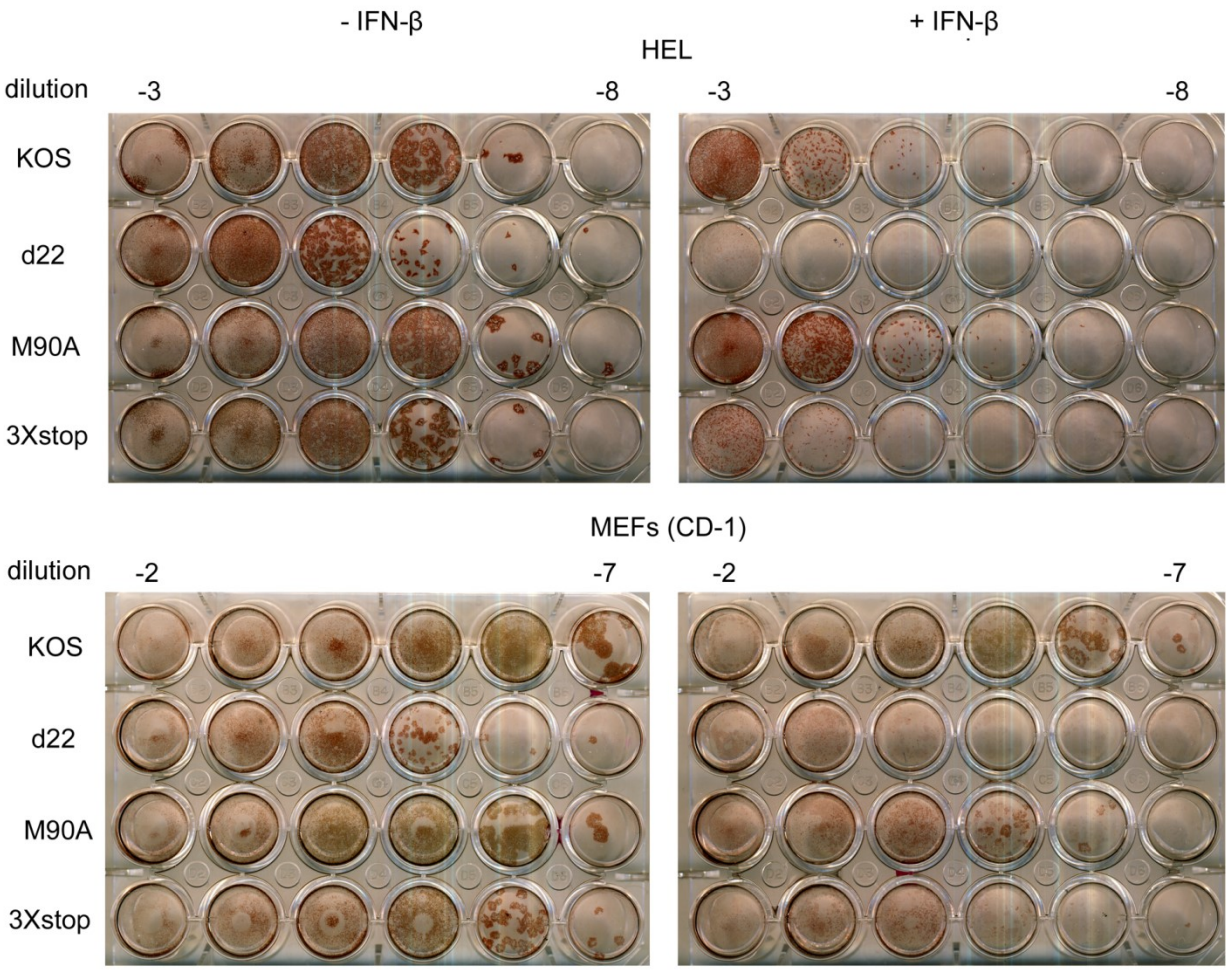

Figure 5.9. **Plaque reduction assay**s. HEL cells or CD-1 MEFs cells were infected with serial dilutions of the indicated viruses in the absence or the presence of 1000 U/mL IFN-β. Three days post-infection, cells were fixed and immunostained for plaque formation.

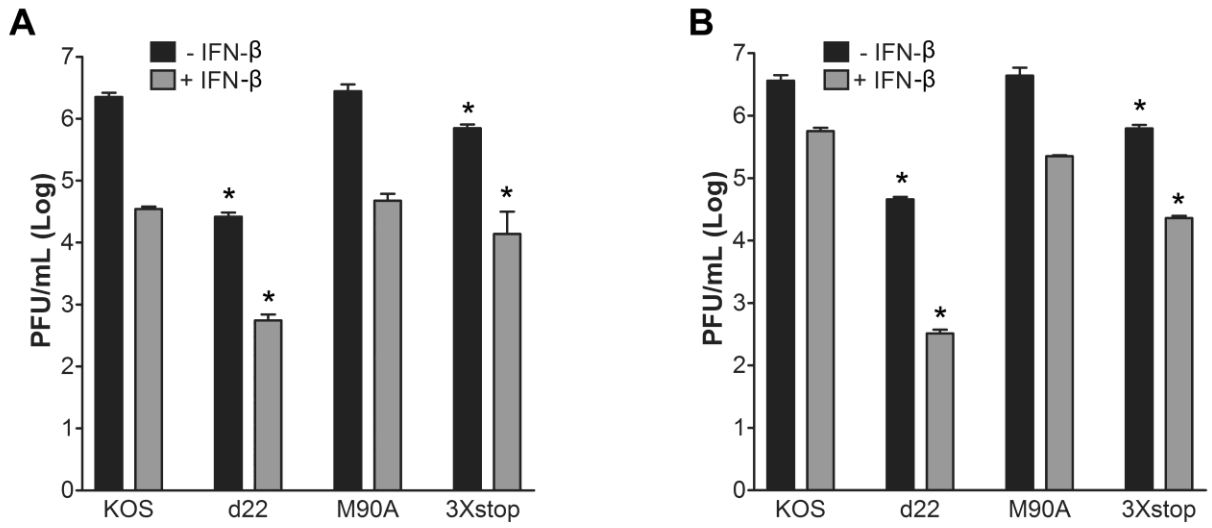

Figure 5.10. **Growth of M90A and 3Xstop with and without IFN-β**. A) HEL cells or B) CD-1 MEFs were infected at MOI of 0.1 in the presence or in the absence of 1000 U/mL IFN-β with the indicated viruses. Twenty-four hours post-infection, cells were collected, and the viral titers were determined by a standard plaque assay. * Student's *t*-test; P< 0.05 compared to KOS. Error bars represent the standard errors of the means (SEMs).

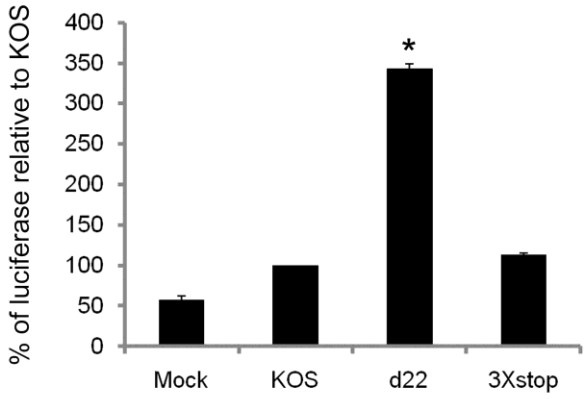

Figure 5.11. **Induction of IFN-β promoter by d22**. HepRG cells, stably expressing Luciferase under the control of IFN-β promoter, were mock infected or infected at MOI of 5 with KOS, d22, or 3Xstop for 24 hours. Cell extracts were analyzed in luciferase assays to monitor the induction of IFN-β promotor. * Mann-Whitney *U* test; $P < 0.05$ compared to KOS. The error bars indicate the standard errors of the means (SEMs).

Chapter 6

Herpes Simplex virus 1 upregulates the expression of p35 and changes the localization of CDK-5 during acute infection of neurons

6.1 Abstract

We previously reported that the cyclin dependent kinase (CDK)-5 activating protein, p35, is an important determinant of acute HSV-1 replication in mice. In order to determine the mechanism by which p35 facilitates acute viral replication in neurons, we examined the expression and localization of p35 and CDK-5 in response to HSV-1 acute infection. Our data showed that HSV-1 infection triggers an increase in p35 protein levels and relocalizes CDK-5 from the nucleus to the cytoplasm in the infected trigeminal ganglia (TG) neurons. As CDK-5 is required for neuronal survival after DNA damage response, and HSV-1 infection is reported to activate the DNA damage response in non-neuronal cell lines, we tested whether HSV-1 infection of TG would trigger the DNA damage response. We observed that infected neurons stained positive for the DNA damage response marker, γH2AX, which is an early event in the DNA damage pathway. On the other hand, where the activated DNA damage response proteins are expected to localize in the nucleus, we noticed that the DNA damage protein, PARP-1, switched from a nuclear to cytoplasmic localization in HSV-1 infected neurons. Consistent with previous studies, we did not detect signs of apoptosis in infected TG. Our data suggest a model in which acute viral infection of neurons upregulates p35 levels to protect neurons from apoptosis by stabilizing and activating

CDK-5 and we propose that the upregulation of p35 is a downstream event to the DNA damage response triggered by viral infection.

6.2 Materials and Methods

Cells and viruses. Two human neuroblastoma cell lines, SK-N-SH and Be-(2)-C cells, were obtained from the American Type Culture Collection (ATCC). SK-N-SH cells were grown in Minimal Essential Medium with Earle's (MEM/EBSS) supplemented with 10% fetal bovine serum (FBS), 2 mM L-glutamine, 100 µg/ml penicillin, and 100 U/ml streptomycin. Be-(2)-C cells were grown in 50% Minimum Essential Medium MEM/EBSS and 50% Ham's F12 supplemented with 10% FBS, and the same concentrations of L-glutamine, and antibiotics as described for SK-N-SH cells. Vero cells were grown in Dulbecco's Modified Eagle's Medium (DMEM) supplemented with 5% fetal bovine serum (FBS), 2 mM L-glutamine, 100 µg/ml penicillin, and 100 U/ml streptomycin. The wild-type HSV-1 strain KOS (passage 11) was used in our study and was propagated and titered on Vero cells.

Acute viral infection of mice. Infections were performed as previously described (92, 236). Briefly, CD-1 outbred female mice (6-7 weeks old) were purchased from Charles Rivers Laboratories (Shrewsbury, MA) and cared for according to Guide for the Care and Use of Laboratory Animals (173). The protocol for using these mice is approved by the University of Kansas Institutional Animal Care and Use Committee. Mice were anesthetized by intraperitoneal injection of ketamine (75-100 mg/kg of body weight) and xylazine (10 mg/kg of body weight). Corneas of mice were scarified with a 26-gauge needle and infected with KOS at $2x10^5$ PFU of virus per eye in 5 µL medium or were mock-infected. TG were collected three days post-infection after euthanizing the mice by CO_2 asphyxiation.

TG immunofluoroscence assays. Harvested TG were immediately fixed in 10% saline-buffered formalin for 16-20 hours. Tissues were then stored in 70% ethanol at 4°C until they were embedded in paraffin. TG were sectioned at 7 μm, and all sections were incubated in xylene for 10 min, 3 times, and then rehydrated through an ethanol series: 100%, 95%, 80%, 70%, and 50%, 5 min each. Sections were then washed in methanol + 0.1% Tween 20 for 15 min on a shaker and then washed twice with methanol, 5 min each. Sections were then washed on a shaker in methanol + 30% hydrogen peroxide (9:1 dilution) for 20 min on the shaker. Samples were boiled in citrate buffer (2.1g citric acid and 1.0g NaOH, in 1L of water, final pH 6) for 25 min in a microwave on high power. Slides were cooled in running distilled water for at least 5 min and washed twice with phosphate buffered saline (PBS), 3 min each. Tissues were incubated with permeablization/blocking buffer (1X PBS, 5% normal goat serum, 0.3% Triton X-100) for 30 min at room temperature. The primary antibody was diluted in PBS (as described below), added to the tissue after removing excess blocking buffer and incubated overnight in a humidity chamber at 4°C. Sections were washed 3 times with PBS for 2 min each. The secondary antibody was diluted in PBS (as described below) and incubated for 1 h at 37°C. Sections were washed in PBS 3 times 2 min each, mounted with Prolong Antifade (Invitrogen), and examined with fluorescence microscopy (Nikon Eclipse TE-2000-U4).

Antibodies used. i) Primary antibodies: ICP0 mouse monoclonal (11060 sc-53070, Santa Cruz Biotechnology) was diluted 1:250; CDK-5 rabbit polyclonal (AHP1270, AbD Serotec) diluted 1:250; CDK-5 rabbit polyclonal (C8 sc-173, Santa Cruz Biotechnology) was diluted 1:250, and p35 rabbit polyclonal (C19 sc-820, Santa Cruz

Biotechnology) was diluted 1:100. HSV-1 rabbit polyclonal (B0114, Dako) was diluted 1:250; PARP-1 rabbit polyclonal,was (237) diluted 1:250; and γH2AX mouse monoclonal (ab18311, Abcam) was diluted 1:150. ii) Secondary antibodies: donkey anti-rabbit dy594 Immunoresearch) diluted 1:1000, donkey anti-mouse dy488 diluted 1:500, and goat anti-rabbit dy594 diluted 1:1000, all obtained from Jackson Immunoresearch.

Western blotting: SK-N-SH and Be-(2)-C cells were plated on 12-well plates at $1x10^5$ cells per well. Twenty-four hours post-plating, cells were infected at an MOI of 2 for each virus. Samples were harvested 24 hours post-infection in 50 µL 1X Laemmli buffer (238) (100ºC) supplemented with 1X protease inhibitors (1µg/mL Leupeptin, 1µg/mL Aprotinin, 1mM PMSF). Samples were heated at 95ºC for 5 min, vortexed, and centrifuged, and resolved on a gradient 4-12% Bis-Tris gel (Novex). Proteins were transferred to nitrocellulose membranes using a semidry transfer unit (GE Health Care, cat. no. TE77). Each membrane was blocked in 5% bovine serum albumin (BSA) in 0.1% Tween-20 diluted in tris-buffered saline (TBS-T) for 1 h at room temperature. Primary antibodies used were: ICP4 mouse monoclonal (H1A021, EastCoast Bio) diluted 1:1000, CDK-5 rabbit polyclonal (C8 sc-173, Santa Cruz Biotechnology) diluted 1:500, p35 rabbit polyclonal (C19 sc-820, Santa Cruz Biotechnology) diluted 1:500, and β-Actin, a rabbit polyclonal antibody (sc-1616, Santa Cruz Biotechnology) diluted 1:1000; The membranes were washed 3 times in TBS-T, and probed with appropriate secondary antibodies: peroxidase conjugated goat anti-rabbit (Jackson Immunoresearch) was diluted 1:1000 and peroxidase conjugated goat anti-mouse (Jackson Immunoresearch) was diluted 1:1000 at room temperature for 1 h.

Membranes were washed 3 times in TBS-T and developed using SuperSignal West Pico chemiluminescent substrate (Thermo Fisher Scientific). Images were captured with a Kodak 4000R image station.

TUNEL assay: Harvested TG were immediately fixed in 10% saline-buffered formalin for 16-20 hours. Tissues were then stored in 70% ethanol at 4°C until they were embedded in paraffin. TG were sectioned at 7 μm and processed following the instructions of Promega DeadEnd^{TM} Fluorometric TUNEL system product G3250. 7134, an ICP0 null mutant virus, was included as a positive control in our staining as this virus has a deletion in LATs as well.

6.3. Results

HSV-1 infection induces p35 protein levels. We previously showed that HSV-1 doesn't replicate efficiently in p35 knockout mice (120). To examine the influence of HSV-1 infection on p35 protein during acute infection of TG, KOS-infected TG were harvested 3 days post-infection, and were sectioned and immuno-stained for both the IE protein, ICP0, which was used as a marker for productively infected neurons, and p35. As shown in Figure 6.1, HSV-1-infected neurons had increased intensity of p35 staining compared to uninfected cells, with a distribution that was primarily cytoplasmic. Similar phenotype was observed in SK-N-SH cells (data not shown). To confirm that the increased intensity for p35 staining was due to elevated p35 protein levels, we performed western blots on mock- and KOS-infected SK-N-SH cell extract samples. As

shown in Figure 6.2, p35 protein was not detected in the mock-infected cells, whereas it was readily detected in HSV-1-infected cells.

HSV-1 infection changes the localization of CDK-5: because the only function of p35 identified so far is being the activating partner for CDK-5, we next wanted to test the effect of HSV-1 acute infection and the associated p35 upregulation on CDK-5 protein. To examine the localization of CDK-5 during acute infection in the TG, mice were infected with KOS for 3 days, and TG sections from these mice were immuno-stained for ICP0, and CDK-5. As shown in Figure 6.3, In contrast to the uninfected neurons where CDK-5 location was primarily nuclear, HSV-1-infected neurons, which stained positive for ICP0, had a CDK-5 localization that was primarily punctate and both cytoplasmic and nuclear. In about 30% of the ICP0-positive neurons, CDK-5 colocalized with ICP0 in the nucleus but showed punctate staining (Figure 6.3).

To test whether this phenotype is accompanied by the degradation of CDK-5, we looked at CDK-5 protein levels after KOS infection in the neuronal cell line SK-N-SH by western blot. As shown in figure 6.3, CDK-5 protein levels were comparable to the mock-infected SK-N-SH cells. This indicates that the alteration in CDK-5 localization observed in figure 6.4 is likely not accompanied by protein degradation.

HSV-1 infection induces the DNA damage response in TG. In order to test the hypothesis that p35 upregulation is a neuronal response to the stress caused by HSV-1 infection which will benefit the viral replication through stabilization of CDK-5, we wanted to examine whether HSV-1 infection triggers a DNA damage response in

infected TG. Previous studies showed that HSV-1 infection induces the DNA damage response in cell culture, an effect that is counteracted by the viral protein, ICP0 (47). To determine whether HSV-1 infection triggers a similar event in infected neurons, KOS-infected TG were isolated 3 days post-infection and immunostained with the DNA damage marker, γH2AX. γH2AX is a histone variant that is the most proximal marker of the DNA damage response and is phosphorylated at serine 139 in response to DNA damage (239-241). Our results showed that neurons stained positive for HSV-1 antigens also stained positive for γH2AX, whereas uninfected neurons had no apparent γH2AX staining (Figure 6.4). This data indicates that acute HSV-1 neuronal infection triggers the DNA damage response.

HSV-1 infection changes the localization of PARP-1 in acutely infected TG. Poly ADP-ribosylation (PAR) is a posttranslational modification which regulates several cellular activities, including DNA damage repair. The PAR polymerase, PARP-1, is one of 17 PAR enzymes that function to transfer the ADP-ribose group from NAD^+ to an acceptor protein ((242, 243) and reviewed in (244)). PARP-1 binds to sites of DNA breaks, depending on the degree of its activation, the cell will either progress to DNA damage repair or apoptosis. PARP-1 is involved in early recruitment of the MRN complex to the sites of DNA damage and is required for rapid accumulation of MRE11 and NBS1(245). A recent study showed that HSV-1 infection activates PARP-1, a phenotype that was dependent on viral DNA replication (49). We examined PARP-1 expression and subcellular localization in infected TG as a marker for the DNA damage response. Once again, KOS-infected TG were harvested at 3 days post-infection and

stained for PARP-1 and ICP0. Un-infected neurons showed PARP-1 nuclear staining, whereas HSV-1-infected neurons (ICP0 positive) showed both nuclear and cytoplasmic punctate PARP-1 staining (Figure 6.5). This phenotype suggests that the change in PARP-1 localization could be a mechanism by which the virus counteracts the activity of PARP-1 in the nucleus to interrupt the DNA damage response. Taken together, our data suggest that HSV-1 infection initiates a DNA damage response in neurons, as indicated by γH2AX staining, which might be counteracted by viral factor(s) that alter PARP-1 localization.

6.4. Discussion

In this study we initially examined the expression and localization of p35 and the cellular kinase, CDK-5 in neurons, in response to acute HSV-1 infection. We showed that p35 protein levels increase in response to HSV-1 acute infection of neurons. In addition, CDK-5 localization was altered in infected cells (nuclear to nuclear and cytoplasmic). CDK-5 is important for neuronal survival in response to stressful conditions, including the DNA damage response (137-141). In this context, HSV-1 infection has been shown to trigger and counteract the DNA damage response in cell culture in non-neuronal cell lines (47, 48, 144, 145, 246); however, the induction of the DNA damage response in neurons using an animal model of infection has not been reported (144). We demonstrated that the most upstream component of the DNA damage response is triggered by HSV-1 in TG (shown as a positive staining of γH2AX), which is apparently counteracted at a downstream step (as suggested by a change in PARP-1 localization). Our study indicates that HSV-1 has evolved mechanisms to

counteract the potential pro-apoptotic pathways and stimulates the pro-survival events during an acute infection of neurons.

What is the mechanism of p35 upregulation during HSV-1 infection? p35 levels are induced secondary to neurotrophic factors that stimulate Extracellular signal Regulated Kinase (ERK)1/2, and this requires the activation of the transcription factor Egr1 (247-249). Interestingly, a previous report has shown that HSV-1 infection activates the ERK/MAPK signaling pathway (250) which may contribute to p35 upregulation. Moreover, it has been shown that HSV-1 lytic infection induces Egr1 in rabbit corneal cells (251). This indicates that enhancing Egr1 in response to HSV-1 infection may be the causative factor of increased p35 levels observed in our study. Moreover, previous reports have shown that p35 expression can be upregulated by oxidative stress in a neuroblastoma cell line (252). Oxidative stress may initiate DNA damage (253) and is reported to enhance the expression of Egr1 (254). In addition, HSV-1 has been shown to induce neuronal oxidative stress (255) in addition to the DNA damage response observed in our study. Taken together, oxidative stress and DNA damage response during acute HSV-1 infection of neurons may stimulate p35 levels through an upregulation of the transcription factor Egr1 (Figure 6.7).

What are the consequences of CDK-5 localization and p35 upregulation during HSV-1 infection? The activity of CDK-5 was shown to directly correlate with the levels of its major activator, p35 (131). In addition, the induction of p35 via nerve growth factor (NGF)/ ERK pathway has been shown to enhance CDK-5 activity (247). Several studies reported that CDK-5/p35 activity counteracts neuronal cell death triggered by the DNA damage response (135, 140). Additionally, published reports have indicated that

cytoplasmic CDK-5 inhibits apoptosis by preventing neurons from entering mitosis (140, 256) and its levels are stabilized by p35 (257). The changes in CDK-5 localization and induction of p35 are consistent with these data, allowing us to propose a model in which HSV-1 stimulates these changes in CDK-5 and p35, stimulating the kinase activity CDK-5, to protect lytically infected neurons from dying while enhancing latent infections (Figure 6.7). In support of this possibility, we examined acutely infected TG neurons for signs of apoptosis 3 days post-infection using TUNEL staining, and we were unable to detect apoptotic neurons (Figure 6.6), as has been previously reported in other studies (258-260). Furthermore, a previous report from our laboratory showed that p35 (and presumably CDK-5) are required for efficient acute ocular and neuronal infection in mice (120), indicating that these proteins play an important role in *in vivo* viral replication. Aberrant pro-apoptotic CDK-5 activity can result when p35 is cleaved to create an N-terminally truncated form, P25 (261), which may induce neuronal death. As the p35 antibody used in our experiments recognizes p35 and p25, our western blots show that only p35 was detected in SK-N-SH and Be-(2)-C cells after HSV-1 infection. This result indicates that HSV-1 infection does not appear to stimulate the cleavage of p35 to p25, thus avoiding the potential deleterious effects of CDK-5 activation by p25.

Several questions remain to be answered including how is p35 upregulated and by which viral factor(s)? What viral factor(s) counteract parts of the DNA damage response in infected neurons? Is CDK-5 kinase activity needed to phosphorylate and modulate viral proteins? Future studies will address these questions.

6.6 **Figures and Figure legends**

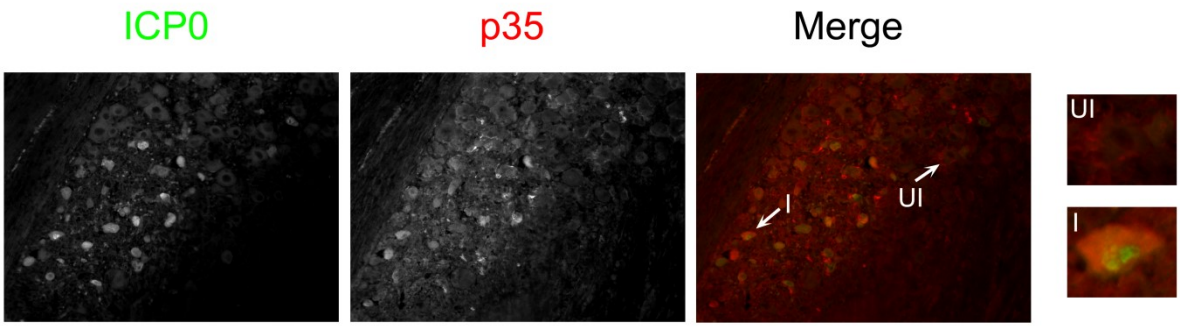

Figure 6.1. p35 localization in response to HSV-1 infection. CD-1 mice were infected with $2x10^5$ PFU per eye. Three days post-infection, mice were sacrificed, and TG were collected, fixed, paraffin embedded, and processed for immunofluorscence staining of ICP0 and p35. UI: an uninfected neuron as indicated by negative staining of ICP0 and consistent with our mock-infected TG sections (data not shown). I: infected neuron as indicated by positive ICP0 staining.

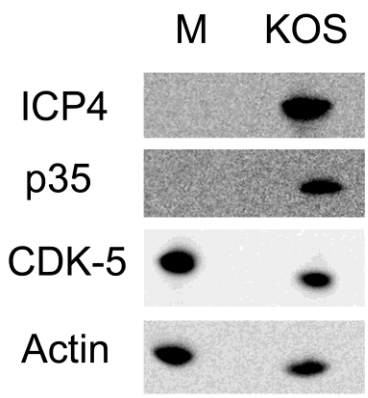

Figure 6.2. p35 and CDK-5 protein levels after KOS infection. SK-N-SH cells were mock infected (M) or infected at an MOI of 2 with KOS. Twenty-four hours post-infection, cells were harvested, and protein levels from cell extracts were determined by western blot analysis.

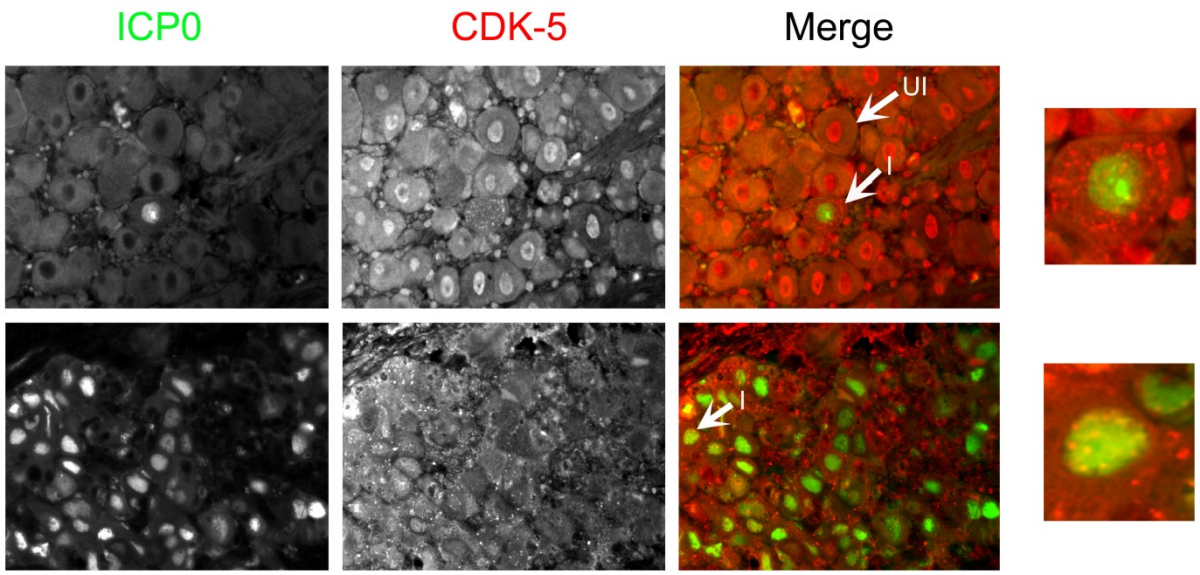

Figure 6.3. CDK-5 localization in response to HSV-1 infection. CD-1 mice were infected with $2x10^5$ PFU per eye. Three days post-infection, mice were sacrificed, and TG were collected, fixed, paraffin embedded, and processed for immunofluorscence staining of ICP0 and CDK-5. UI: an uninfected neuron as indicated by negative staining of ICP0 and consistent with our mock-infected TG sections (data not shown). I: infected neuron as indicated by positive ICP0 staining. Two representative sets of images are shown.

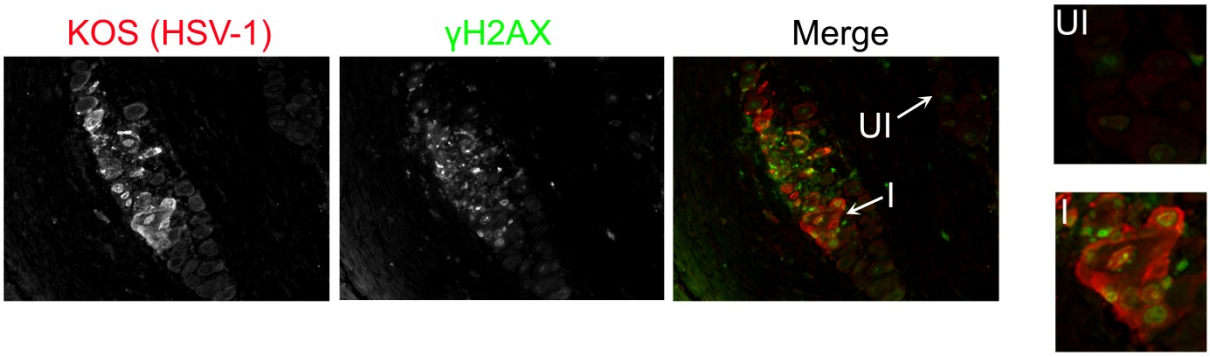

Figure 6.4. DNA damage response to HSV-1 infection. CD-1 mice were infected with KOS at $2x10^5$ PFU per eye. Three days post-infection, mice were sacrificed, and TG were collected, fixed, paraffin embedded, and processed for immunofluoroscence staining of HSV-1 and γH2AX. UI: un-infected neurons as indicated by negative staining of HSV-1 antigens and consistent with our mock-infected TG sections (data not shown). I: infected neurons as indicated by positive staining of HSV-1 antigens.

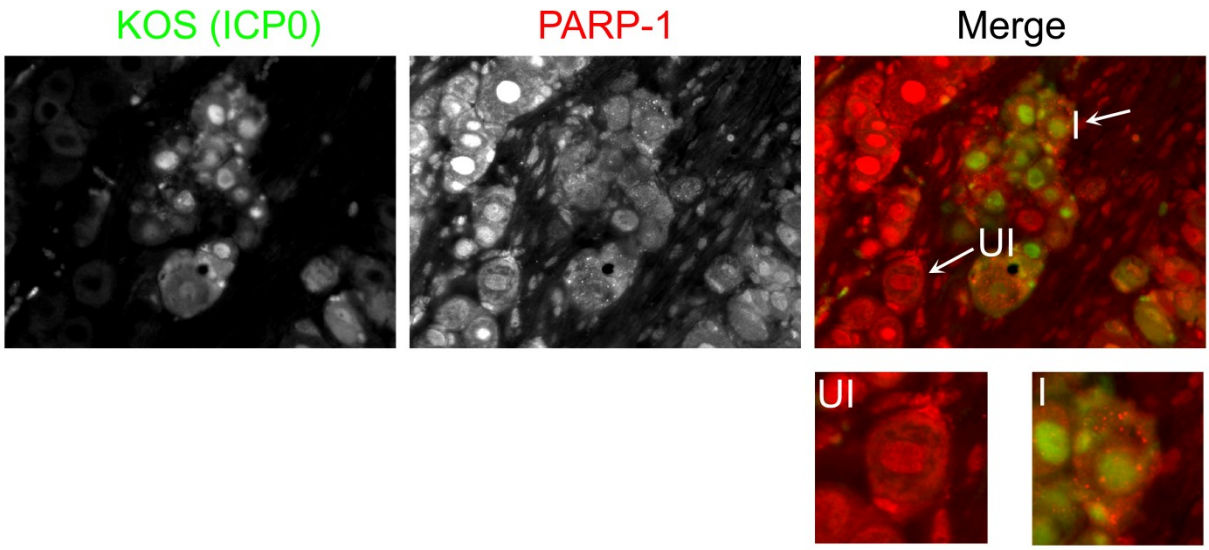

Figure 6.5. PARP-1 staining in response to HSV-1 infection. CD-1 mice were infected with KOS at $2x10^5$ PFU per eye. Three days post-infection, mice were sacrificed and TG were collected, fixed, paraffin embedded, and processed for immunofluorscence staining of ICP0 and PARP-1. UI: un-infected neurons as indicated by negative staining of ICP0, which is consistent with our mock-infected TG sections (data not shown). I: infected neurons as indicated by positive staining of ICP0.

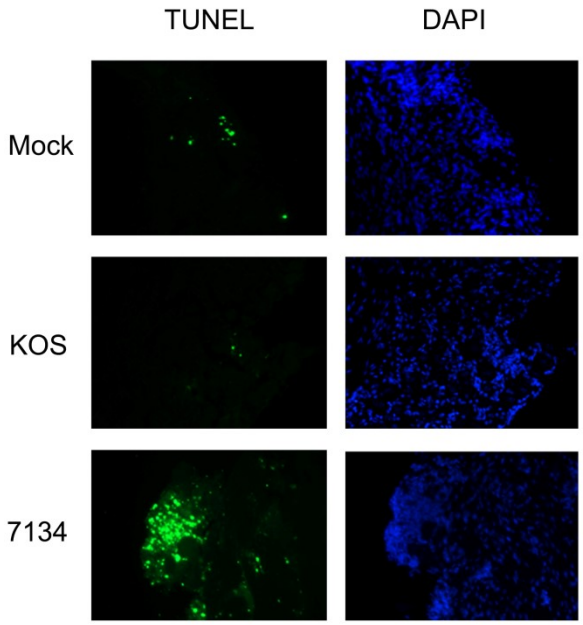

Figure 6.6. TUNEL staining in response to HSV-1 infection. CD-1 mice were infected with KOS at $2x10^5$ PFU per eye. Three days post-infection, mice were sacrificed and TG were collected, fixed, paraffin embedded, and processed for TUNEL staining. 7134 is an ICP0 null mutant included as a control.

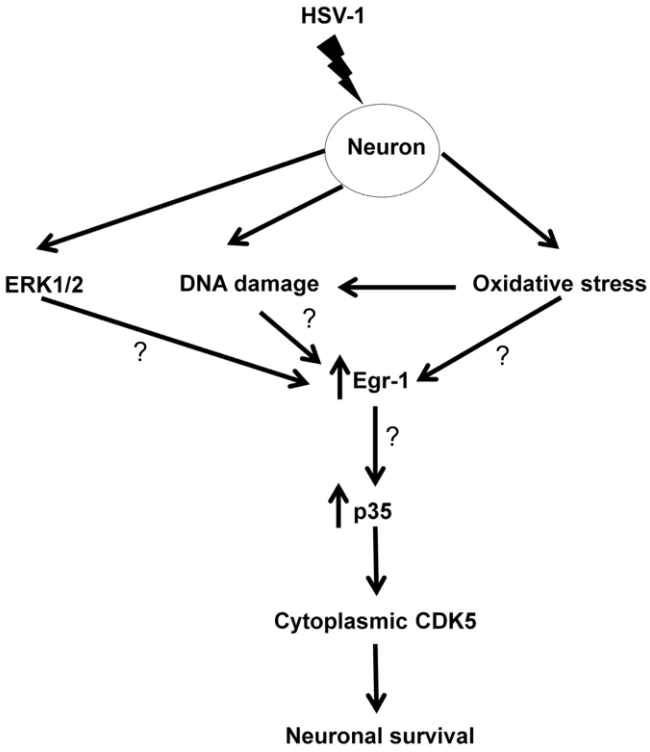

Figure 6.7. Model of p35 upregulation in response to HSV-1 infection. HSV-1 infection of neurons stimulates the ERK pathway, activates at least one component of the DNA damage response, and triggers the oxidative stress response which could lead to DNA damage. This may increase the expression of Egr-1, leading to the induction of p35. Elevated p35 protein levels result in the cytoplasmic localization of CDK-5, which promotes neuronal survival of the infected cell.

Chapter 7

Discussion

Virus-host interactions are important for regulating the HSV-1 life cycle. In understanding the contribution of viral proteins in this process, I studied the role of two key viral IE proteins: infected cell protein 0 (ICP0) and infected cell protein 22 (ICP22). Specifically, I examined how ICP0's functions are regulated via phosphorylation and impact HSV-1 infection, and the role of $U_S1.5$, truncated form of ICP22, in viral replication. I also identified a novel relation between the cellular kinase CDK-5, its activating partner p35 and HSV-1 acute infection of neurons. In addition, I characterized a novel mutation within the viral encoded protein, ICP6 which led to less stable protein, attenuated phenotypes *in vivo,* and a great protective potential making a virus carrying this mutation a great vaccine candidate.

In this dissertation, I showed that ICP0 phosphorylation regulates several of its activity (Chapters 2 and 3). Specifically, one phosphorylation site, S224, appears critical for its E3 Ub ligase activity, transactivation activity, and acute viral replication in cultured cells and in mice (Chapter 3). We propose a potential mechanism by which phosphorylated S224 regulates ICP0's E3 ubiquitin ligase activity, which is by enhancing the contact with the E2 ubiquitin conjugating enzyme, UbcH5a (Chapter 3, Figure 3.12). This observation could explain why the Phos 1 and S224A mutations are impaired for ICP0's E3 ubiquitin ligase activity (Chapter 3, Figure 3.10). The diminished E3 ubiquitin ligase activity of Phos 1likely explains its reduced ability to enhance acute replication and reactivation, while preferentially establishing a latent infection (Chapter 2). Of note, Phos 1 is impaired in its ability to direct the degradation of USP-7compared

to the wild type virus KOS (Chapter 3, Figure 3.6). USP-7 plays a role in transcriptional repression through stabilization of polycomb repressive complex (PRC) subunits (262) and the repressor element 1-silencing transcription factor (REST) (263). As repression of HSV genome is associated with polycomb proteins during viral latency (264, 265). Thus, ICP0 phosphorylation may play a role in mediating the degradation of USP7 in order to counteract this cellular defense mechanism. ICP0 has been shown to be important for reactivation of the quiescent genome (53, 78) by preventing the accumulation of repressive histones marks. Moreover, ICP0 interacts with histone deacetylases (HDACs) causing their relocalization (79). Furthermore, a C-terminal domain in ICP0 binds to the cellular factor RE1-silencing transcription factor corepressor (CoREST) causing disruption of the repressor complex REST/CoREST/ HDAC1/2/LSD1, an activity which was shown to inhibit silencing of the HSV genome (54, 80). Interestingly, the ring finger domain of ICP0 was shown to be critical and more important than the CoREST binding domain for disrupting this complex (78). Thus, I propose that the inability of Phos 1 to direct the degradation of USP-7 might be related to its inability to counteract the cellular transcription repressive mechanisms in acutely infected neurons and reactivation (Figure 7.1). Future studies would be to examine the capability of Phos 1 in reversing the silencing or inhibiting hetero-chromatinization of viral genomes during acute and latent infection.

In addition to ICP0, I discovered a new role for the viral encoded protein, ICP22, in counteracting the type 1interferon (IFN) response. Plaque reduction assays (Chapter 5, Figure 5.9) showed that the plaque sizes of both d22 ($ICP22^{-}$ / $U_S1.5^{-}$) and 3Xstop ($ICP22^{-}$/ $U_S1.5^{+}$) mutants were reduced relative to the wild type HSV-1 plaques on

several restrictive cell lines. Interestingly, the size of plaques of 3Xstop mutant on HEL cells was comparable to the wild type plaques prior to IFN-β treatment. After the addition of IFN-β, the plaque sizes of d22 and 3Xstop mutants were remarkably reduced compared to wild type HSV-1.Surprisingly, the growth yield assays failed to correlate to the plaquing phenotypes in the presence of IFN-β and complementation of viral replication was not observed on MEFs of α/β IFN receptors knockout mice (unpublished data). These results suggest that plaque size in IFN-β-treated cells can be independent from viral replication. Interestingly, these data indicate that IFN-β triggers a cell to cell spread restriction factor against HSV-1 that is counteracted directly or indirectly by ICP22 (Figure 7.1). In the context of *in vivo* replication, viral spread from cell to cell is very important specifically because HSV-1 spreads locally and doesn't usually reach the blood stream or cause viremia (266). This might explain the difference between the phenotypes of ICP22 mutants in cell culture and *in vivo*. Cell culture studies showed only ~100-fold reduction in acute replication of d22 in restrictive cell lines, whereas 3Xstop replication was reduced 4 fold. *In vivo* phenotypes were more apparent. 3Xstop replication was reduced 17- to 184-fold at days 1 and 5 post-infection in the eyes and 59-to 429-fold in TG at days 3 and 5 post-infection relative to wild type HSV-1. The d22 acute replication in the eyes by 1722, 255 and 554 at days 1, 3, and 5 post-infection, and acute replication in the TG was undetectable. More experiments are required to characterize the IFN stimulated restriction factor/s responsible for limiting HSV-1 cell to cell spread.

Related to an established type I IFN response, I also noticed that ICP22 inhibits stimulation of the IFN-β promoter in response to viral infection (Chapter 5, Figure 5.11).

This novel phenotype was only apparent when full length ICP22 protein was not expressed in cells (data not shown). This may explain the defective replication capabilities of d22 in restrictive cell lines and *in vivo* versus the permissive Vero cells, which cannot stimulate type 1 IFNs in response to viral infection (226) (Figure 7.1). In addition, my data confined the region of ICP22 required for the formation of VICE domains to the first 89 AA (Figure 7.1) and highlighted that the regulation of the translocation of one VICE domains marker, Hsc70, to the nucleus is separate from the formation of VICE domains (Chapter 5, Figure 5.7). This observation is important as the inability to form VICE domains with the 3Xstop mutant correlated with a decrease in acute viral growth in mice, suggesting a possible role for VICE domains in enhancing *in vivo* viral replication. Future studies will examine this possibility.

Lastly, in examining the contribution of host factors in the HSV-1 life cycle, I characterized the interrelationship between HSV-1 acute neuronal infection and the cyclin dependent kinase-5 (CDK-5)/ p35 and DNA damage response (Chapter 6). CDK-5/p35 are necessary for efficient HSV-1 replication in mice (120), and I wanted to examine whether their properties were altered during productive infection *in vivo*. Upon lytic infection of neurons, I observed an increase in the protein levels of the CDK-5 activating protein, p35 and a change in the localization of CDK-5 (Chapter 6, Figures 6.1 and 6.4). Furthermore, I detected activation of the DNA damage marker, γH2AX (Figure 6.7). Studying the role of cellular factors in the HSV-1 replication in neuronal cell lines versus neurons *in vivo* has been challenging as the regulation or properties of the cellular factors in HSV-1 replication may not be apparent in proliferating neuroblastoma cells. For instance, we were unable to detect a defect in viral replication when CDK-5

was depleted in the neuronal cell line, SK-N-SH (data not shown). This result contrasts with the *in vivo* defect in HSV-1 replication in p35 knockout mice (120). Together these observations highlight the great difference between the behavior of post-mitotic neurons and neuronal cell lines and indicate that there is a lack of a robust system to study the biology of HSV-1 in neurons, which is a great limitation in the HSV-1 field.

My dissertation illustrates the importance of conducting *in vivo* studies to characterize the biological impact of a certain mutation of a viral encoded protein. E.g. KOS.NA behaved like wild type virus in all the cell culture based experiment (data not shown) and was severely attenuated in mice with a great protective potential as a vaccine (chapter 4 and unpublished data). Additionally, the phosphorylation mutant, Phos 2 was not impaired in replication in cell culture (91) and was impaired in acute replication in TG and in reactivation from latency (chapter 2). My data also highlights that variables exist between different cell lines, a phenotype which was noticed with ICP0 mutants as well as ICP22 mutants, and indicates the importance of choosing an appropriate cell line when characterizing a particular function or diagnosing the behavior of a certain mutant.

Figures and Figure legends

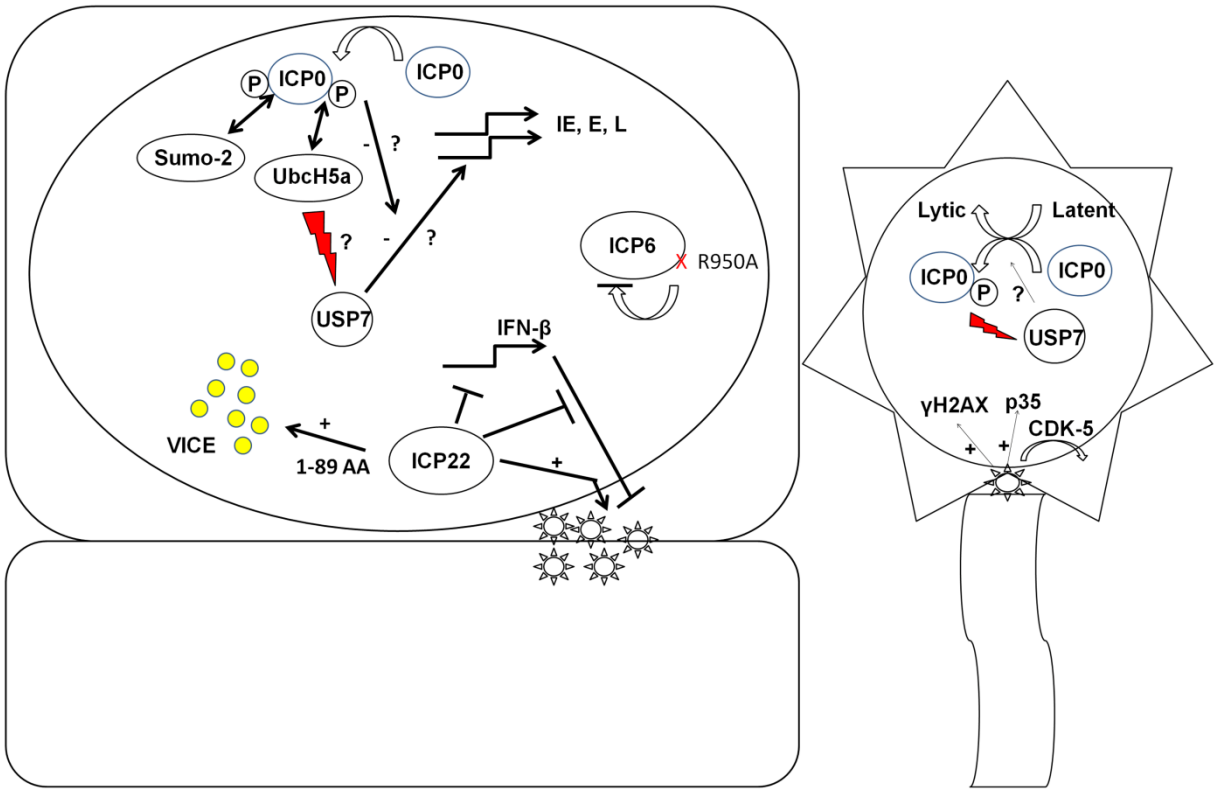

Figure 7.1. **Summary and hypothesized models**. ICP0 phosphorylation enhances the contact with the E2 enzyme, UbcH5a, directing the degradation of USP7. Degradation of USP7 inhibits its transcriptional repressive activities and consequently reduce viral genome repression and directs the virus to a lytic versus latent infection. Phosphorylation of region 2 of ICP0 enhances the contact with Sumo-2 (refer to Figure 2.6). ICP22 is required for enhancing viral cell to cell spread, counteracting IFN-β mediated restriction of cell to cell spread, and inhibiting the activation of IFN-β promoter. The first 89 AA of ICP22 are required for the formation of VICE domains (refer to Chapter 5). HSV-1 acute infection of neurons induces an upregulation of γH2AX and

p35 and changes the localization of CDK-5 (refer to Chapter 6). R950H mutation in ICP6 reduces ICP6 protein levels, attenuating acute viral replication, latency, and reactivation (refer to Chapter 4).

References

1. **Roizman R. KDM, Whitley R. J. .** 2007. Herpes simplex viruses, p. 2501–2601. *In* Knipe D. M. HPM (ed.), Fields virology, vol. 2. Lippincott Williams & Wilkins, New York, NY.
2. **Kimberlin DW.** 2005. Herpes simplex virus infections in neonates and early childhood. Seminars in pediatric infectious diseases **16:**271-281.
3. **Dupuis S, Jouanguy E, Al-Hajjar S, Fieschi C, Al-Mohsen IZ, Al-Jumaah S, Yang K, Chapgier A, Eidenschenk C, Eid P, Al Ghonaium A, Tufenkeji H, Frayha H, Al-Gazlan S, Al-Rayes H, Schreiber RD, Gresser I, Casanova JL.** 2003. Impaired response to interferon-alpha/beta and lethal viral disease in human STAT1 deficiency. Nature genetics **33:**388-391.
4. **Dorsky DI, Crumpacker CS.** 1987. Drugs five years later: acyclovir. Annals of internal medicine **107:**859-874.
5. **Andrei G, Snoeck R.** 2013. Herpes simplex virus drug-resistance: new mutations and insights. Current opinion in infectious diseases **26:**551-560.
6. **Richter ER, Dias JK, Gilbert JE, 2nd, Atherton SS.** 2009. Distribution of herpes simplex virus type 1 and varicella zoster virus in ganglia of the human head and neck. The Journal of infectious diseases **200:**1901-1906.
7. **Wysocka J, Herr W.** 2003. The herpes simplex virus VP16-induced complex: the makings of a regulatory switch. Trends in biochemical sciences **28:**294-304.
8. **Roizman B, Gu H, Mandel G.** 2005. The first 30 minutes in the life of a virus: unREST in the nucleus. Cell Cycle **4:**1019-1021.
9. **Smith CA, Bates P, Rivera-Gonzalez R, Gu B, DeLuca NA.** 1993. ICP4, the major transcriptional regulatory protein of herpes simplex virus type 1, forms a tripartite complex with TATA-binding protein and TFIIB. Journal of virology **67:**4676-4687.
10. **Carrozza MJ, DeLuca NA.** 1996. Interaction of the viral activator protein ICP4 with TFIID through TAF250. Molecular and cellular biology **16:**3085-3093.
11. **DeLuca NA, McCarthy AM, Schaffer PA.** 1985. Isolation and characterization of deletion mutants of herpes simplex virus type 1 in the gene encoding immediate-early regulatory protein ICP4. Journal of virology **56:**558-570.
12. **Sandri-Goldin RM.** 2011. The many roles of the highly interactive HSV protein ICP27, a key regulator of infection. Future microbiology **6:**1261-1277.
13. **Bauer D, Tampe R.** 2002. Herpes viral proteins blocking the transporter associated with antigen processing TAP--from genes to function and structure. Current topics in microbiology and immunology **269:**87-99.
14. **Antinone SE, Smith GA.** 2010. Retrograde axon transport of herpes simplex virus and pseudorabies virus: a live-cell comparative analysis. Journal of virology **84:**1504-1512.
15. **Bertke AS, Swanson SM, Chen J, Imai Y, Kinchington PR, Margolis TP.** 2011. A5-positive primary sensory neurons are nonpermissive for productive infection with herpes simplex virus 1 in vitro. Journal of virology **85:**6669-6677.
16. **Stevens JG.** 1987. Defining herpes simplex genes involved in neurovirulence and neuroinvasiveness. Current eye research **6:**63-67.

17. **Knipe DM, Cliffe A.** 2008. Chromatin control of herpes simplex virus lytic and latent infection. Nature reviews. Microbiology **6:**211-221.
18. **Bloom DC, Giordani NV, Kwiatkowski DL.** 2010. Epigenetic regulation of latent HSV-1 gene expression. Biochimica et biophysica acta **1799:**246-256.
19. **Trousdale MD, Steiner I, Spivack JG, Deshmane SL, Brown SM, MacLean AR, Subak-Sharpe JH, Fraser NW.** 1991. In vivo and in vitro reactivation impairment of a herpes simplex virus type 1 latency-associated transcript variant in a rabbit eye model. Journal of virology **65:**6989-6993.
20. **Carpenter D, Hsiang C, Brown DJ, Jin L, Osorio N, BenMohamed L, Jones C, Wechsler SL.** 2007. Stable cell lines expressing high levels of the herpes simplex virus type 1 LAT are refractory to caspase 3 activation and DNA laddering following cold shock induced apoptosis. Virology **369:**12-18.
21. **Branco FJ, Fraser NW.** 2005. Herpes simplex virus type 1 latency-associated transcript expression protects trigeminal ganglion neurons from apoptosis. Journal of virology **79:**9019-9025.
22. **Wang QY, Zhou C, Johnson KE, Colgrove RC, Coen DM, Knipe DM.** 2005. Herpesviral latency-associated transcript gene promotes assembly of heterochromatin on viral lytic-gene promoters in latent infection. Proceedings of the National Academy of Sciences of the United States of America **102:**16055-16059.
23. **Umbach JL, Kramer MF, Jurak I, Karnowski HW, Coen DM, Cullen BR.** 2008. MicroRNAs expressed by herpes simplex virus 1 during latent infection regulate viral mRNAs. Nature **454:**780-783.
24. **Kriesel JD.** 2002. The roles of inflammation, STAT transcription factors, and nerve growth factor in viral reactivation and herpes keratitis. DNA and cell biology **21:**475-481.
25. **Perng GC, Jones C.** 2010. Towards an understanding of the herpes simplex virus type 1 latency-reactivation cycle. Interdisciplinary perspectives on infectious diseases **2010:**262415.
26. **Sawtell NM, Triezenberg SJ, Thompson RL.** 2011. VP16 serine 375 is a critical determinant of herpes simplex virus exit from latency in vivo. Journal of neurovirology **17:**546-551.
27. **Danaher RJ, Cook RK, Wang C, Triezenberg SJ, Jacob RJ, Miller CS.** 2013. C-terminal trans-activation sub-region of VP16 is uniquely required for forskolin-induced herpes simplex virus type 1 reactivation from quiescently infected-PC12 cells but not for replication in neuronally differentiated-PC12 cells. Journal of neurovirology **19:**32-41.
28. **Halford WP, Schaffer PA.** 2001. ICP0 is required for efficient reactivation of herpes simplex virus type 1 from neuronal latency. Journal of virology **75:**3240-3249.
29. **Webre JM, Hill JM, Nolan NM, Clement C, McFerrin HE, Bhattacharjee PS, Hsia V, Neumann DM, Foster TP, Lukiw WJ, Thompson HW.** 2012. Rabbit and mouse models of HSV-1 latency, reactivation, and recurrent eye diseases. Journal of biomedicine & biotechnology **2012:**612316.

30. **Sacks WR, Schaffer PA.** 1987. Deletion mutants in the gene encoding the herpes simplex virus type 1 immediate-early protein ICP0 exhibit impaired growth in cell culture. Journal of virology **61:**829-839.
31. **Leib DA, Coen DM, Bogard CL, Hicks KA, Yager DR, Knipe DM, Tyler KL, Schaffer PA.** 1989. Immediate-early regulatory gene mutants define different stages in the establishment and reactivation of herpes simplex virus latency. Journal of virology **63:**759-768.
32. **Cai WZ, Schaffer PA.** 1989. Herpes simplex virus type 1 ICP0 plays a critical role in the de novo synthesis of infectious virus following transfection of viral DNA. Journal of virology **63:**4579-4589.
33. **Cai W, Schaffer PA.** 1992. Herpes simplex virus type 1 ICP0 regulates expression of immediate-early, early, and late genes in productively infected cells. Journal of virology **66:**2904-2915.
34. **Maul GG, Ishov AM, Everett RD.** 1996. Nuclear domain 10 as preexisting potential replication start sites of herpes simplex virus type-1. Virology **217:**67-75.
35. **Maul GG, Guldner HH, Spivack JG.** 1993. Modification of discrete nuclear domains induced by herpes simplex virus type 1 immediate early gene 1 product (ICP0). Journal of General Virology **74:**2679-2690.
36. **Maul GG, Guldner HH, Spivack JG.** 1993. Modification of discrete nuclear domains induced by herpes simplex virus type 1 immediate early gene 1 product (ICP0). The Journal of general virology **74 (Pt 12):**2679-2690.
37. **Maul GG, Everett RD.** 1994. The nuclear location of PML, a cellular member of the C3HC4 zinc-binding domain protein family, is rearranged during herpes simplex virus infection by the C3HC4 viral protein ICP0. The Journal of general virology **75 (Pt 6):**1223-1233.
38. **Everett RD, Freemont P, Saitoh H, Dasso M, Orr A, Kathoria M, Parkinson J.** 1998. The disruption of ND10 during herpes simplex virus infection correlates with the Vmw110- and proteasome-dependent loss of several PML isoforms. Journal of virology **72:**6581-6591.
39. **Everett RD, Earnshaw WC, Findlay J, Lomonte P.** 1999. Specific destruction of kinetochore protein CENP-C and disruption of cell division by herpes simplex virus immediate-early protein Vmw110. The EMBO journal **18:**1526-1538.
40. **Lomonte P, Sullivan KF, Everett RD.** 2001. Degradation of nucleosome-associated centromeric histone H3-like protein CENP-A induced by herpes simplex virus type 1 protein ICP0. The Journal of biological chemistry **276:**5829-5835.
41. **Lomonte P, Morency E.** 2007. Centromeric protein CENP-B proteasomal degradation induced by the viral protein ICP0. FEBS letters **581:**658-662.
42. **Everett RD.** 2000. ICP0 induces the accumulation of colocalizing conjugated ubiquitin. Journal of virology **74:**9994-10005.
43. **Boutell C, Everett RD.** 2003. The herpes simplex virus type 1 (HSV-1) regulatory protein ICP0 interacts with and Ubiquitinates p53. J Biol Chem **278:**36596-36602.

44. **Boutell C, Canning M, Orr A, Everett RD.** 2005. Reciprocal activities between herpes simplex virus type 1 regulatory protein ICP0, a ubiquitin E3 ligase, and ubiquitin-specific protease USP7. Journal of virology **79:**12342-12354.
45. **Lees-Miller SP, Long MC, Kilvert MA, Lam V, Rice SA, Spencer CA.** 1996. Attenuation of DNA-dependent protein kinase activity and its catalytic subunit by the herpes simplex virus type 1 transactivator ICP0. Journal of virology **70:**7471-7477.
46. **Parkinson J, Lees-Miller SP, Everett RD.** 1999. Herpes simplex virus type 1 immediate-early protein vmw110 induces the proteasome-dependent degradation of the catalytic subunit of DNA-dependent protein kinase. Journal of virology **73:**650-657.
47. **Lilley CE, Chaurushiya MS, Boutell C, Everett RD, Weitzman MD.** 2011. The intrinsic antiviral defense to incoming HSV-1 genomes includes specific DNA repair proteins and is counteracted by the viral protein ICP0. PLoS pathogens **7:**e1002084.
48. **Lilley CE, Chaurushiya MS, Boutell C, Landry S, Suh J, Panier S, Everett RD, Stewart GS, Durocher D, Weitzman MD.** 2010. A viral E3 ligase targets RNF8 and RNF168 to control histone ubiquitination and DNA damage responses. The EMBO journal **29:**943-955.
49. **Grady SL, Hwang J, Vastag L, Rabinowitz JD, Shenk T.** 2012. Herpes simplex virus 1 infection activates poly(ADP-ribose) polymerase and triggers the degradation of poly(ADP-ribose) glycohydrolase. Journal of virology **86:**8259-8268.
50. **Cliffe AR, Knipe DM.** 2008. Herpes simplex virus ICP0 promotes both histone removal and acetylation on viral DNA during lytic infection. Journal of virology **82:**12030-12038.
51. **Coleman HM, Connor V, Cheng ZS, Grey F, Preston CM, Efstathiou S.** 2008. Histone modifications associated with herpes simplex virus type 1 genomes during quiescence and following ICP0-mediated de-repression. The Journal of general virology **89:**68-77.
52. **Ferenczy MW, DeLuca NA.** 2009. Epigenetic modulation of gene expression from quiescent herpes simplex virus genomes. J Virol **83:**8514-8524.
53. **Ferenczy MW, DeLuca NA.** 2011. Reversal of heterochromatic silencing of quiescent herpes simplex virus type 1 by ICP0. J Virol **85:**3424-3435.
54. **Gu H, Roizman B.** 2007. Herpes simplex virus-infected cell protein 0 blocks the silencing of viral DNA by dissociating histone deacetylases from the CoREST-REST complex. Proceedings of the National Academy of Sciences of the United States of America **104:**17134-17139.
55. **Harle P, Sainz B, Jr., Carr DJ, Halford WP.** 2002. The immediate-early protein, ICP0, is essential for the resistance of herpes simplex virus to interferon-alpha/beta. Virology **293:**295-304.
56. **Leib DA, Harrison TE, Laslo KM, Machalek MA, Moorman NJ, Virgin HW.** 1999. Interferons regulate the phenotype of wild-type and mutant herpes simplex viruses in vivo. J Exp Med **189:**663-672.

57. **Melroe GT, DeLuca NA, Knipe DM.** 2004. Herpes simplex virus 1 has multiple mechanisms for blocking virus-induced interferon production. Journal of virology **78:**8411-8420.
58. **Mossman KL, Saffran HA, Smiley JR.** 2000. Herpes simplex virus ICP0 mutants are hypersensitive to interferon. Journal of virology **74:**2052-2056.
59. **Paladino P, Collins SE, Mossman KL.** 2010. Cellular localization of the herpes simplex virus ICP0 protein dictates its ability to block IRF3-mediated innate immune responses. PloS one **5:**e10428.
60. **Ching RW, Dellaire G, Eskiw CH, Bazett-Jones DP.** 2005. PML bodies: a meeting place for genomic loci? Journal of cell science **118:**847-854.
61. **Cho Y, Lee I, Maul GG, Yu E.** 1998. A novel nuclear substructure, ND10: distribution in normal and neoplastic human tissues. International journal of molecular medicine **1:**717-724.
62. **Zhong S, Salomoni P, Pandolfi PP.** 2000. The transcriptional role of PML and the nuclear body. Nature cell biology **2:**E85-90.
63. **Zhong S, Salomoni P, Ronchetti S, Guo A, Ruggero D, Pandolfi PP.** 2000. Promyelocytic leukemia protein (PML) and Daxx participate in a novel nuclear pathway for apoptosis. The Journal of experimental medicine **191:**631-640.
64. **Lallemand-Breitenbach V, de The H.** 2010. PML nuclear bodies. Cold Spring Harbor perspectives in biology **2:**a000661.
65. **Regad T, Saib A, Lallemand-Breitenbach V, Pandolfi PP, de The H, Chelbi-Alix MK.** 2001. PML mediates the interferon-induced antiviral state against a complex retrovirus via its association with the viral transactivator. The EMBO journal **20:**3495-3505.
66. **McNally BA, Trgovcich J, Maul GG, Liu Y, Zheng P.** 2008. A role for cytoplasmic PML in cellular resistance to viral infection. PloS one **3:**e2277.
67. **Tavalai N, Stamminger T.** 2008. New insights into the role of the subnuclear structure ND10 for viral infection. Biochimica et biophysica acta **1783:**2207-2221.
68. **Everett RD, Parada C, Gripon P, Sirma H, Orr A.** 2008. Replication of ICP0-null mutant herpes simplex virus type 1 is restricted by both PML and Sp100. J Virol **82:**2661-2672.
69. **Everett RD, Rechter S, Papior P, Tavalai N, Stamminger T, Orr A.** 2006. PML contributes to a cellular mechanism of repression of herpes simplex virus type 1 infection that is inactivated by ICP0. J Virol **80:**7995-8005.
70. **Negorev DG, Vladimirova OV, Ivanov A, Rauscher F, 3rd, Maul GG.** 2006. Differential role of Sp100 isoforms in interferon-mediated repression of herpes simplex virus type 1 immediate-early protein expression. J Virol **80:**8019-8029.
71. **Muller S, Dejean A.** 1999. Viral immediate-early proteins abrogate the modification by SUMO-1 of PML and Sp100 proteins, correlating with nuclear body disruption. J Virol **73:**5137-5143.
72. **Chelbi-Alix MK, de The H.** 1999. Herpes virus induced proteasome-dependent degradation of the nuclear bodies-associated PML and Sp100 proteins. Oncogene **18:**935-941.
73. **Everett RD, Freemont P, Saitoh H, Dasso M, Orr A, Kathoria M, Parkinson J.** 1998. The disruption of ND10 during herpes simplex virus infection correlates

with the Vmw110- and proteasome-dependent loss of several PML isoforms. Journal of Virology **72:**6581-6591.
74. **Everett RD, Maul GG.** 1994. HSV-1 IE protein Vmw110 causes redistribution of PML. The EMBO journal **13:**5062-5069.
75. **Parkinson J, Everett RD.** 2000. Alphaherpesvirus proteins related to herpes simplex virus type 1 ICP0 affect cellular structures and proteins. Journal of virology **74:**10006-10017.
76. **Walters MS, Kyratsous CA, Silverstein SJ.** 2010. The RING finger domain of Varicella-Zoster virus ORF61p has E3 ubiquitin ligase activity that is essential for efficient autoubiquitination and dispersion of Sp100-containing nuclear bodies. Journal of virology **84:**6861-6865.
77. **Lukashchuk V, Everett RD.** Regulation of ICP0-null mutant herpes simplex virus type 1 infection by ND10 components ATRX and hDaxx. J Virol **84:**4026-4040.
78. **Ferenczy MW, Ranayhossaini DJ, Deluca NA.** 2011. Activities of ICP0 involved in the reversal of silencing of quiescent herpes simplex virus 1. Journal of virology **85:**4993-5002.
79. **Lomonte P, Thomas J, Texier P, Caron C, Khochbin S, Epstein AL.** 2004. Functional interaction between class II histone deacetylases and ICP0 of herpes simplex virus type 1. Journal of virology **78:**6744-6757.
80. **Gu H, Liang Y, Mandel G, Roizman B.** 2005. Components of the REST/CoREST/histone deacetylase repressor complex are disrupted, modified, and translocated in HSV-1-infected cells. Proceedings of the National Academy of Sciences of the United States of America **102:**7571-7576.
81. **Meredith M, Orr A, Elliott M, Everett R.** 1995. Separation of sequence requirements for HSV-1 Vmw110 multimerisation and interaction with a 135-kDa cellular protein. Virology **209:**174-187.
82. **Meredith M, Orr A, Everett R.** 1994. Herpes simplex virus type 1 immediate-early protein Vmw110 binds strongly and specifically to a 135-kDa cellular protein. Virology **200:**457-469.
83. **Everett RD, Meredith M, Orr A, Cross A, Kathoria M, Parkinson J.** 1997. A novel ubiquitin-specific protease is dynamically associated with the PML nuclear domain and binds to a herpesvirus regulatory protein. The EMBO journal **16:**1519-1530.
84. **Everett RD, Meredith M, Orr A.** 1999. The ability of herpes simplex virus type 1 immediate-early protein Vmw110 to bind to a ubiquitin-specific protease contributes to its roles in the activation of gene expression and stimulation of virus replication. Journal of virology **73:**417-426.
85. **Canning M, Boutell C, Parkinson J, Everett RD.** 2004. A RING finger ubiquitin ligase is protected from autocatalyzed ubiquitination and degradation by binding to ubiquitin-specific protease USP7. The Journal of biological chemistry **279:**38160-38168.
86. **Mostafa HH, Thompson TW, Davido DJ.** 2012. N-terminal phosphorylation sites of herpes simplex virus type 1 ICP0 differentially regulate its activities and enhance viral replication. Journal of virology.

87. **Daubeuf S, Singh D, Tan Y, Liu H, Federoff HJ, Bowers WJ, Tolba K.** 2009. HSV ICP0 recruits USP7 to modulate TLR-mediated innate response. Blood **113:**3264-3275.
88. **Ackermann M, Braun DK, Pereira L, Roizman B.** 1984. Characterization of herpes simplex virus 1 alpha proteins 0, 4, and 27 with monoclonal antibodies. Journal of virology **52:**108-118.
89. **Davido DJ, Leib DA, Schaffer PA.** 2002. The cyclin-dependent kinase inhibitor roscovitine inhibits the transactivating activity and alters the posttranslational modification of herpes simplex virus type 1 ICP0. Journal of virology **76:**1077-1088.
90. **Davido DJ, von Zagorski WF, Lane WS, Schaffer PA.** 2005. Phosphorylation site mutations affect herpes simplex virus type 1 ICP0 function. Journal of virology **79:**1232-1243.
91. **Boutell C, Everett R, Hilliard J, Schaffer P, Orr A, Davido D.** 2008. Herpes simplex virus type 1 ICP0 phosphorylation mutants impair the E3 ubiquitin ligase activity of ICP0 in a cell type-dependent manner. Journal of virology **82:**10647-10656.
92. **Mostafa HH, Thompson TW, Kushnir AS, Haenchen SD, Bayless AM, Hilliard JG, Link MA, Pitcher LA, Loveday E, Schaffer PA, Davido DJ.** 2011. Herpes simplex virus 1 ICP0 phosphorylation site mutants are attenuated for viral replication and impaired for explant-induced reactivation. Journal of virology **85:**12631-12637.
93. **Macdonald SJ, Mostafa HH, Morrison LA, Davido DJ.** 2012. Genome sequence of herpes simplex virus 1 strain KOS. Journal of virology **86:**6371-6372.
94. **Averett DR, Lubbers C, Elion GB, Spector T.** 1983. Ribonucleotide reductase induced by herpes simplex type 1 virus. Characterization of a distinct enzyme. The Journal of biological chemistry **258:**9831-9838.
95. **Ponce de Leon M, Eisenberg RJ, Cohen GH.** 1977. Ribonucleotide reductase from herpes simplex virus (types 1 and 2) infected and uninfected KB cells: properties of the partially purified enzymes. The Journal of general virology **36:**163-173.
96. **Goldstein DJ, Weller SK.** 1988. Herpes simplex virus type 1-induced ribonucleotide reductase activity is dispensable for virus growth and DNA synthesis: isolation and characterization of an ICP6 lacZ insertion mutant. Journal of virology **62:**196-205.
97. **Goldstein DJ, Weller SK.** 1988. Factor(s) present in herpes simplex virus type 1-infected cells can compensate for the loss of the large subunit of the viral ribonucleotide reductase: characterization of an ICP6 deletion mutant. Virology **166:**41-51.
98. **Jacobson JG, Leib DA, Goldstein DJ, Bogard CL, Schaffer PA, Weller SK, Coen DM.** 1989. A herpes simplex virus ribonucleotide reductase deletion mutant is defective for productive acute and reactivatable latent infections of mice and for replication in mouse cells. Virology **173:**276-283.

99. **Brandt CR, Kintner RL, Pumfery AM, Visalli RJ, Grau DR.** 1991. The herpes simplex virus ribonucleotide reductase is required for ocular virulence. The Journal of general virology **72 (Pt 9):**2043-2049.
100. **Post LE, Roizman B.** 1981. A generalized technique for deletion of specific genes in large genomes: alpha gene 22 of herpes simplex virus 1 is not essential for growth. Cell **25:**227-232.
101. **Poffenberger KL, Raichlen PE, Herman RC.** 1993. In vitro characterization of a herpes simplex virus type 1 ICP22 deletion mutant. Virus genes **7:**171-186.
102. **Sears AE, Halliburton IW, Meignier B, Silver S, Roizman B.** 1985. Herpes simplex virus 1 mutant deleted in the alpha 22 gene: growth and gene expression in permissive and restrictive cells and establishment of latency in mice. Journal of virology **55:**338-346.
103. **Purves FC, Roizman B.** 1992. The UL13 gene of herpes simplex virus 1 encodes the functions for posttranslational processing associated with phosphorylation of the regulatory protein alpha 22. Proceedings of the National Academy of Sciences of the United States of America **89:**7310-7314.
104. **Asai R, Ohno T, Kato A, Kawaguchi Y.** 2007. Identification of proteins directly phosphorylated by UL13 protein kinase from herpes simplex virus 1. Microbes and infection / Institut Pasteur **9:**1434-1438.
105. **Smith-Donald BA, Roizman B.** 2008. The interaction of herpes simplex virus 1 regulatory protein ICP22 with the cdc25C phosphatase is enabled in vitro by viral protein kinases US3 and UL13. Journal of virology **82:**4533-4543.
106. **Orlando JS, Balliet JW, Kushnir AS, Astor TL, Kosz-Vnenchak M, Rice SA, Knipe DM, Schaffer PA.** 2006. ICP22 is required for wild-type composition and infectivity of herpes simplex virus type 1 virions. Journal of virology **80:**9381-9390.
107. **Rice SA, Long MC, Lam V, Schaffer PA, Spencer CA.** 1995. Herpes simplex virus immediate-early protein ICP22 is required for viral modification of host RNA polymerase II and establishment of the normal viral transcription program. Journal of virology **69:**5550-5559.
108. **Purves FC, Ogle WO, Roizman B.** 1993. Processing of the herpes simplex virus regulatory protein alpha 22 mediated by the UL13 protein kinase determines the accumulation of a subset of alpha and gamma mRNAs and proteins in infected cells. Proceedings of the National Academy of Sciences of the United States of America **90:**6701-6705.
109. **Durand LO, Advani SJ, Poon AP, Roizman B.** 2005. The carboxyl-terminal domain of RNA polymerase II is phosphorylated by a complex containing cdk9 and infected-cell protein 22 of herpes simplex virus 1. Journal of virology **79:**6757-6762.
110. **Fraser KA, Rice SA.** 2007. Herpes simplex virus immediate-early protein ICP22 triggers loss of serine 2-phosphorylated RNA polymerase II. Journal of virology **81:**5091-5101.
111. **Rice SA.** 2011. Multiple Roles of Immediate-Early Protein ICP22 in HSV-1 Replication. *In* Weller SK (ed.). Caister Academic Press, Alphaherpesviruses.

112. **Bastian TW, Livingston CM, Weller SK, Rice SA.** 2010. Herpes simplex virus type 1 immediate-early protein ICP22 is required for VICE domain formation during productive viral infection. Journal of virology **84:**2384-2394.
113. **Burch AD, Weller SK.** 2004. Nuclear sequestration of cellular chaperone and proteasomal machinery during herpes simplex virus type 1 infection. Journal of virology **78:**7175-7185.
114. **Burch AD, Weller SK.** 2005. Herpes simplex virus type 1 DNA polymerase requires the mammalian chaperone hsp90 for proper localization to the nucleus. Journal of virology **79:**10740-10749.
115. **Livingston CM, Ifrim MF, Cowan AE, Weller SK.** 2009. Virus-Induced Chaperone-Enriched (VICE) domains function as nuclear protein quality control centers during HSV-1 infection. PLoS pathogens **5:**e1000619.
116. **Carter KL, Roizman B.** 1996. The promoter and transcriptional unit of a novel herpes simplex virus 1 alpha gene are contained in, and encode a protein in frame with, the open reading frame of the alpha 22 gene. Journal of virology **70:**172-178.
117. **Bowman JJ, Schaffer PA.** 2009. Origin of expression of the herpes simplex virus type 1 protein U(S)1.5. Journal of virology **83:**9183-9194.
118. **Ogle WO, Roizman B.** 1999. Functional anatomy of herpes simplex virus 1 overlapping genes encoding infected-cell protein 22 and US1.5 protein. Journal of virology **73:**4305-4315.
119. **Bastian TW, Rice SA.** 2009. Identification of sequences in herpes simplex virus type 1 ICP22 that influence RNA polymerase II modification and viral late gene expression. Journal of virology **83:**128-139.
120. **Haenchen SD, Utter JA, Bayless AM, Dobrowsky RT, Davido DJ.** 2010. Role of a cdk5-associated protein, p35, in herpes simplex virus type 1 replication in vivo. Journal of neurovirology **16:**405-409.
121. **Tang D, Wang JH.** 1996. Cyclin-dependent kinase 5 (Cdk5) and neuron-specific Cdk5 activators. Progress in cell cycle research **2:**205-216.
122. **Hisanaga S, Saito T.** 2003. The regulation of cyclin-dependent kinase 5 activity through the metabolism of p35 or p39 Cdk5 activator. Neuro-Signals **12:**221-229.
123. **Zhang J, Li H, Yabut O, Fitzpatrick H, D'Arcangelo G, Herrup K.** 2010. Cdk5 suppresses the neuronal cell cycle by disrupting the E2F1-DP1 complex. The Journal of neuroscience : the official journal of the Society for Neuroscience **30:**5219-5228.
124. **Hisanaga S, Endo R.** 2010. Regulation and role of cyclin-dependent kinase activity in neuronal survival and death. Journal of neurochemistry **115:**1309-1321.
125. **Lew J, Huang QQ, Qi Z, Winkfein RJ, Aebersold R, Hunt T, Wang JH.** 1994. A brain-specific activator of cyclin-dependent kinase 5. Nature **371:**423-426.
126. **Tsai LH, Delalle I, Caviness VS, Jr., Chae T, Harlow E.** 1994. p35 is a neural-specific regulatory subunit of cyclin-dependent kinase 5. Nature **371:**419-423.
127. **Tang D, Yeung J, Lee KY, Matsushita M, Matsui H, Tomizawa K, Hatase O, Wang JH.** 1995. An isoform of the neuronal cyclin-dependent kinase 5 (Cdk5) activator. The Journal of biological chemistry **270:**26897-26903.

128. **Humbert S, Dhavan R, Tsai L.** 2000. p39 activates cdk5 in neurons, and is associated with the actin cytoskeleton. Journal of cell science **113 (Pt 6):**975-983.
129. **Tarricone C, Dhavan R, Peng J, Areces LB, Tsai LH, Musacchio A.** 2001. Structure and regulation of the CDK5-p25(nck5a) complex. Molecular cell **8:**657-669.
130. **Ko J, Humbert S, Bronson RT, Takahashi S, Kulkarni AB, Li E, Tsai LH.** 2001. p35 and p39 are essential for cyclin-dependent kinase 5 function during neurodevelopment. The Journal of neuroscience : the official journal of the Society for Neuroscience **21:**6758-6771.
131. **Lee KY, Rosales JL, Tang D, Wang JH.** 1996. Interaction of cyclin-dependent kinase 5 (Cdk5) and neuronal Cdk5 activator in bovine brain. The Journal of biological chemistry **271:**1538-1543.
132. **Philpott A, Porro EB, Kirschner MW, Tsai LH.** 1997. The role of cyclin-dependent kinase 5 and a novel regulatory subunit in regulating muscle differentiation and patterning. Genes & development **11:**1409-1421.
133. **Ohshima T, Ward JM, Huh CG, Longenecker G, Veeranna, Pant HC, Brady RO, Martin LJ, Kulkarni AB.** 1996. Targeted disruption of the cyclin-dependent kinase 5 gene results in abnormal corticogenesis, neuronal pathology and perinatal death. Proceedings of the National Academy of Sciences of the United States of America **93:**11173-11178.
134. **Tanaka T, Veeranna, Ohshima T, Rajan P, Amin ND, Cho A, Sreenath T, Pant HC, Brady RO, Kulkarni AB.** 2001. Neuronal cyclin-dependent kinase 5 activity is critical for survival. The Journal of neuroscience : the official journal of the Society for Neuroscience **21:**550-558.
135. **Li BS, Zhang L, Takahashi S, Ma W, Jaffe H, Kulkarni AB, Pant HC.** 2002. Cyclin-dependent kinase 5 prevents neuronal apoptosis by negative regulation of c-Jun N-terminal kinase 3. The EMBO journal **21:**324-333.
136. **Cheung ZH, Gong K, Ip NY.** 2008. Cyclin-dependent kinase 5 supports neuronal survival through phosphorylation of Bcl-2. The Journal of neuroscience : the official journal of the Society for Neuroscience **28:**4872-4877.
137. **Li BS, Ma W, Jaffe H, Zheng Y, Takahashi S, Zhang L, Kulkarni AB, Pant HC.** 2003. Cyclin-dependent kinase-5 is involved in neuregulin-dependent activation of phosphatidylinositol 3-kinase and Akt activity mediating neuronal survival. The Journal of biological chemistry **278:**35702-35709.
138. **Wang CX, Song JH, Song DK, Yong VW, Shuaib A, Hao C.** 2006. Cyclin-dependent kinase-5 prevents neuronal apoptosis through ERK-mediated upregulation of Bcl-2. Cell death and differentiation **13:**1203-1212.
139. **Vartiainen N, Keksa-Goldsteine V, Goldsteins G, Koistinaho J.** 2002. Aspirin provides cyclin-dependent kinase 5-dependent protection against subsequent hypoxia/reoxygenation damage in culture. Journal of neurochemistry **82:**329-335.
140. **O'Hare MJ, Kushwaha N, Zhang Y, Aleyasin H, Callaghan SM, Slack RS, Albert PR, Vincent I, Park DS.** 2005. Differential roles of nuclear and cytoplasmic cyclin-dependent kinase 5 in apoptotic and excitotoxic neuronal death. The Journal of neuroscience : the official journal of the Society for Neuroscience **25:**8954-8966.

141. **Brinkkoetter PT, Olivier P, Wu JS, Henderson S, Krofft RD, Pippin JW, Hockenbery D, Roberts JM, Shankland SJ.** 2009. Cyclin I activates Cdk5 and regulates expression of Bcl-2 and Bcl-XL in postmitotic mouse cells. The Journal of clinical investigation **119:**3089-3101.
142. **Kusakawa G, Saito T, Onuki R, Ishiguro K, Kishimoto T, Hisanaga S.** 2000. Calpain-dependent proteolytic cleavage of the p35 cyclin-dependent kinase 5 activator to p25. The Journal of biological chemistry **275:**17166-17172.
143. **Shirata N, Kudoh A, Daikoku T, Tatsumi Y, Fujita M, Kiyono T, Sugaya Y, Isomura H, Ishizaki K, Tsurumi T.** 2005. Activation of ataxia telangiectasia-mutated DNA damage checkpoint signal transduction elicited by herpes simplex virus infection. The Journal of biological chemistry **280:**30336-30341.
144. **Lilley CE, Carson CT, Muotri AR, Gage FH, Weitzman MD.** 2005. DNA repair proteins affect the lifecycle of herpes simplex virus 1. Proceedings of the National Academy of Sciences of the United States of America **102:**5844-5849.
145. **Wilkinson DE, Weller SK.** 2004. Recruitment of cellular recombination and repair proteins to sites of herpes simplex virus type 1 DNA replication is dependent on the composition of viral proteins within prereplicative sites and correlates with the induction of the DNA damage response. Journal of virology **78:**4783-4796.
146. **Samaniego LA, Wu N, DeLuca NA.** 1997. The herpes simplex virus immediate-early protein ICP0 affects transcription from the viral genome and infected-cell survival in the absence of ICP4 and ICP27. Journal of Virology **71:**4614-4625.
147. **Schaffer PA, Aron GM, Biswal N, Benyesh-Melnick M.** 1973. Temperature-sensitive mutants of herpes simplex virus type 1: isolation, complementation and partial characterization. Virology **52:**57-71.
148. **Cai WZ, Schaffer PA.** 1989. Herpes simplex virus type 1 ICP0 plays a critical role in the de novo synthesis of infectious virus following transfection of viral DNA. Journal of Virology **63:**4579-4589.
149. **Council NR.** 1996. Guide for the care and use of laboratory animals. *In* Sciences NAo (ed.), National Academy Press, Washington, D.C.
150. **Balliet JW, Schaffer PA.** 2006. Point mutations in herpes simplex virus type 1 oriL, but not in oriS, reduce pathogenesis during acute infection of mice and impair reactivation from latency. Journal of virology **80:**440-450.
151. **Halford WP, Schaffer PA.** 2000. Optimized viral dose and transient immunosuppression enable herpes simplex virus ICP0-null mutants To establish wild-type levels of latency in vivo. Journal of Virology **74:**5957-5967.
152. **Schrimpf JE, Tu EM, Wang H, Wong YM, Morrison LA.** 2011. B7 costimulation molecules encoded by replication-defective, vhs-deficient HSV-1 improve vaccine-induced protection against corneal disease PloS one **In Press**.
153. **Strand SS, Leib DA.** 2004. Role of the VP16-binding domain of vhs in viral growth, host shutoff activity, and pathogenesis. Journal of virology **78:**13562-13572.
154. **Livak KJ, Schmittgen TD.** 2001. Analysis of relative gene expression data using real-time quantitative PCR and the 2(-Delta Delta C(T)) Method. Methods **25:**402-408.

155. **Link MA, Schaffer PA.** 2007. Herpes simplex virus type 1 C-terminal variants of the origin binding protein (OBP), OBPC-1 and OBPC-2, cooperatively regulate viral DNA levels in vitro, and OBPC-2 affects mortality in mice. Journal of virology **81:**10699-10711.
156. **Sainz B, Jr., Halford WP.** 2002. Alpha/Beta interferon and gamma interferon synergize to inhibit the replication of herpes simplex virus type 1. Journal of virology **76:**11541-11550.
157. **Halford WP, Weisend C, Grace J, Soboleski M, Carr DJ, Balliet JW, Imai Y, Margolis TP, Gebhardt BM.** 2006. ICP0 antagonizes Stat 1-dependent repression of herpes simplex virus: implications for the regulation of viral latency. Virology journal **3:**44.
158. **Summers BC, Margolis TP, Leib DA.** 2001. Herpes simplex virus type 1 corneal infection results in periocular disease by zosteriform spread. Journal of virology **75:**5069-5075.
159. **Leib DA, Bogard CL, Kosz-Vnenchak M, Hicks KA, Coen DM, Knipe DM, Schaffer PA.** 1989. A deletion mutant of the latency-associated transcript of herpes simplex virus type 1 reactivates from the latent state with reduced frequency. Journal of virology **63:**2893-2900.
160. **Katz JP, Bodin ET, Coen DM.** 1990. Quantitative polymerase chain reaction analysis of herpes simplex virus DNA in ganglia of mice infected with replication-incompetent mutants. Journal of virology **64:**4288-4295.
161. **Boutell C, D. C, Antrobus R, Vanni E, Orr A, Everett RD.** 2010. 35th International Herpesvirus Workshop, Salt Lake City, UT.
162. **Hecker CM, Rabiller M, Haglund K, Bayer P, Dikic I.** 2006. Specification of SUMO1- and SUMO2-interacting motifs. The Journal of biological chemistry **281:**16117-16127.
163. **Hannich JT, Lewis A, Kroetz MB, Li SJ, Heide H, Emili A, Hochstrasser M.** 2005. Defining the SUMO-modified proteome by multiple approaches in Saccharomyces cerevisiae. The Journal of biological chemistry **280:**4102-4110.
164. **Stehmeier P, Muller S.** 2009. Phospho-regulated SUMO interaction modules connect the SUMO system to CK2 signaling. Molecular cell **33:**400-409.
165. **Liang Y, Roizman B.** 2006. State and role of SRC family kinases in replication of herpes simplex virus 1. Journal of virology **80:**3349-3359.
166. **Liang Y, Kurakin A, Roizman B.** 2005. Herpes simplex virus 1 infected cell protein 0 forms a complex with CIN85 and Cbl and mediates the degradation of EGF receptor from cell surfaces. Proceedings of the National Academy of Sciences of the United States of America **102:**5838-5843.
167. **Ackermann M, Braun DK, Pereira L, Roizman B.** 1984. Characterization of herpes simplex virus 1 alpha proteins 0, 4, and 27 with monoclonal antibodies. Journal of Virology **52:**108-118.
168. **Advani SJ, Hagglund R, Weichselbaum RR, Roizman B.** 2001. Posttranslational processing of infected cell proteins 0 and 4 of herpes simplex virus 1 is sequential and reflects the subcellular compartment in which the proteins localize. Journal of virology **75:**7904-7912.

169. **Ogle WO, Ng TI, Carter KL, Roizman B.** 1997. The UL13 protein kinase and the infected cell type are determinants of posttranslational modification of ICP0. Virology **235:**406-413.
170. **Wilcox KW, Kohn A, Sklyanskaya E, Roizman B.** 1980. Herpes simplex virus phosphoproteins. I. Phosphate cycles on and off some viral polypeptides and can alter their affinity for DNA. Journal of virology **33:**167-182.
171. **Samaniego LA, Wu N, DeLuca NA.** 1997. The herpes simplex virus immediate-early protein ICP0 affects transcription from the viral genome and infected-cell survival in the absence of ICP4 and ICP27. Journal of virology **71:**4614-4625.
172. **Kushnir AS, Davido DJ, Schaffer PA.** 2010. Role of nuclear factor Y in stress-induced activation of the herpes simplex virus type 1 ICP0 promoter. Journal of virology **84:**188-200.
173. **National-Research-Council.** 2011. Guide for the Care and Use of Laboratory Animals, 8th ed, National Academies Press, Washington, DC.
174. **Rojas S, Corbin-Lickfett KA, Escudero-Paunetto L, Sandri-Goldin RM.** 2010. ICP27 phosphorylation site mutants are defective in herpes simplex virus 1 replication and gene expression. Journal of virology **84:**2200-2211.
175. **Sekhar V, McBride AA.** 2012. Phosphorylation regulates binding of the HPV8 E2 protein to host chromosomes. Journal of virology.
176. **Levkowitz G, Waterman H, Ettenberg SA, Katz M, Tsygankov AY, Alroy I, Lavi S, Iwai K, Reiss Y, Ciechanover A, Lipkowitz S, Yarden Y.** 1999. Ubiquitin ligase activity and tyrosine phosphorylation underlie suppression of growth factor signaling by c-Cbl/Sli-1. Molecular cell **4:**1029-1040.
177. **Vodermaier HC.** 2004. APC/C and SCF: controlling each other and the cell cycle. Current biology : CB **14:**R787-796.
178. **Debonneville C, Flores SY, Kamynina E, Plant PJ, Tauxe C, Thomas MA, Munster C, Chraibi A, Pratt JH, Horisberger JD, Pearce D, Loffing J, Staub O.** 2001. Phosphorylation of Nedd4-2 by Sgk1 regulates epithelial Na(+) channel cell surface expression. The EMBO journal **20:**7052-7059.
179. **Gu H, Roizman B.** 2003. The degradation of promyelocytic leukemia and Sp100 proteins by herpes simplex virus 1 is mediated by the ubiquitin-conjugating enzyme UbcH5a. Proceedings of the National Academy of Sciences of the United States of America **100:**8963-8968.
180. **Boutell C, Sadis S, Everett RD.** 2002. Herpes simplex virus type 1 immediate-early protein ICP0 and is isolated RING finger domain act as ubiquitin E3 ligases in vitro. Journal of virology **76:**841-850.
181. **Nagel CH, Albrecht N, Milovic-Holm K, Mariyanna L, Keyser B, Abel B, Weseloh B, Hofmann TG, Eibl MM, Hauber J.** 2011. Herpes simplex virus immediate-early protein ICP0 is targeted by SIAH-1 for proteasomal degradation. Journal of virology **85:**7644-7657.
182. **Chaurushiya MS, Lilley CE, Aslanian A, Meisenhelder J, Scott DC, Landry S, Ticau S, Boutell C, Yates JR, 3rd, Schulman BA, Hunter T, Weitzman MD.** 2012. Viral E3 ubiquitin ligase-mediated degradation of a cellular E3: viral mimicry of a cellular phosphorylation mark targets the RNF8 FHA domain. Molecular cell **46:**79-90.

183. **Ciufo DM, Mullen MA, Hayward GS.** 1994. Identification of a dimerization domain in the C-terminal segment of the IE110 transactivator protein from herpes simplex virus. Journal of virology **68:**3267-3282.
184. **Rabellino A, Carter BJ, Konstantinidou G, Shwu-Yuan W, Rimessi A, Byers LA, Heymach JV, Girard L, Chiang CM, Teruya-Feldstein J, Scaglioni PP.** 2012. The SUMO E3-ligase PIAS1 regulates the tumor suppressor PML and its oncogenic counterpart PML-RARA. Cancer research.
185. **Ng TI, Ogle WO, Roizman B.** 1998. UL13 protein kinase of herpes simplex virus 1 complexes with glycoprotein E and mediates the phosphorylation of the viral Fc receptor: glycoproteins E and I. Virology **241:**37-48.
186. **Cai W, Schaffer PA.** 1991. A cellular function can enhance gene expression and plating efficiency of a mutant defective in the gene for ICP0, a transactivating protein of herpes simplex virus type 1. Journal of virology **65:**4078-4090.
187. **Boutell C, Everett RD, Hilliard J, Shaffer PA, Orr A, Davido DJ.** 2008. Herpes Simplex Virus Type 1 ICP0 Phosphorylation Mutants Impair the E3 Ubiquitin Ligase Activity of ICP0 in a Cell Type-Dependent Manner. Journal of virology **82:**10647-10656.
188. **Mostafa HH, Thompson TW, Davido DJ.** 2013. N-terminal phosphorylation sites of herpes simplex virus 1 ICP0 differentially regulate its activities and enhance viral replication. Journal of virology **87:**2109-2119.
189. **Cox MP, Peterson DA, Biggs PJ.** 2010. SolexaQA: At-a-glance quality assessment of Illumina second-generation sequencing data. BMC bioinformatics **11:**485.
190. **Langmead B, Trapnell C, Pop M, Salzberg SL.** 2009. Ultrafast and memory-efficient alignment of short DNA sequences to the human genome. Genome biology **10:**R25.
191. **Zerbino DR, Birney E.** 2008. Velvet: algorithms for de novo short read assembly using de Bruijn graphs. Genome research **18:**821-829.
192. **Otto TD, Dillon GP, Degrave WS, Berriman M.** 2011. RATT: Rapid Annotation Transfer Tool. Nucleic acids research **39:**e57.
193. **Bradley RK, Roberts A, Smoot M, Juvekar S, Do J, Dewey C, Holmes I, Pachter L.** 2009. Fast statistical alignment. PLoS computational biology **5:**e1000392.
194. **council Nr.** 2011. Guide for the Care and Use of Laboratory Animals, 8th ed.
195. **Halford WP, Schaffer PA.** 2000. Optimized viral dose and transient immunosuppression enable herpes simplex virus ICP0-null mutants To establish wild-type levels of latency in vivo. Journal of virology **74:**5957-5967.
196. **Bacchetti S, Evelegh MJ, Muirhead B, Sartori CS, Huszar D.** 1984. Immunological characterization of herpes simplex virus type 1 and 2 polypeptide(s) involved in viral ribonucleotide reductase activity. Journal of virology **49:**591-593.
197. **Cohen GH.** 1972. Ribonucleotide reductase activity of synchronized KB cells infected with herpes simplex virus. Journal of virology **9:**408-418.
198. **Frame MC, Marsden HS, Dutia BM.** 1985. The ribonucleotide reductase induced by herpes simplex virus type 1 involves minimally a complex of two

polypeptides (136K and 38K). The Journal of general virology **66 (Pt 7):**1581-1587.
199. **Ingemarson R, Lankinen H.** 1987. The herpes simplex virus type 1 ribonucleotide reductase is a tight complex of the type alpha 2 beta 2 composed of 40K and 140K proteins, of which the latter shows multiple forms due to proteolysis. Virology **156:**417-422.
200. **Swain MA, Galloway DA.** 1986. Herpes simplex virus specifies two subunits of ribonucleotide reductase encoded by 3'-coterminal transcripts. Journal of virology **57:**802-808.
201. **Nordlund P, Reichard P.** 2006. Ribonucleotide reductases. Annual review of biochemistry **75:**681-706.
202. **Honess RW, Roizman B.** 1973. Proteins specified by herpes simplex virus. XI. Identification and relative molar rates of synthesis of structural and nonstructural herpes virus polypeptides in the infected cell. Journal of virology **12:**1347-1365.
203. **Honess RW, Roizman B.** 1974. Regulation of herpesvirus macromolecular synthesis. I. Cascade regulation of the synthesis of three groups of viral proteins. Journal of virology **14:**8-19.
204. **Watson RJ, Preston CM, Clements JB.** 1979. Separation and characterization of herpes simplex virus type 1 immediate-early mRNA's. Journal of virology **31:**42-52.
205. **Wymer JP, Chung TD, Chang YN, Hayward GS, Aurelian L.** 1989. Identification of immediate-early-type cis-response elements in the promoter for the ribonucleotide reductase large subunit from herpes simplex virus type 2. Journal of virology **63:**2773-2784.
206. **Conner J, Macfarlane J, Lankinen H, Marsden H.** 1992. The unique N terminus of the herpes simplex virus type 1 large subunit is not required for ribonucleotide reductase activity. The Journal of general virology **73 (Pt 1):**103-112.
207. **Dufour F, Sasseville AM, Chabaud S, Massie B, Siegel RM, Langelier Y.** 2011. The ribonucleotide reductase R1 subunits of herpes simplex virus types 1 and 2 protect cells against TNFalpha- and FasL-induced apoptosis by interacting with caspase-8. Apoptosis : an international journal on programmed cell death **16:**256-271.
208. **Dufour F, Bertrand L, Pearson A, Grandvaux N, Langelier Y.** 2011. The ribonucleotide reductase R1 subunits of herpes simplex virus 1 and 2 protect cells against poly(I . C)-induced apoptosis. Journal of virology **85:**8689-8701.
209. **Chabaud S, Lambert H, Sasseville AM, Lavoie H, Guilbault C, Massie B, Landry J, Langelier Y.** 2003. The R1 subunit of herpes simplex virus ribonucleotide reductase has chaperone-like activity similar to Hsp27. FEBS letters **545:**213-218.
210. **Cooper J, Conner J, Clements JB.** 1995. Characterization of the novel protein kinase activity present in the R1 subunit of herpes simplex virus ribonucleotide reductase. Journal of virology **69:**4979-4985.
211. **Salvucci LA, Bonneau RH, Tevethia SS.** 1995. Polymorphism within the herpes simplex virus (HSV) ribonucleotide reductase large subunit (ICP6) confers type

specificity for recognition by HSV type 1-specific cytotoxic T lymphocytes. Journal of virology **69:**1122-1131.
212. **Conner J, Cross A, Murray J, Marsden H.** 1994. Identification of structural domains within the large subunit of herpes simplex virus ribonucleotide reductase. The Journal of general virology **75 (Pt 12):**3327-3335.
213. **Conner J, Furlong J, Murray J, Meighan M, Cross A, Marsden H, Clements JB.** 1993. Herpes simplex virus type 1 ribonucleotide reductase large subunit: regions of the protein essential for subunit interaction and dimerization. Biochemistry **32:**13673-13680.
214. **Nikas I, McLauchlan J, Davison AJ, Taylor WR, Clements JB.** 1986. Structural features of ribonucleotide reductase. Proteins **1:**376-384.
215. **Nikas I, Darling AJ, Lankinen HM, Cross AM, Marsden HS, Clements JB.** 1990. A single amino acid substitution in the large subunit of herpes simplex virus type 1 ribonucleotide reductase which prevents subunit association. The Journal of general virology **71 (Pt 10):**2369-2376.
216. **Preston VG, Palfreyman JW, Dutia BM.** 1984. Identification of a herpes simplex virus type 1 polypeptide which is a component of the virus-induced ribonucleotide reductase. The Journal of general virology **65 (Pt 9):**1457-1466.
217. **Balan P, Davis-Poynter N, Bell S, Atkinson H, Browne H, Minson T.** 1994. An analysis of the in vitro and in vivo phenotypes of mutants of herpes simplex virus type 1 lacking glycoproteins gG, gE, gI or the putative gJ. The Journal of general virology **75 (Pt 6):**1245-1258.
218. **Long MC, Leong V, Schaffer PA, Spencer CA, Rice SA.** 1999. ICP22 and the UL13 protein kinase are both required for herpes simplex virus-induced modification of the large subunit of RNA polymerase II. Journal of virology **73:**5593-5604.
219. **Read GS, Karr BM, Knight K.** 1993. Isolation of a herpes simplex virus type 1 mutant with a deletion in the virion host shutoff gene and identification of multiple forms of the vhs (UL41) polypeptide. Journal of virology **67:**7149-7160.
220. **Flory E, Weber CK, Chen P, Hoffmeyer A, Jassoy C, Rapp UR.** 1998. Plasma membrane-targeted Raf kinase activates NF-kappaB and human immunodeficiency virus type 1 replication in T lymphocytes. Journal of virology **72:**2788-2794.
221. **Poffenberger KL, Idowu AD, Fraser-Smith EB, Raichlen PE, Herman RC.** 1994. A herpes simplex virus type 1 ICP22 deletion mutant is altered for virulence and latency in vivo. Archives of virology **139:**111-119.
222. **Everett RD.** 1984. Trans activation of transcription by herpes virus products: requirement for two HSV-1 immediate-early polypeptides for maximum activity. The EMBO journal **3:**3135-3141.
223. **Bowman JJ, Orlando JS, Davido DJ, Kushnir AS, Schaffer PA.** 2009. Transient expression of herpes simplex virus type 1 ICP22 represses viral promoter activity and complements the replication of an ICP22 null virus. Journal of virology **83:**8733-8743.
224. **Guo L, Wu WJ, Liu LD, Wang LC, Zhang Y, Wu LQ, Guan Y, Li QH.** 2012. Herpes simplex virus 1 ICP22 inhibits the transcription of viral gene promoters by binding to and blocking the recruitment of P-TEFb. PloS one **7:**e45749.

225. **Cun W, Guo L, Zhang Y, Liu L, Wang L, Li J, Dong C, Wang J, Li Q.** 2009. Transcriptional regulation of the Herpes Simplex Virus 1alpha-gene by the viral immediate-early protein ICP22 in association with VP16. Science in China. Series C, Life sciences / Chinese Academy of Sciences **52:**344-351.
226. **Emeny JM, Morgan MJ.** 1979. Regulation of the interferon system: evidence that Vero cells have a genetic defect in interferon production. The Journal of general virology **43:**247-252.
227. **Chee AV, Roizman B.** 2004. Herpes simplex virus 1 gene products occlude the interferon signaling pathway at multiple sites. Journal of virology **78:**4185-4196.
228. **Yang M, Wang C, Zhu X, Tang S, Shi L, Cao X, Chen T.** 2011. E3 ubiquitin ligase CHIP facilitates Toll-like receptor signaling by recruiting and polyubiquitinating Src and atypical PKC{zeta}. The Journal of experimental medicine **208:**2099-2112.
229. **Shang L, Tomasi TB.** 2006. The heat shock protein 90-CDC37 chaperone complex is required for signaling by types I and II interferons. The Journal of biological chemistry **281:**1876-1884.
230. **Yang K, Shi H, Qi R, Sun S, Tang Y, Zhang B, Wang C.** 2006. Hsp90 regulates activation of interferon regulatory factor 3 and TBK-1 stabilization in Sendai virus-infected cells. Molecular biology of the cell **17:**1461-1471.
231. **Rice SA, Davido DJ.** 2013. HSV-1 ICP22: hijacking host nuclear functions to enhance viral infection. Future microbiology **8:**311-321.
232. **Hook LM, Lubinski JM, Jiang M, Pangburn MK, Friedman HM.** 2006. Herpes simplex virus type 1 and 2 glycoprotein C prevents complement-mediated neutralization induced by natural immunoglobulin M antibody. Journal of virology **80:**4038-4046.
233. **Friedman HM, Cohen GH, Eisenberg RJ, Seidel CA, Cines DB.** 1984. Glycoprotein C of herpes simplex virus 1 acts as a receptor for the C3b complement component on infected cells. Nature **309:**633-635.
234. **Hung SL, Peng C, Kostavasili I, Friedman HM, Lambris JD, Eisenberg RJ, Cohen GH.** 1994. The interaction of glycoprotein C of herpes simplex virus types 1 and 2 with the alternative complement pathway. Virology **203:**299-312.
235. **Kostavasili I, Sahu A, Friedman HM, Eisenberg RJ, Cohen GH, Lambris JD.** 1997. Mechanism of complement inactivation by glycoprotein C of herpes simplex virus. J Immunol **158:**1763-1771.
236. **Mostafa HH, Davido DJ.** 2013. HSV-1 ICP22 but not US1.5 is Required for Efficient Acute Replication in Mice and VICE Domain Formation. Journal of virology.
237. **Ryu H, Al-Ani G, Deckert K, Kirkpatrick D, Gygi SP, Dasso M, Azuma Y.** 2010. PIASy mediates SUMO-2/3 conjugation of poly(ADP-ribose) polymerase 1 (PARP1) on mitotic chromosomes. The Journal of biological chemistry **285:**14415-14423.
238. **Laemmli UK.** 1970. Cleavage of structural proteins during the assembly of the head of bacteriophage T4. Nature **227:**680-685.
239. **Fernandez-Capetillo O, Lee A, Nussenzweig M, Nussenzweig A.** 2004. H2AX: the histone guardian of the genome. DNA repair **3:**959-967.

240. **Rogakou EP, Pilch DR, Orr AH, Ivanova VS, Bonner WM.** 1998. DNA double-stranded breaks induce histone H2AX phosphorylation on serine 139. The Journal of biological chemistry **273:**5858-5868.
241. **Bekker-Jensen S, Mailand N.** 2010. Assembly and function of DNA double-strand break repair foci in mammalian cells. DNA repair **9:**1219-1228.
242. **Chapman JD, Gagne JP, Poirier GG, Goodlett DR.** 2013. Mapping PARP-1 Auto-ADP-ribosylation Sites by Liquid Chromatography-Tandem Mass Spectrometry. Journal of proteome research.
243. **Riquelme PT, Burzio LO, Koide SS.** 1979. ADP ribosylation of rat liver lysine-rich histone in vitro. The Journal of biological chemistry **254:**3018-3028.
244. **Tallis M, Morra R, Barkauskaite E, Ahel I.** 2013. Poly(ADP-ribosyl)ation in regulation of chromatin structure and the DNA damage response. Chromosoma.
245. **Haince JF, McDonald D, Rodrigue A, Dery U, Masson JY, Hendzel MJ, Poirier GG.** 2008. PARP1-dependent kinetics of recruitment of MRE11 and NBS1 proteins to multiple DNA damage sites. The Journal of biological chemistry **283:**1197-1208.
246. **Mohni KN, Livingston CM, Cortez D, Weller SK.** 2010. ATR and ATRIP are recruited to herpes simplex virus type 1 replication compartments even though ATR signaling is disabled. Journal of virology **84:**12152-12164.
247. **Harada T, Morooka T, Ogawa S, Nishida E.** 2001. ERK induces p35, a neuron-specific activator of Cdk5, through induction of Egr1. Nature cell biology **3:**453-459.
248. **Tokuoka H, Saito T, Yorifuji H, Wei F, Kishimoto T, Hisanaga S.** 2000. Brain-derived neurotrophic factor-induced phosphorylation of neurofilament-H subunit in primary cultures of embryo rat cortical neurons. Journal of cell science **113 (Pt 6):**1059-1068.
249. **Lee JH, Kim KT.** 2004. Induction of cyclin-dependent kinase 5 and its activator p35 through the extracellular-signal-regulated kinase and protein kinase A pathways during retinoic-acid mediated neuronal differentiation in human neuroblastoma SK-N-BE(2)C cells. Journal of neurochemistry **91:**634-647.
250. **Qin D, Feng N, Fan W, Ma X, Yan Q, Lv Z, Zeng Y, Zhu J, Lu C.** 2011. Activation of PI3K/AKT and ERK MAPK signal pathways is required for the induction of lytic cycle replication of Kaposi's sarcoma-associated herpesvirus by herpes simplex virus type 1. BMC microbiology **11:**240.
251. **Bedadala GR, Palem JR, Graham L, Hill JM, McFerrin HE, Hsia SC.** 2011. Lytic HSV-1 infection induces the multifunctional transcription factor Early Growth Response-1 (EGR-1) in rabbit corneal cells. Virology journal **8:**262.
252. **Strocchi P, Pession A, Dozza B.** 2003. Up-regulation of cDK5/p35 by oxidative stress in human neuroblastoma IMR-32 cells. Journal of cellular biochemistry **88:**758-765.
253. **Canugovi C, Misiak M, Ferrarelli LK, Croteau DL, Bohr VA.** 2013. The role of DNA repair in brain related disease pathology. DNA repair **12:**578-587.
254. **Ohba M, Shibanuma M, Kuroki T, Nose K.** 1994. Production of hydrogen peroxide by transforming growth factor-beta 1 and its involvement in induction of egr-1 in mouse osteoblastic cells. The Journal of cell biology **126:**1079-1088.

255. **Schachtele SJ, Hu S, Little MR, Lokensgard JR.** 2010. Herpes simplex virus induces neural oxidative damage via microglial cell Toll-like receptor-2. Journal of neuroinflammation **7:**35.
256. **Zhang J, Li H, Herrup K.** 2010. Cdk5 nuclear localization is p27-dependent in nerve cells: implications for cell cycle suppression and caspase-3 activation. The Journal of biological chemistry **285:**14052-14061.
257. **Zhang J, Li H, Zhou T, Zhou J, Herrup K.** 2012. Cdk5 levels oscillate during the neuronal cell cycle: Cdh1 ubiquitination triggers proteosome-dependent degradation during S-phase. The Journal of biological chemistry **287:**25985-25994.
258. **Jiang X, Chentoufi AA, Hsiang C, Carpenter D, Osorio N, BenMohamed L, Fraser NW, Jones C, Wechsler SL.** 2011. The herpes simplex virus type 1 latency-associated transcript can protect neuron-derived C1300 and Neuro2A cells from granzyme B-induced apoptosis and CD8 T-cell killing. Journal of virology **85:**2325-2332.
259. **Perng GC, Jones C, Ciacci-Zanella J, Stone M, Henderson G, Yukht A, Slanina SM, Hofman FM, Ghiasi H, Nesburn AB, Wechsler SL.** 2000. Virus-induced neuronal apoptosis blocked by the herpes simplex virus latency-associated transcript. Science **287:**1500-1503.
260. **Thompson RL, Sawtell NM.** 2001. Herpes simplex virus type 1 latency-associated transcript gene promotes neuronal survival. Journal of virology **75:**6660-6675.
261. **Lee MS, Kwon YT, Li M, Peng J, Friedlander RM, Tsai LH.** 2000. Neurotoxicity induces cleavage of p35 to p25 by calpain. Nature **405:**360-364.
262. **de Bie P, Zaaroor-Regev D, Ciechanover A.** 2010. Regulation of the Polycomb protein RING1B ubiquitination by USP7. Biochemical and biophysical research communications **400:**389-395.
263. **Huang Z, Wu Q, Guryanova OA, Cheng L, Shou W, Rich JN, Bao S.** 2011. Deubiquitylase HAUSP stabilizes REST and promotes maintenance of neural progenitor cells. Nature cell biology **13:**142-152.
264. **Kwiatkowski DL, Thompson HW, Bloom DC.** 2009. The polycomb group protein Bmi1 binds to the herpes simplex virus 1 latent genome and maintains repressive histone marks during latency. Journal of virology **83:**8173-8181.
265. **Cliffe AR, Coen DM, Knipe DM.** 2013. Kinetics of facultative heterochromatin and polycomb group protein association with the herpes simplex viral genome during establishment of latent infection. mBio **4**.
266. **Kinchington PR, Leger AJ, Guedon JM, Hendricks RL.** 2012. Herpes simplex virus and varicella zoster virus, the house guests who never leave. Herpesviridae **3:**5.